ON UNDERSTANDING OF PIEZORESISTIVE RESPONSE IN CARBON NANOTUBE NETWORKS UNDER IN-PLANE STRAINING

A Thesis Submitted to the College of

Graduate Studies and Research

In Partial Fulfillment of the Requirements

For the Degree of Doctor of Philosophy

In the Mechanical Engineering

University of Saskatchewan

Saskatoon

By

YU MIAO

PERMISSION TO USE

In presenting this thesis in partial fulfilment of the requirements for a Postgraduate degree from the University of Saskatchewan, I agree that the Libraries of this University may make it freely available for inspection. I further agree that permission for copying of this thesis in any manner, in whole or in part, for scholarly purposes may be granted by the professor or professors who supervised my thesis work or, in their absence, by the Chair of the Division or the Dean of the College in which my thesis work was done. It is understood that any copying or publication or use of this thesis or parts thereof for financial gain shall not be allowed without my written permission. It is also understood that due recognition shall be given to me and to the University of Saskatchewan in any scholarly use which may be made of any material in my thesis.

Requests for permission to copy or to make other use of material in this thesis in whole or part should be addressed to:

Head of the Department of Mechanical Engineering

University of Saskatchewan

Saskatoon, Saskatchewan CANADA S7N 5A9

ABSTRACT

Strain detecting with carbon nanotube (CNT) networks is one of the encouraging findings in sensor technologies. Two types of CNT based films are available for strain detection, namely CNT composite films and CNT films. Configurations of the CNT networks in these films can be made into random and aligned distributions. Understanding of fundamental knowledge regarding piezoresistive response in CNT networks in particular of the CNT film is not quite available, and this is the motivation of the present thesis.

In this thesis, piezoresistive response of CNT networks under in-plane straining was studies in details first. Based on the stick percolation model, the relation between the density and conductance in CNT networks (with randomly distributed) was established and then the models which describe the relation between the density and piezoresistive sensitivity and the relation between density and piezoresistive linearity, respectively, were developed. After that, fabrication of CNT networks with aligned distributions was studied. Likewise, the models as developed for CNT network with random distributions were developed for ones with aligned distributions. Finally, modeling of the stress transfer between the nanotubes and polymer matrix was studied.

This study has led to the following conclusions: (1) piezoresistive response in CNT networks of the CNT film follows the stick percolation model with the critical exponent coefficient (α) in the model being 1.938; (2) it is feasible to fabricate aligned CNT networks of varying densities with the technique which combines the spray deposition and externally applied magnetic field; (3) the configuration of CNT networks, in addition

to their density, was a primary factor governing their piezoresistive response; (4) slipping occurs at the interface between the nanotube and polymer matrix when the films are subject to in-plane straining.

The contributions of this study are: (1) the knowledge along with a percolation model for piezoresistive response of CNT networks of the CNT film, (2) a fabrication technique to align CNT networks of the CNT film, and (3) the knowledge along with a model for interaction between the CNT and polymer substrate in the CNT film.

ACKNOWLEDGMENTS

I would like to take this opportunity to express my appreciation to my supervisors, Prof. W. J. Zhang, Prof. Q. Q. Yang and Dr. R. Sammynaiken, whose encouragement, support, expertise, and guidance led me to complete this thesis. Their enthusiasm and dedication to this research have greatly influenced and inspired me.

I would like to thank the support from the Saskatchewan Structural Sciences Centre (SSSC), particularly Mr. J. Maley and Dr G. Schatte, who gave me guidance and advice for synthesis process; material characterization and for their participation in the experiments.

I would like to give thanks to Prof. Dolovich from the Department of Mechanical Engineer, who has given me guidance and advice in the field of solid mechanics and Finite Element Analysis (FEA).

I also would like to give thanks to Mr. Hans-Jürgen Steinmetz from the Material Test Laboratory for giving my advice for the tensile experiment set-up and providing me the testing materials. I am grateful to the staff at Engineering Workshop at the University of Saskatchewan, who has helped me design and fabricate research instruments and samples used in my studies.

I would like to extend my appreciation to Mr. R. Peace from the Department of Mechanical Engineering and Dr. G.S. Liu from the Department of Biology for their guidance and valuable suggestion on the micro/nano-scopic scanning.

Finally, this research has been financially supported by NSERC through the discovery grant and Canadian Research Chair program and SHRF through a Phase I project grant (BioNEMS), and these supports are acknowledged.

DEDICATED TO

My family

Thank you for encouraging me in all of my pursuits

And for teaching me that the engagement of life is to learn, to understand yourself and to be happy

TABLE OF CONTENTS

LIST OF FIGURES

LIST OF TABLES

LIST OF ACRONYMS

AFM:	Atomic Force Microscope
CNT:	Carbon Nanotube
CVD:	Chemical Vaper Deposition
DEG:	Diethylene Glycol
EPR:	Electron Paramagnetic Resonance
GF:	Gauge Factor
IR:	Infrared (IR) absorption
LFD:	Laminar Flow Deposition
LBL:	Layer-by-Layer
MRI:	Magnetic Resonance Imaging
MMS:	Molecular Mechanical Simulation
MWNT:	Multi-Walled Nanotube
DMF:	N-Dimethylformamide
PMMA:	Poly (methyl methacrylate)
PDMS:	Polydimethylsiloxane
PSS:	Poly (sodium 4-styrenesulfonate)
PVA:	Polyvinyl alcohol
PET:	Polyethylene Terephthalate

PVC:	Polyvinyl Chloride
SEM:	Scanning Electron Microscope
SHM:	Structural Health Monitoring
SWNT:	Single-Walled Nanotubes
SDS:	Sodium Dodecyl Sulfate
TEM:	Transmission Electron Microscopy
VDW:	Van der Waals

CHAPTER 1

INTRODUCTION

1.1 Background

1.1.1 Electrical Based Strain Gauge: Macroscale and Nanoscale Thin Film

Strain gauges, also known as strain sensors, are one of the most common devices used for the Structural Health Monitoring (SHM) system. Fundamentally, all strain gauges are designed to convert a mechanical deformation into an electrical signal, which is further processed in the SHM system. In electrical based strain gauges, the strain is measured as a function of resistance change due to the displacement change of a gauge. Mladenvic et al. (1998) mentioned: "The discovery of the basic principle of such gauges dates back to 1856; Lord Kelvin reported that certain metallic conductors exhibited the change in their electrical resistance after subjected to a mechanical straining." This property was referred to as piezoresistive response, as shown in Figure 1.1. More importantly, this change in resistance is linearly proportional to the amount of strains in the material. Piezoresistive sensitivity is defined as the ratio of the resistance change over the strain, and it is also called gauge factor (GF). GF can be found by equation 1.1.

$$GF = \frac{\Delta R/R}{\Delta L/L} = \frac{\Delta R/R}{\varepsilon} \tag{1.1}$$

where ε is the strain; R is the resistance of material; ΔR is the changes in resistance.

Figure 1.1 Schematic model of piezoresistive response in the material

Various types of electrical based strain gauges have been developed over years. As a type of the electrical based strain gauge, nanoscale thin films exhibit great potential in strain measurements and particularly as neuron sensor which can be attached onto the surface of a structure to form a sensor network (Kang et al., 2002). Compared with conventional strain gauges, the nanoscale thin film sensor provides several benefits in strain detections, such as film flexibility; ease of processing; and installation.

Initial developments in nanoscale thin films were focused on conductive polymer composites that contain polymeric matrix and conductive filler materials. In general, conductance of the films can be tuned by introduction of conductive filler materials, such as carbon black (Cochrane et al., 2010), carbon fibers (Feller et al., 2002). During strain measurements, changes in resistance of thin films are only due to conductive filler materials (note: polymeric matrix is insulator material). However, the idea of the conductive polymer composite as aforementioned requires a high concentration of filler materials to form a conductive network, and this may affect the mechanical properties of an entire film (Liu et al., 2009). Nanoscale conductive fillers are certainly a trade-off solution to this problem.

Carbon nanotubes (CNTs), a type of nanoscale materials, were published in 1991 by Iijima et al. (1991). CNTs are considered to be an excellent filler material in the conductive polymer films. It is known (Dresselhaus et al., 2004) that the diameter of CNTs ranges from 0.7 to 10.0 nm and aspect ratio (L/D, L: Length of CNT; D: Diameter of CNT) ranges from 10^4 -10^5. Further, there are two types of CNTs: Single Wall Nanotubes (SWNTs) and Multi Wall Nanotubes (MWNTs). More importantly, their high L/D ratio and excellent electronic properties allow conductive networks to be formed with low threshold concentration in the film (Peijs et al., 2009). In addition, their nanoscale size allows for fabricating small films with high gauge factor and for optimizing the films with an improved performance.

Two types of thin films with CNTs have been developed for strain measurements so far, namely CNT composite films and CNT films. The major difference between them is that CNT networks free of surfactant are distributed on a polymeric matrix in CNT films, while CNT networks in CNT composite films are embedded with polymeric surfactants. The basic fabrication methods for both types of films will be discussed below.

1.1.2 Fabrication of CNT Composite Films

The first CNT composite films applied as strain gauge were fabricated and named as buckypaper by Dharap et al. (2004). In their fabrication process, CNTs (SWNTs) were first dispersed in the N-Dimethylformamide (DMF) solution. Then, the CNT/DMF solution was poured gently through a filter paper, and the paper was dried in a vacuum

oven to slowly evaporate the solvent. Finally, the free standing CNT/DMF composite film was peeled off, as shown in Figure 1.2. In such films, CNT networks are randomly distributed and interacted with polymeric surfactant (DMF) through the physical bondings. Under the in-plane straining, the film exhibited linear changes in its resistance to the applied strain. Because of the insulator property of DMF polymers, Dharap et al. (2004) further believed that the changes in resistance of the film are due to CNTs.

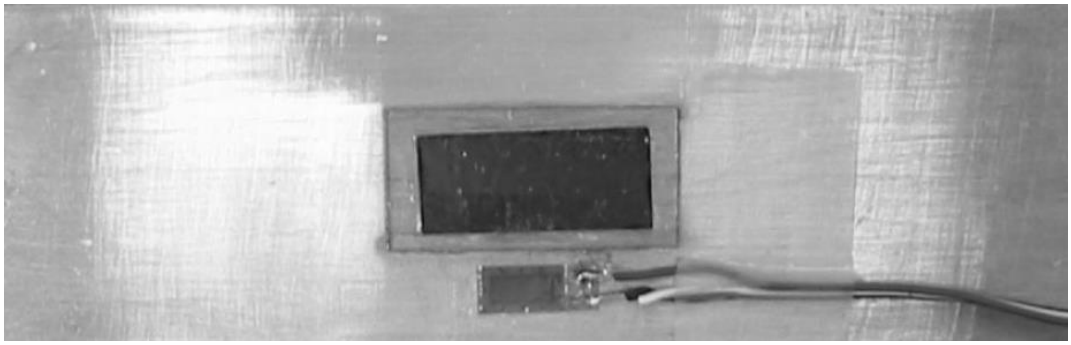

Figure 1.2 The buckypaper with insulating PVC attached to the structure, and a traditional strain gauge attached next to the film (Dharap et al., 2004)

In general, the fabrication of CNT composite films requires the use of surfactants to improve dispersion of CNTs in aqueous solutions. The suspensions were then filtered through a membrane under pressure (vacuum) to yield thin films or to evaporate (in oven) the solvent to yield thin films. Other methods to fabricate CNT composite films, constructed from both SWNTs and MWNTs, have been proposed in recent years, including Mechanical Stirring Fabrication by Thostenson et al. (2006), Molding Transfer Fabrication by Liu et al. (2009), Layer-by-Layer Fabrication by (Lynch et al., 2008).

1.1.3 Fabrication of CNT Films

The CNT films constructed from CNT networks free of surfactants were first presented by Kaempgen et al. (2005). In their fabrication methods, the following steps were followed. First, CNTs (SWNTs) were dispersed in aqueous Sodium Dodecyl Sulfate (SDS). Second, the CNT/SDS suspension was deposited on a polymeric substrate during the coating process. Third, the film was dipped into distilled water to rinse off the SDS surfactant. Consequently, the CNT networks resided on the substrate owing to the hydrophobic properties of CNTs and strong adhesion between CNTs and the polymer substrate.

As compared with the CNT composite films, the CNT films exhibit a higher conductance (owing to the absence of polymeric surfactant) and have a lower threshold concentration. As shown in Figure 1.3, CNT films usually are transparent films due to the low concentration of CNTs. In the studies by Miao et al. (2010), they discovered that CNT films constructed with the Layer-by-Layer deposition method had good piezoresistive sensitivity as a strain gauge. Under the in-plane straining, their results have shown that the films maintain a linear behavior between their resistance and the applied strain up to the 0.8 strain. In addition, the applications of CNT films have been proposed in numerous reports, such as transistors (Gruner et al., 2005); touch panel (Hecht et al., 2007) and pH sensors (Kaempgen et al., 2006).

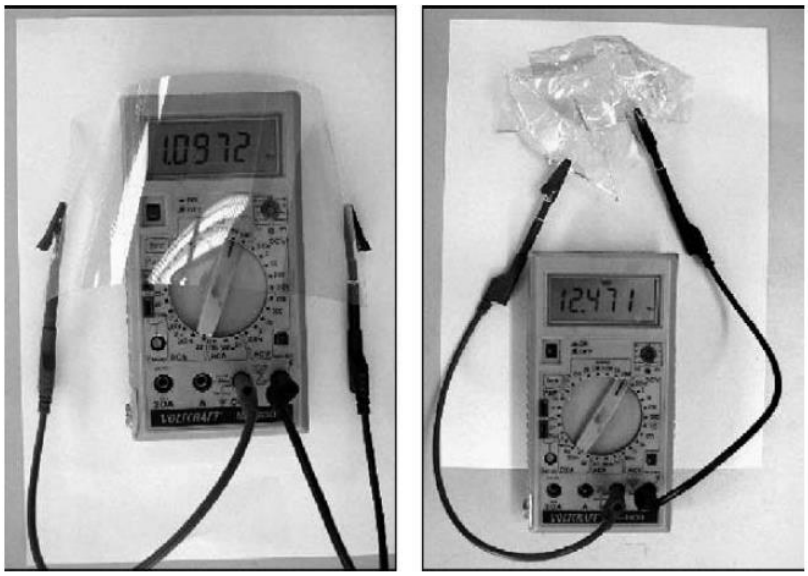

Figure 1.3 Flexible transparent CNT film: CNT deposited on a polymeric substrate (Kaempgen et al., 2005)

In the fabrication of CNT films, the substrate surface in general requires to be pre-treated to enhance its adhesion for bonding with CNTs. In addition, the aforementioned fabrication methods are only limited to the CNT films constructed from SWNTs.

1.1.4 Chemical Vapor Deposition (CVD) Fabrication

In the study by Yong et al. (2003), the CNTs were synthesized by hot filament CVD with mixed catalysts Ni and Fe and perpendicularly grown on the Ni/Fe/Si substrate, as shown in Figure 1.4. The film was loaded under a three-point test device for strain measurements and yielded gauge factor 60 up to 500 microstrains. Different from the aforementioned CNT based films, the film fabricated by the CVD method function as a strain sensor based on the principle called “band gap” of individual tubes. The films

based on this principle have a high gauge factor, but such films are difficult to fabricate (compared with deposition method), install and highly sensitive to the temperature.

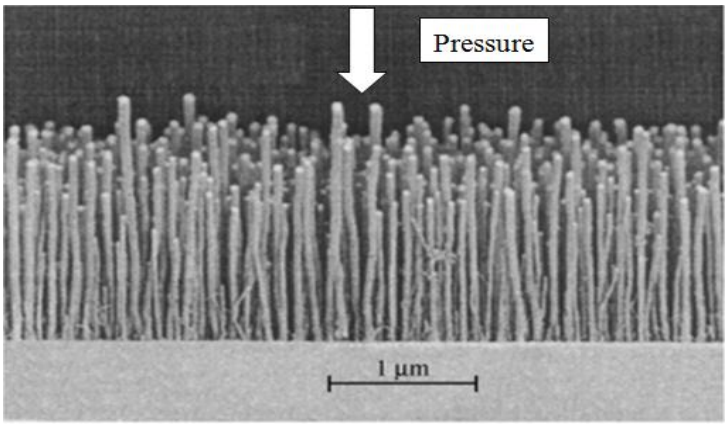

Figure 1.4 Scanning Electron Microscopy (SEM) micrographs of CNTs grown perpendicularly on the substrate (Yong et al., 2003)

1.2 Research Motivation and Objectives

In our previous studies (Miao et al., 2010), CNT films made by the deposition method yielded randomly distributed CNT networks on polymer substrates. More importantly the piezoresistive response in such CNT films was found and optimized with a specific of density of CNTs. Hecht et al. (2004) proposed that in CNT networks, the nanotubes, including metallic and semiconductive tubes, be considered as randomly distributed conducting sticks, and the networks be modeled by the stick model used in the percolation theory. As results, it was expected that piezoresistive response of CNT networks can be modeled based on the percolation theory.

In both CNT film and CNT composite film, numerous studies have reported the existence of piezoresistive response in randomly distributed CNT networks (Chapter 2). However, few (if none) have studied piezoresistive response in aligned CNT networks. It was hypothesized that piezoresistive response also exists in the aligned CNT networks and it should have an improved quality as opposed to randomly distributed CNT networks.

In CNT composite films, nanotubes were completely embedded in the polymer matrix. Under the in-plane straining, several models have been established to study the stress transition between the nanotubes and polymer matrix. Compared with CNT composite films, the nanotubes in CNT films were considered to be partially (if not completely) embedded in the polymer matrix. As a result, it was expected that the nanotubes in CNT films would experience the axial stress through the interfacial cohesion, instead of external pressure from the surrounding polymer matrix (Wagner et al. 1998).

From the aforementioned discussion, this thesis study defined three specific objectives, and they are stated as follows:

(1) To verify whether the relation between the conductance and density in randomly distributed CNT networks follows the stick percolation model and (if this does) then to model the peizoreostive response in CNT networks.

(2) To fabricate CNT films with aligned CNT networks and to investigate their piezoresistive response.

(3) To study the interaction of CNTs with the polymer matrix in CNT films as under in-plane straining.

1.3 Organization of the Thesis

This thesis comprises of 8 chapters:

Chapter 1 gives an introduction to this thesis research, necessary background, research motivations and research objectives.

Chapter 2 presents a literature review of modelling of piezoresistive response in CNT based films for strain detection. This review will outline some important concepts and results in the current literature regarding piezoresistive response in CNT networks; including band gap theory, percolation theory, and influence of the density of CNT networks on gauge factors. More importantly, several modelling approaches will be introduced which attempt to establish the relation between the density and conductance in randomly distributed CNT networks. The discrepancies between the theoretical and experimental results will also be discussed in this chapter. The goal of this review was to make a critical assessment of these experimental results/methods and to justify the choice of the percolation theory as the most suitable approach for modeling piezoresistive response in CNT networks in this thesis study.

Chapter 3 presents a literature review on fabrication techniques for the films with aligned CNT networks. This review will outline some important techniques to align CNT networks under various externally applied forces, including air flow, mechanical force,

and magnetic force. In addition, several methods related to decoration of CNTs with nanoparticles will also be discussed. The goal of this review was to make a critical assessment of the methods in the current literature and to justify the choice of the magnetic field with the aid of magnetic nanoparticles as the most suitable approach for aligning CNT networks in this thesis study.

Chapter 4 presents a literature review of knowledge of physical interaction of CNTs with the polymer matrix in CNT based films. This review will outline several methods and models in the current literature for estimating stress transfer between the CNT and polymer matrix in the films, including Molecular Mechanical Simulation (MMS) method, TEM fragmentation method, Raman Induced D Band method. The goal of this review was to make a critical assessment of the existing methods/models and to justify the choice of Raman Induced D Band method as the most suitable approach for understanding interactions of CNTs with the polymer matrix in this thesis study.

Chapter 5 presents the model of piezoresistive response in CNT films with randomly distributed CNT networks. In this chapter, fabrication of CNT films with randomly distributed CNT networks by the Layer-by-Layer deposition method will be discussed. The density and conductance in randomly distributed CNT networks were determined by Raman Microscopy and Two Probe measurement, respectively. The relation between the density and conductance in such CNT networks were thus established by following the stick percolation model. Finally, theoretical models are presented to describe the

relationship between the density of CNTs and gauge factor and the relationship between the density of CNTs and linearity in CNT networks.

Chapter 6 presents a study of piezoresistive response in CNT films with aligned CNT networks. In this study, CNTs were first decorated with iron oxide nanoparticles (enhancing the magnetic property) after the acid treatment and sol-gel process. With the enhanced magnetism, the CNTs decorated with iron oxide nanoparticles were aligned along with the direction of an externally applied magnetic field to form aligned CNT networks on the polymer substrate. The CNT films with aligned CNT networks were further investigated under two probe measurements and in-plane straining.

Chapter 7 presents a study of interaction of CNTs with the polymer matrix in CNT films under in-plane straining. In this study, the Raman Microscopy was employed to study the axial strain on the nanotube, which was transformed from the surrounding polymeric matrix. When the CNT film was under the in-plane straining (tensile strain applied on the polymeric matrix), it was found that the D band* wavenumber peak of CNTs shifted linearly with the applied strain. Based on the experimental results, a model was established to describe the stress transfer between the CNT and polymeric matrix during in-plane straining. In CNT films, it was found that the interfacial slipping between the nanotube and polymeric matrix happens along with the in-plane straining. The mechanism which explains the interaction was explored with the mode.

CHAPTER 2

MODELLING OF CNT BASED THIN FILMS: LITERATURE REVIEW

2.1 Piezoresistive Response Based on Band Gap of Individual Nanotubes

An experiment conducted by Tombler et al. (2000) has shown that conductance of the a single nanotube decreases when it is strained; in particular Figure 2.1 gives a schematic diagram of their experiment where a SWNT is strained by impressing a force with an Atomic Force Microscope (AFM) tip at its middle location. Further, they believed that when a single nanotube is strained, the local distortion of band gap occurs, which is the cause of the drop in conductance.

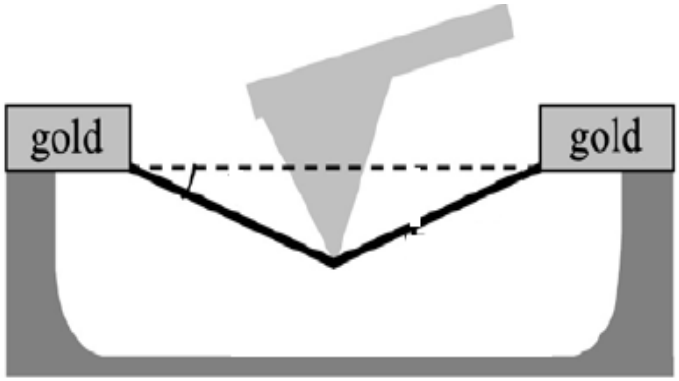

Figure 2.1 Schematic model of an AFM needle pushing down a SWNT to detect voltage changes on gold pads (Tombler et al., 2000)

Many studies of the band gap theory for piezoresistive response of CNTs have been made in literature. Minot et al. (2003) presented measurements to demonstrate the effects of strain on the band structure of the tube and further predicted the rate of change of band gap with respect to strain. In the study by Yang et al. (2007), they developed a

mathematical model to describe the relation between band gap and applied strain, which is as follows:

$$R_{tot}(\varepsilon) = R_S + \frac{1}{|t|^2}\frac{h}{8e^2}\left[1+\exp\left(\frac{E_g}{kT}\right)\right] \tag{2.1}$$

$$E_g = E_g^0 + \frac{dE_g}{d\varepsilon}\varepsilon \tag{2.2}$$

$$R_{tot}(0) = R_S + \frac{1}{|t|^2}\frac{h}{8e^2}\left[1+\exp(\frac{E_g^0}{kT})\right] \tag{2.3}$$

where ε is applied strain, t is 0.5, h is Plank's constant, k is $1.38\text{x}10^{-23}$j/k, e is $1.6\text{x}10^{-19}$C, T is laboratory temperature (300K) and R_s is negligible. More importantly, they further calculated the gage factor by using equation 2.4 and their results were listed in Table 2.1.

$$GF = \frac{\Delta R/R}{\varepsilon} = \frac{[R_{tot} - R_{tot}(0)]/R_{tot}(0)}{\varepsilon} \tag{2.4}$$

where R_{tot} is the current resistance of CNTs, R_{tot} (0) is the original resistance of CNTs.

Table 2.1 Model predicted parameters for three different kinds of CNTs (Yang et al., 2007)

	Metallic-CNT	Semiconductor-CNT	SGS-CNT
E_g (meV)	0	160	40.5
$dE_g/d\varepsilon$ (meV/%)	35	-53	180

2.2 Piezoresistive Response of CNT Networks

CNT networks with piezoresistive response were first reported by Dharap et al. (2004) in CNT/DMF composite films. They further proposed that piezoresistive response was only due to CNTs because the polymer was an insulator. Lynch et al (2007) concluded that piezoresistive response in CNT based films was due to the change of CNT network configurations within the polymer matrix. Their reasoning follows some important findings on CNT networks by others, including Liao et al. (2001), Wagner et al. (1998), Salvetat et al. (1999) and Ajayan et al. (2000). In particular, Liao et al. (2001) showed that the bonding between CNTs and polymeric matrix was based on Van der Waals (VDW) force and/or the electrostatic in the films. According to the highest shear stress, about 500 MPa at the interface between SWNT and polymeric matrix (polyurethane) was reported by Wagner et al. (1998). The effective elastic modulus for SWNTs (MWNTs) was around 1 ~ 3 TPa (0.1 ~1TPa) according to Salvetat et al. (1999). Therefore, the nanotube displaces with the polymeric matrix as the film is under in-plane straining according to Ajayan et al. (2000). Further, one can infer that the topology and density of CNT networks would have significant effects on piezoresistive response of CNT base films.

2.2.1 Optimizing Piezoresistive Response of CNT networks based Films

In CNT network based films, there have been studies in optimizing the films for an improved piezoresistive response in literature. Kang et al. (2002) reported that the gauge factor of the CNT/DMF/Poly (methyl methacrylate) (PMMA) films is highly related to the density of CNT networks. In particular, the gauge factor decreased from 5 to 1 when

the weight percentage of CNTs in their fabrication process increased from 0.5% to 10%. In addition, they also reported that the resistance of the films decreased dramatically with the increase of weigh percentage of CNTs. Liu et al. (2009) reported that the gauge factor of the CNT/Polydimethylsiloxane (PDMS) film varied from 0.01 to 1.25 when the suspension volume of CNTs varies from 5 ml to 80 ml. Using the Layer-By-Layer (LBL) fabrication method, Lynch et al. (2008) reported that the CNT/ Poly (sodium 4-styrenesulfonate) (PSS)/ Polyvinyl alcohol (PVA) film (multilayered) exhibited variation in its gauge factor from 0.1 to 1.8 when the number of layers varied from 50 to 100 and the concentration of CNT suspension varied 0.5mg/ml to 0.8mg/ml. Using the LBL fabrication method, Miao et al. (2011) reported that the gauge factor of CNT films (multilayered) decreases from 4 to 1 with the increase of the number of layers.

It is noted that the change of gauge factor may also happen with the change of distribution of microscale conductive fillers in films. Martinez et al. (2010) reported that the highest gauge factor was achieved in the lowest density of the carbon black (as conductive filler) in their polymer composite films.

2.2.2 Percolation and Conductance

Percolation theory was first introduced by Broaden et al. (1957) to model the behavior of connected clusters in a random graph. Later, the theory was extended to model transport in amorphous and porous media and composites and to model the properties of polymers, gels, and ionic conductors (Bunde et al., 2000). According to Bunde et al. (1996), in percolation theory, the important concept is the so-called percolation threshold (N_c)

which is related the density (N) that a particular site in a square lattice is occupied or unoccupied (1-N) as shown in Figure 2.2; the occupied and unoccupied sites may have different physical properties. For instance, occupied sites may be electrical conductors, while unoccupied sites may be insulators where electrical current can only flow between nearest-neighbor conductor sites (Liang et al., 1998).

Further according to Bunde et al. (1996), when density N is smaller than critical density N_c (N_c =0.59 in this case) as shown in Figure 2.2a, the conducting sites are either isolated or form small clusters, but the clusters are isolated to each other and therefore, the lattice is an insulator (because there is no unbroken conducting path from the top to bottom of the lattice). When N is larger than N_c as shown in Figure 2.2c, many conducting paths are formed from top to bottom, where the currents can flow through, and the lattice is thus a conductor. Therefore, there must be a so-called critical density N_c as shown in Figure 2.2b, above which the current can follow from the top to bottom side at the first time. They further suggested the relation between the conductivity (P) and the density (N) of the square lattice as: $P\sim (N-N_c)^{\alpha}$, where α is the critical exponent parameter which depends on different application systems.

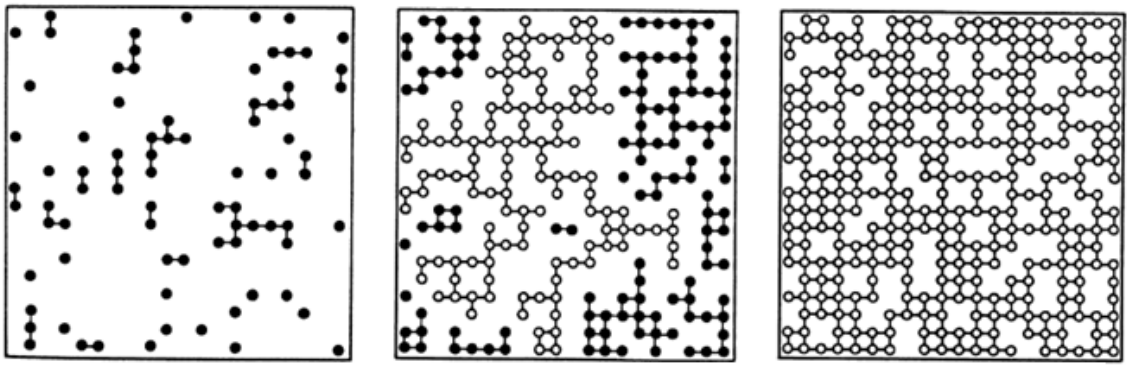

Figure 2.2 Site percolation on the square lattice: the small circles represent the occupied site for three different concentrations: N=0.2, 0.59 and 0.8. Nearest-neighbor cluster sites are connected by lines representing the current paths. Filled circle are used for broken (finite) clusters, while open circles mark the unbroken (infinite) cluster (Available online: http://www.uni-giessen.de/physik/theorie/theorie3/publications/Intro_bunde1.pdf)

The percolation threshold N_c and parameters α depend on details of a percolation model, including the dimension and the shape of the lattice (Pike et al., 1975). For different models, the Monte Carlo simulation can be performed to determine N_c and α. For instance, Pike et al. (1975) used the Monte Carlo simulation to classify many different percolation models in two and three dimensions, which include circle model, sphere model (three dimension), square model and stick model. In the stick model, they further proposed that conductivity P is proportional to the site densities N and critical density N_c as: $P\sim (N-Nc)^{\alpha}$, where α is equal to 1.33 in a two dimensional region and 1.94 in a three dimensional region and the critical density N_c (percolation threshold: the first conductive path formed in networks) is determined by the length (L) of the stick as: $\sqrt[L]{\pi N c}=4.236$. Following the study of Pike et al. (1975), Li et al. (2009) developed a high-efficiency

algorithm for the Monte Carlo simulation to investigate the stick percolation model (Figure 2.3), which is consistent with, but more precise than, the result from Pike et al. (1975).

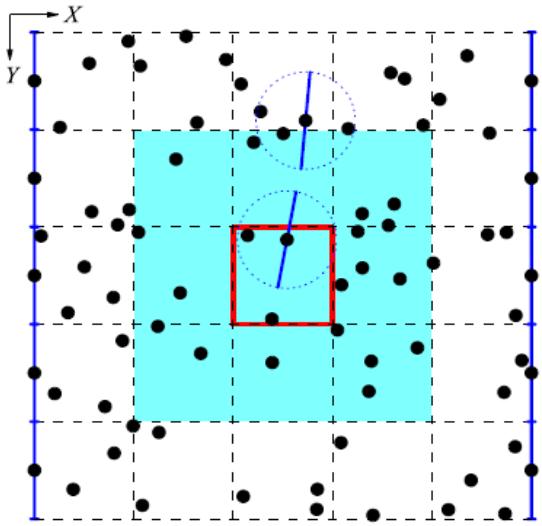

Figure 2.3 Schematic illustration of stick percolation on a square system (L=5). Each stick is of unity length l=1 and are presented here only by their centers (filled circles). The two boundaries (the left and right ones) are described also by L connecting stick (Li et al., 2009)

2.2.3 Percolation and Conductance in Randomly Distributed CNT Networks

In CNT networks, Hecht et al. (2004) proposed that the nanotubes can be considered as conducting sticks and appear randomly oriented with no preferential directions, which is analogous to the stick model in the percolation theory.

2.2.3.1 Influence of Tube-to-Tube Contact on Percolation and Conductance

In CNT networks, Straderman et al. (2004) proposed that the conductance of the tube to tube contacts dominates the overall conductance in the network. In their studies, CNT networks were formed between two golden electrodes on the silicon substrate. By varying the separation lengths of electrodes, their two-probe measurements have shown that the conductance of CNT networks does not decrease linearly with the distance from the electrodes. In addition, CNT networks contained both metallic and semiconducting sticks where Schottky Barrier can present between their interconnections, which can further affect their conductive path and thus conductance in CNT networks (Straderman et al., 2004).

2.2.3.2 Influence of the Tube Length on Percolation and Conductance

Hecht et al. (2006) reported that the sonication hours can severely affects the size of CNTs and CNT bundles during the dispersion process. In particular, the average length of tubes decreased with the increase of sonication time. They subsequently fabricated a series of CNT networks under the same density but with different average length of the nanotubes. Based on the experimental results, they further derived the model of $\sigma \sim L^{1.46}$ as shown in Figure 2.4, which represents the relation between the conductance (σ) and the average length of nanotubes (L) in CNT networks. According to their model, it can be seen that the increased length of tubes can lower the threshold concentration (critical density) in CNT networks.

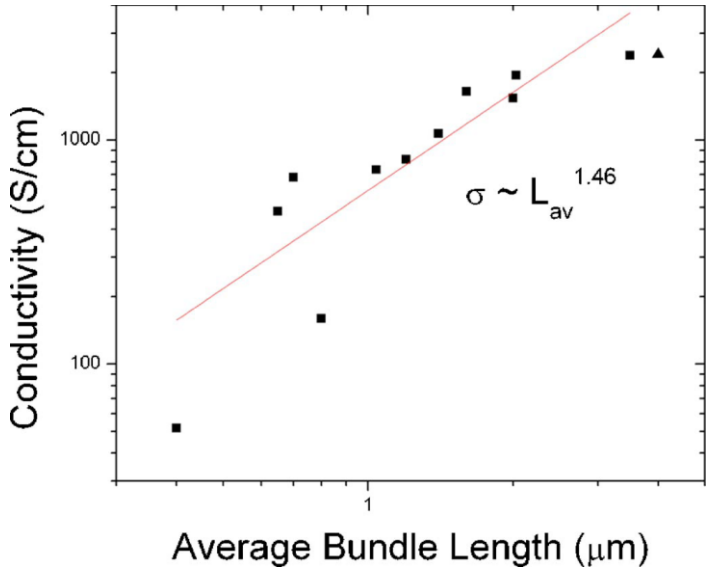

Figure 2.4 DC conductivity of CNT networks vs. average bundle length in the network (Hetch et al., 2006)

2.2.3.3 Influence of CNT Density on Percolation and Conductance

Hecht et al. (2004) established a relation between the conductance and the density in CNT networks. In their experiments, uniform CNT networks with varying densities were deposited on the thin aluminum plate at room temperature by the vacuum filtration method, as shown in Figure 2.5, and the density of CNT networks was controlled by varying the volume of solution, where the critical density is the critical volume value of 6 ml. They further performed two-probe measurement on the film. Based on the measurements as shown in Figure 2.6, they found that $\alpha = 1.5$, which is close to, but somewhat higher than the theoretical values (in 2-dimensions, $\alpha = 1.33$, while in 3-dimensions, $\alpha = 1.94$). They suggested that the discrepancies between the theoretical and experimental value be caused by: 1) the CNT networks were not perfectly two

dimensional; 2) the theoretical value was based on the same conducting stick model, while the CNT networks contained both metallic and semiconducting sticks.

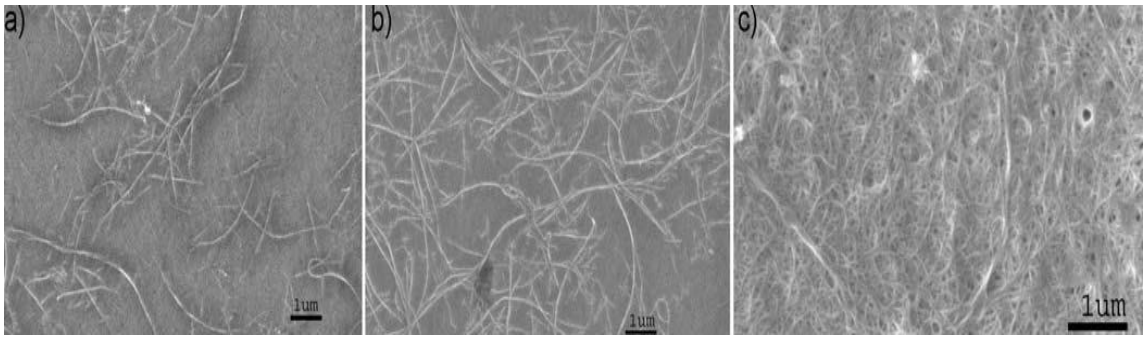

Figure 2.5 SEM images of the SWNT networks on alumina substrates with different filtration volumes: a) 7 ml of SWNT solution b) 10 ml of SWNT solution and c) 400 ml of solution (Hecht et al., 2004)

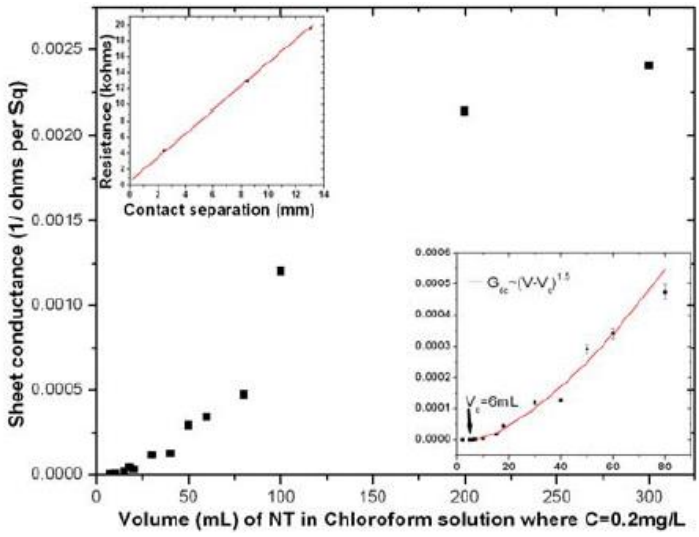

Figure 2.6 Sheet conductance vs. volume of CNTs in Chloroform solution. Notice the onset of conduction when the first percolative path across the sample is formed, indicated by V_c = 6ml on the lower right inset (Hecht et al., 2004)

2.2.3.4 **Influence of the Interface on Percolation and Conductance**

In CNT composite films, the percolation and conductance in CNT networks can be affected by the interface between CNTs and polymeric matrix. Kim et al. (2004) reported that the critical density of CNTs can be reduced by the surface treatment of CNTs. In particular, the CNT/Epoxy composite films exhibited better conductance by oxidizing CNTs (using acid mixture) to improve their dispersion in polymer matrix. Similar results were also reported in the CNT/PET composite films fabricated by Shin et al. (2006). Based on the percolation theory, Xue et al. (2007) proposed a model of the effective electrical conductivity by incorporating the interface effect between nanotubes and polymer matrix. Their results were shown that the percolation threshold of CNT networks decreases with the increased interface thickness

2.2.3.5 Percolation and Conductance in Aligned CNT Networks

In the method proposed by Lay et al. (2009), aligned CNT networks were fabricated by the Laminar Flow Deposition (LFD) method. By varying the number of deposition cycles, various densities of aligned CNT networks were formed. Based on the experimental results, they proposed that the percolation be applicable to such aligned cases with the argument that despite the presence of many aligned CNTs there were sufficient amounts of randomly distributed CNTs in the film, exhibiting the macroscopic conduction to follow the percolation theory. In consistence with their proposal, the conductance and density in aligned CNT networks follow percolation theory as shown in Figure 2.6. The best fit to their data yields an experimentally measured value of $\alpha = 1.8$, which is higher than the theoretical ones (in 2-dimensions, theory predicts $\alpha = 1.33$).

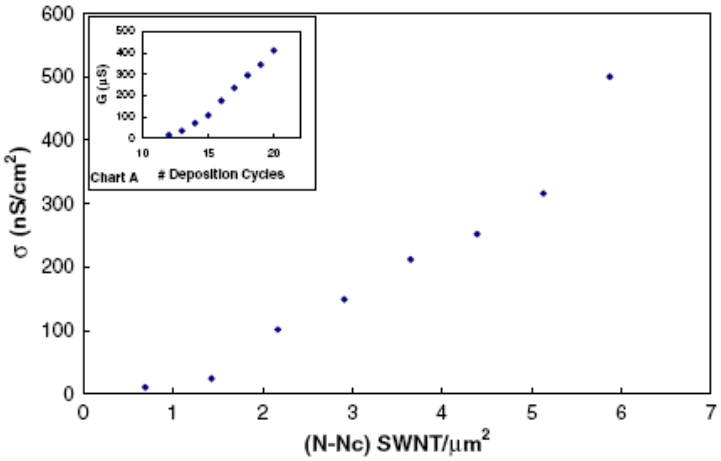

Figure 2.7 Current density versus (N–Nc) for aligned CNT networks; σ is the current density for the network (Lay et al., 2010)

2.3 Summary

(1) The principle that governs piezoresistive response in CNT based films is as this. 1) when individual CNTs were under a load, the local distortion in band gap can cause the conductance change of the tube, which further gives rise to the piezoresistive response in the film. Piezoresistive sensitivity of the film depends on the type of CNTs and varies from 30 to 180; and 2) when CNT networks were under a load, the CNT displacements cause variation of their network configuration and thus change their conductive paths, which gives rise to the piezoresistive response in the film. Piezoresistive sensitivity of the films depends on the density of CNT networks and varies from 0.1 to 5.

(2) In randomly distributed CNT networks, the nanotubes can be considered as conducting sticks and appear oriented with no preferential directions; that is to say piezoresistive response follows the stick model in percolation theory.

CHAPTER 3

FABRICATION OF ALIGNED CNT NETWORKS: LITERATURE REVIEW

3.1 Introduction

In CNT based films, configurations of CNT networks can be divided into random and aligned distributions. The fabrication methods for randomly distributed CNT networks were introduced in the preceding two chapters, including Layer-by-Layer Deposition Method by Miao et al. (2010), Buckypaper Method by Dharap *et al.* (2004) and Filtering Deposition Method by Hetch et al. (2006).

To make aligned CNT networks, there were two essential steps in most available techniques. First, the CNTs were dispersed in solutions where CNTs can easily be rotated relative to the solutions. Second, an external force was imposed to the solutions to rotate CNTs towards one desired direction. The air flow and magnetic force are the common external forces used to rotate CNTs into alignments (discussed in Section 3.2 and 3.3 respectively). In addition, other approaches related to align CNTs have been proposed, such as Melt processing method by Haggenmueller et al. (2000), Electrophoresis method by Yamamoto et al. (1996). The thin films with aligned CNT networks exhibited enhanced thermal, mechanical and electrical properties in many studies, such as the reinforced polymer composites by Shi *et al.* (2005), the enhanced thermal properties by Choi *et al.* (2003).

3.2 Laminar Flow Deposition Method

In the method proposed by Lay et al. (2009), aligned CNT networks were achieved by the Laminar Flow Deposition (LFD) method as shown in Figure 3.1. In their method, CNTs - SDS solution was first added to the substrate to create a thin layer of the suspension. The laminar flow (as a kind of external force) was then applied at a certain angle to the CNTs in suspension, which causes CNTs rotate toward the flow direction (Lay et al., 2009). After the solvent was dried out, the substrate was washed with water to remove any remaining SDS residue. The above process is defined as one deposition and the density in CNT networks thus can be determined by the number of deposition cycles.

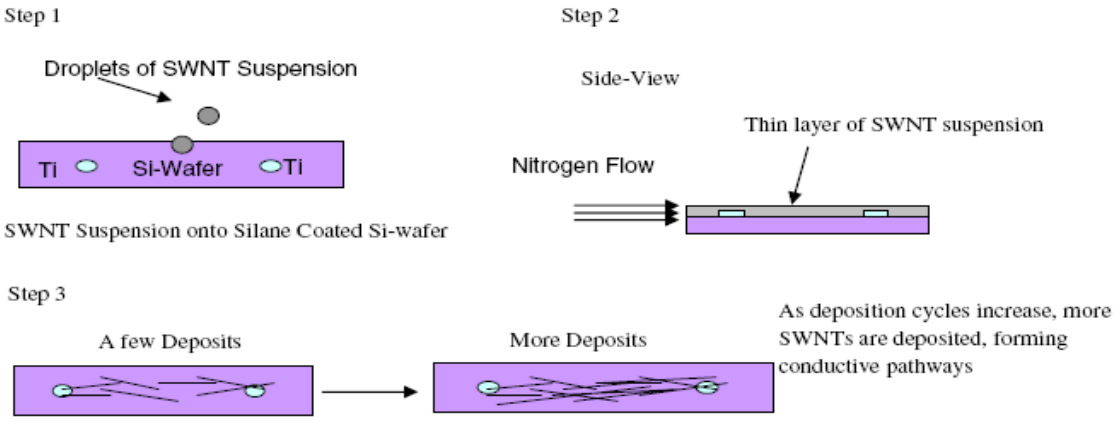

Figure 3.1 Flow chart of flow deposition method used to fabricate aligned CNT networks. Step 1: CNT suspension was drop-cast on a Si wafer, Step 2: Directional nitrogen flow was to evaporate solvent and align SWNTs in a thin layer of the suspension; and Step 3: Repeated deposition cycles were used to increase the network density (Lay et al., 2009)

By varying the number of deposition cycles, different densities of aligned CNT networks were deposited on the Si wafer for the studies of percolation, as shown in Figure 3.2.

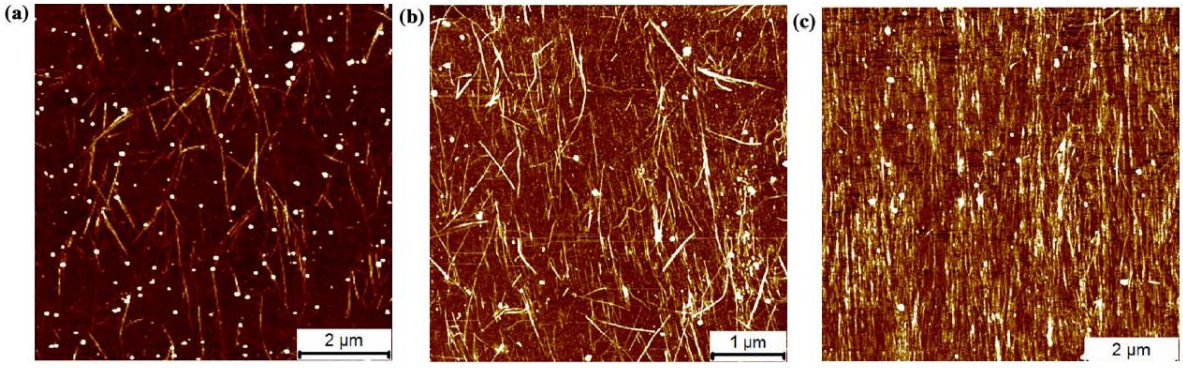

Figure 3.2 AFM Images of aligned SWNT deposits formed via LFD method: (a) after 5, (b) 10, and (c) 15 deposition cycles (Lay et al., 2009)

By using the LFD method, Lay et al. (2009) further proposed a method to fabricate the CNT networks with multi-orientations. In this method, high-purity nitrogen flow were manipulated in two directions, resulting in arrays of CNTs aligned in two directions as shown in Figure 3.3.

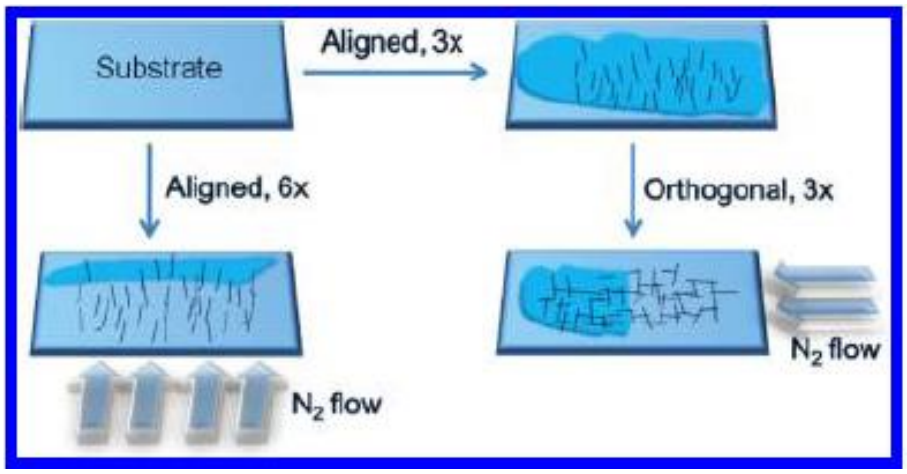

Figure 3.3 Laminar flow deposition (LFD) was used to form two types of macroscopic SWNT networks; "aligned" networks were formed from six successive deposition cycles, whereas "orthogonal" networks were formed from three deposition cycles in one direction, followed by three more at an orthogonal angle (Lay et al., 2010)、

3.3 Magnetic Field Alignment Method

In the method proposed by Tannenbaum et al. (2010), aligned CNT networks were achieved under an externally applied magnetic field. When nanotubes were placed between a pair of magnets, nanotubes in suspensions were oriented parallel to the direction of the externally applied magnetic field (or field line). After the solvent was dried out, the aligned CNT networks were formed on the substrate as shown in Figure 3.4. This method however needs to decorate CNTs with magnetic nanoparticles (Tannenbaum et al., 2010). In the decoration process, various types of magnetic nanoparticles can be used to attach on the nanotubes including iron oxide nanoparticles, Pt nanoparticles, Ag nanoparticles, etc. (discussed in Section 3.3.1 and 3.3.2). With the attached nanoparticles, the magnetic susceptibility of CNTs was improved where nanoparticles imparted

magnetic characteristics to CNTs. In the studies by Tannenbaum et al. (2010), the alignment of CNTs can happen at a low magnetic field (0.3T), because of the magnetization of CNTs through the tethering of maghemite nanoparticles, compared with the alignment of undecorated CNTs under 7T magnetic field (Walters et al., 2001).

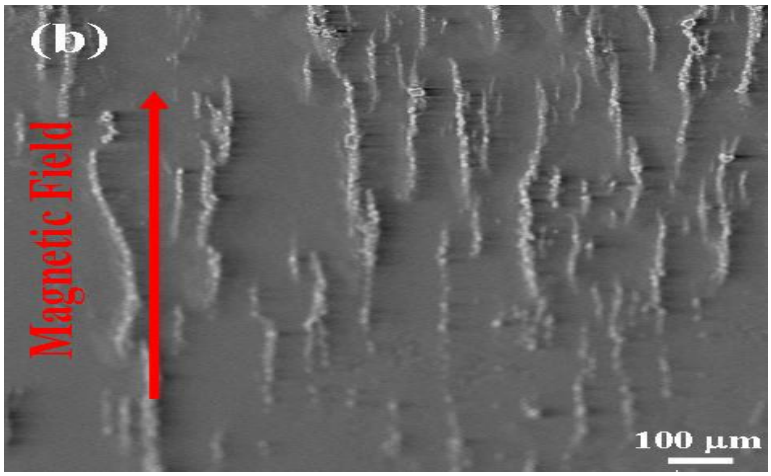

Figure 3.4 Aligned maghemite-CNT (4:1 mass ratio) (Tannenbaum et al., 2010)

3.3.1 Iron oxide nanoparticles

It is well known that iron oxides are one of the most important nanoparticles. Iron oxides have sixteen phases in total, and among them, magnetite Fe_3O_4 and maghemite γ-Fe_2O_3 have excellent magnetic properties. Laurent et al. (2008) described that Oxides of iron are one of the most studied inverse spinel structure where both Fe^{3+} and Fe^{2+} are in the octahedral sites and only Fe^{3+} is in the tetrahedral sites of face-centered cubic oxygen. The cationic site in magnetite is fully occupied whereas maghemite has cation vacancies in the octahedral sites. Characterization of these oxide compounds can be done by X-ray

diffractions, Infrared (IR) absorption spectrometry, Raman Microscopy, Electron Paramagnetic Resonance (EPR), and so forth.

The magnetite and maghemite in nanoscale can be obtained by the various solution-based syntheses, such as the chemical precipitation process of Ali-zade et al. (2009); the Sol-Gel processes of Sugimoto *et al*. (1993); the hydrothermal process of Horner et al. (2009). The studies by Domingo et al. (1994) have shown that the solution-based synthesis with different fabrication factors, such as pH value, concentration of the reactants, temperature, method of mixing, give different characteristics of magnetite and maghemite in the nano range. In the Sol-Gel synthesis by Sugimoto et al. (1993) for instance, α-Fe_2O_3 particles were obtained from $FeCl_3$ solutions in Sodium Hydroxide (NaOH) after aging the gel at100°C for 8 days. In the Sol-Gel synthesis by He et al. (2010), magnetite Fe_3O_4 particles obtained from $FeCl_3$ solutions in NaOH after aging at 220°C for 30mins.

3.3.2 Decorate CNTs with Nanoparticles to Enhance Magnetism

Decoration of CNTs with iron oxide nanoparticles was of interest in obtaining nanotube-nanoparticles composite materials with enhanced magnetic properties. The CNTs decorated with iron oxides are one of the most useful composite materials in nanoscale due to the combined feature of magnetism and CNTs, and they have many applications, such as the bio-manipulations by Li et al. (2006), the alignment networks by Tannenbaum et al. (2010), the Magnetic Resonance Imaging (MRI) by Richard et al. (2008).

Recently, several approaches for attaching iron oxide nanoparticles to the CNTs have been proposed, among which three are most important. In the first approach, CNTs attached with the iron oxide nanoparticles were formed during the process of fabricating CNTs (He et al., 2010). In the studies by Qiu et al. (2006) for instance, CNTs with attached iron oxide were obtained by Chemical Vapor Deposition (CVD) where ferrocene Fe $(C_5H_5)_2$ was used as catalyst as shown in Figure 3.5. In the studies by Jang et al. (2005), CNTs containing iron oxide were obtained by the carbonization process where ferric chloride-embedded ployimide was used as a precursor.

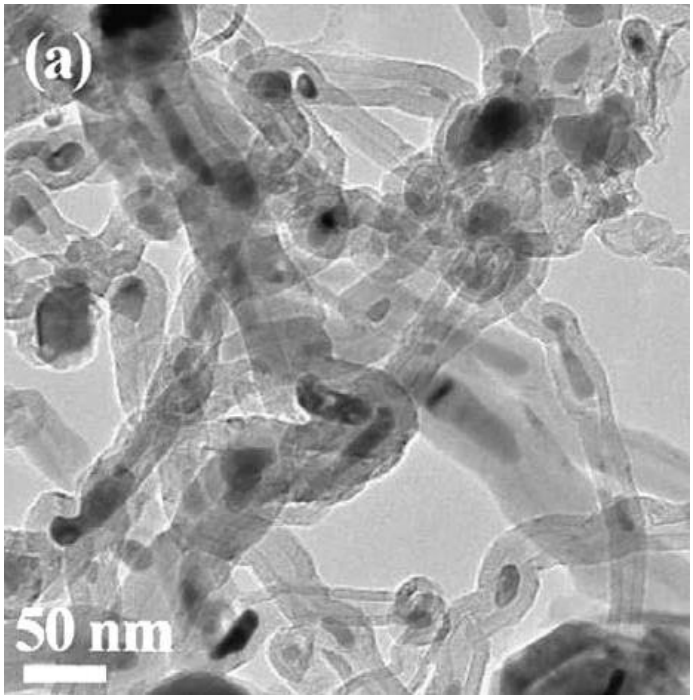

Figure 3.5 TEM images of iron oxide filled CNTs obtained via CVD of coal-gas (Qiu et al., 2006)

In the second approach, iron oxide nanoparticles were attached into the hollow structures of CNTs (He et al., 2011). In the studies by Korneva et al. (2005) for instance, CNTs

(formed on the aluminum template via CVD) were washed through by water-based ferrofluids, resulting iron oxide filled inside of the tubes as shown in Figure 3.6. Other studies also have been proposed to obtain CNTs with filled nanoparticles, such as the Fe_2O_3 filled CNTs by Chen et al. (2006) and Fe_3O_4-filled CNTs by Cao et al. (2007).

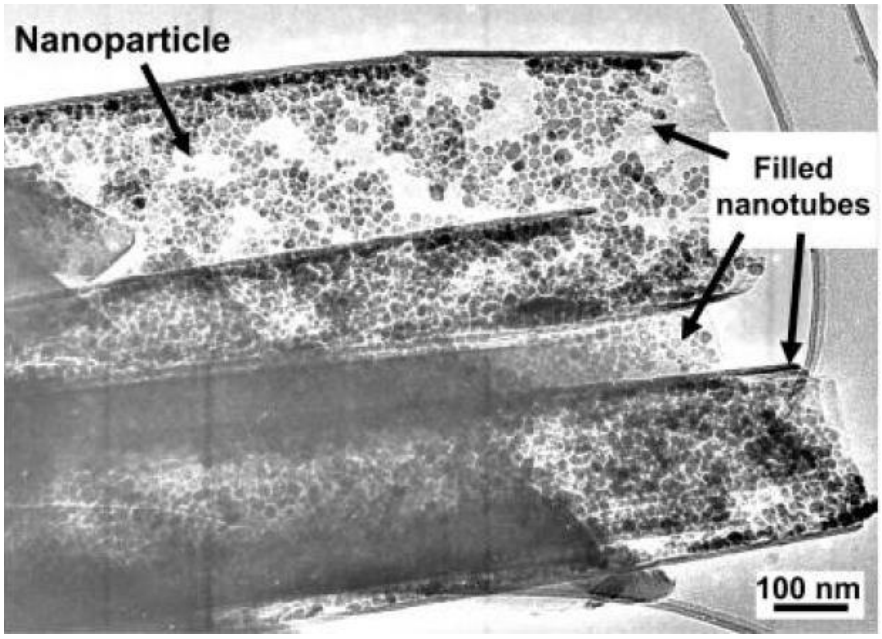

Figure 3.6 TEM images of the inside of CNTs filled with iron oxide nanoparticles (Korneva et al., 2005)

In the third approach, iron oxide nanoparticles were attached onto the outer surfaces of CNTs via covalent or non-covalent links, as shown in Figure 3.7. This method can generally be preceded with two steps. The first step is involved with the CNT functionalization where the functional groups were formed on the surfaces, which further bind iron oxide nanoparticles. Various methods related to functionalize CNTs have been designed, including the polymer wrapping method by Miguel et al. (2005), the ionic

chemistry (doping) method by Niyogi et al. (2002) and the oxidation method (acid treatment) by Zhang et al. (2004). By means of different functionalization methods, different functional groups can be formed on the outer surfaces of CNTs, such as the carboxylic acid group by Tannenbaum et al. (2010), the quinine group by Kuznetsova et al. (2000) and the phenol group by Yu et al. (1998).

The second step is to attach iron oxide nanoparticles onto the surface of CNTs. The procedure used here is similar to the solution-based synthesis method for generating iron oxide nanoparticles as previously discussed

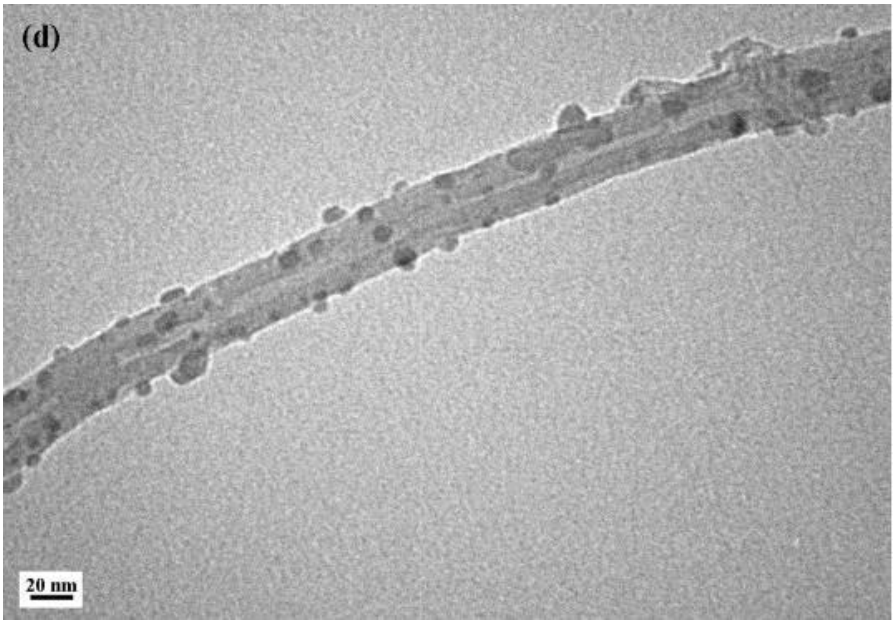

Figure 3.7 TEM image of maghemite-CNT: Fe_3O_4 nanoparticles attached on the outer convex surface of the tube (Tannenbaum et al., 2010)

In addition, the surfaces of CNTs were suitable to bonding with other metal nanoparticles. The studies by Chun et al. (2008) have shown that the CNTs with curved surface changed the π-bonding in the graphene sheets, leading to different electronic structures that further enhance the interaction between CNTs and metal nanoparticles. Many studies related to decoration of CNTs with metal nanoparticles have been conducted, including the CNTs attached with Pt by Kaniyoor et al. (2009), the CNTs attached with Ag by Day et al. (2005), and the CNTs attached with Au by Choi et al. (2002).

3.4 Summary

In this chapter, several methods related to formation of aligned CNT networks and to decoration of CNT with magnetic nanoparticles were reviewed and more specifically:

(1) In CNT based films, configurations of CNT networks can be divided into random and aligned distribution. In order to obtain aligned CNT networks, an external force in general needs to be employed to rotate CNTs in suspension into alignments.

(2) An air flow can be used as an external mechanical force to align CNTs on the substrate. With this method, the density of aligned CNT networks can be controlled by suspension volume and the deposition cycle but the uniformity of aligned CNT networks is difficult to be controlled.

(3) A magnetic force can be used as an external mechanical force to rotate CNTs into alignment. The method, however, requires the decoration of CNTs with magnetic nanoparticles to enhance their magnetic strength of the CNTs.

CHAPTER 4

INTERACTION OF CNT WITH POLYMER MATRIX IN THIN FILMS

4.1 Introduction

In CNT based films, CNT embedded in the polymer matrix may serve as a material to reinforce the strength of the polymer matrix. At the interface between the nanotube and polymer matrix, Liao et al. (2003) suggested that the physical bonding such as Van der Waals interactions, cohesion (polymer chain wrap around the tube), may play an important role on the strength of fiber polymer composites. When the films were subjected to an in-plane straining, there is a significant stress transfer between the polymer matrix and the nanotubes (Frankland et al., 2002). To date, numerous methods have been proposed for describing such stress transfer at the interface, and among them, three are most important: Molecular Mechanical Simulation by Frankland et al. (2002), TEM Fragmentation by Wagner et al.(1998), Raman induced D band microscopy by Young et al. (2001). This chapter provides a review of these three methods.

4.2 Molecular Mechanical Simulation

Frankland et al. (2002) proposed a model which describes the interaction among the nanotube and polymer matrix (crystalline or amorphous) with the Molecular Mechanical Simulation (MMS), and the model is shown in Figure 4.1. The simulation was performed under several different circumstances of nanotubes (different L/D ratio), polymer chain and cross link. The estimated shear stress τ_t was further described by

$$\tau t = \frac{\sigma f D}{L} \quad (4.1)$$

where σ_f is the tensile strength of CNT, D is the diameter of CNT and L is the critical length of CNT. According to the simulation results, the shear stress between CNT and polymer varied from 2.7 to 110MPa depending on shapes of CNTs and types of polymer. It is noted that the MMS results by Lordi et al. (2001) have shown that the shear stress ranges from 18 to 130 MPa. Although the results obtained from MMS methods are based on the simulation, they are an important reference for estimating the interfacial interaction in CNT films, specifically for any new development.

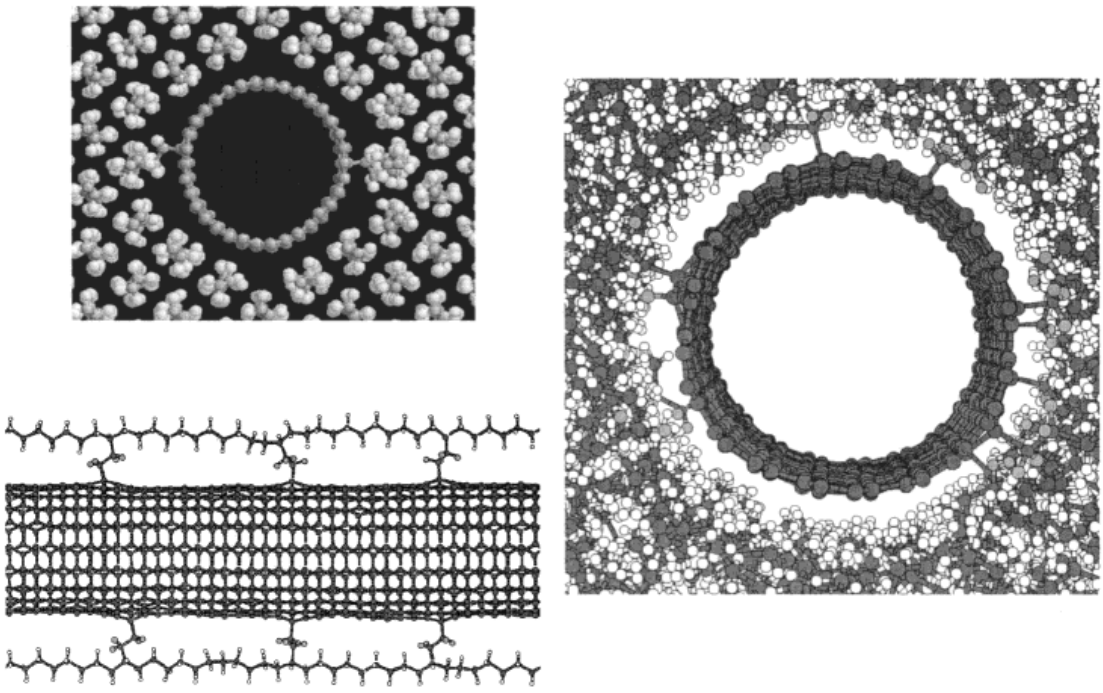

Figure 4.1 Illustration of the cross-linked systems. Left: crystalline matrix. Right: amorphous matrix (Frankland et al., 2002)

4.3 TEM Fragmentation Examination

By applying tensile stress on CNT based films, Wagner et al. (1997) reported an experimental observation of CNT fragmentation. Under the Transmission Electron Microscopy (TEM) scanning, the fragmentation lengths of CNT were measured, as shown in Figure 4.2, and the ratio of fragmentation length (L_c) to the outer diameter (D_c) is about 50. Further, the shear stress can be found by the Kelly and Tyson model in (Kelly et al., 1965):

$$\tau_c = \left(\frac{\sigma_c(L_c)}{2(L_c/D_c)}\right)\left(1 - \frac{{d_c}^2}{{D_c}^2}\right) \tag{4.2}$$

where d_c and D_c are the inner and outer diameters of the tube (respectively), L_c is the length of the tube (fragmentation length in this case), τ_c is the shear stress. They used equation (4.2) to estimate τ_c, resulting in around 500MPa and up (Note: σ_c was taken to be 50GPa as a conservative value). The stress transfer efficiency in the CNT-polymer matrix was shown to be higher than that in the conventional fiber-polymer matrix, approximately more than one order of magnitude (Wagner et al., 1998). However, this method is not applicable to CNT films where shear stress at the interface is comparatively low and thus is more likely to displace the nanotubes with polymer matrix instead of breaking them (see discussion later in section 7.3).

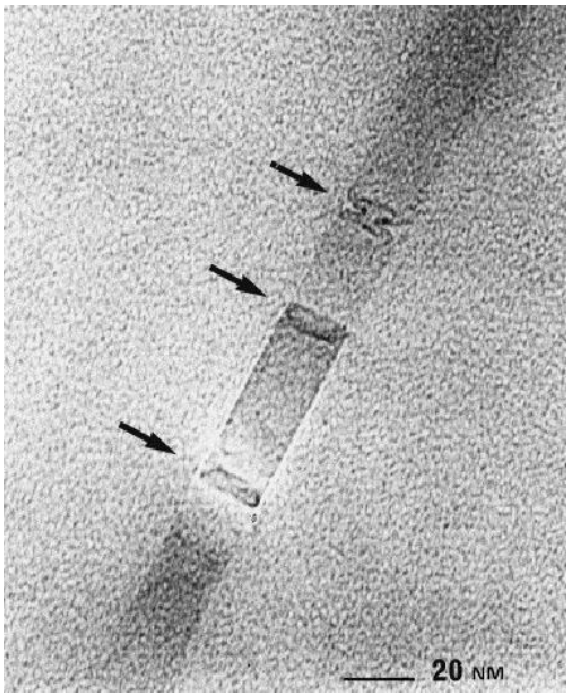

Figure 4.2 TEM image of a multilayer carbon nanotube at the polymer film, revealing the extent of nanotube fragmentation (arrows) (Wagner et al., 1998)

4.4 Wavenumber Shift in Raman D* band

Tuinstra et al. (1970) reported that the disorder-induced D* band in Raman microscopy, reflects a breathing vibrational mode in graphite. According to Dresselhaus et al. (1997), the D* band represents a symmetric vibration mode (A_{1g}) which is further related to the so-called breathing mode. It is noted that a breathing mode in Raman microscopy represents the vibrations in the radial direction or along the nanotube axis.

By placing CNTs in liquids or embedding CNTs in a polymeric matrix and then scanning it under the Raman microscopy, it was found by Wagner et al. (1998) that the wavenumber of the peak of D* band shifts upon immersion or embedding tubes in a

polymer matrix with respect to its position in air (Figure 4.3). They further proposed that the shift in Raman wavenumber is originally attributed to the transfer of strain and stresses to the tubes from the surrounding liquid or polymeric matrix.

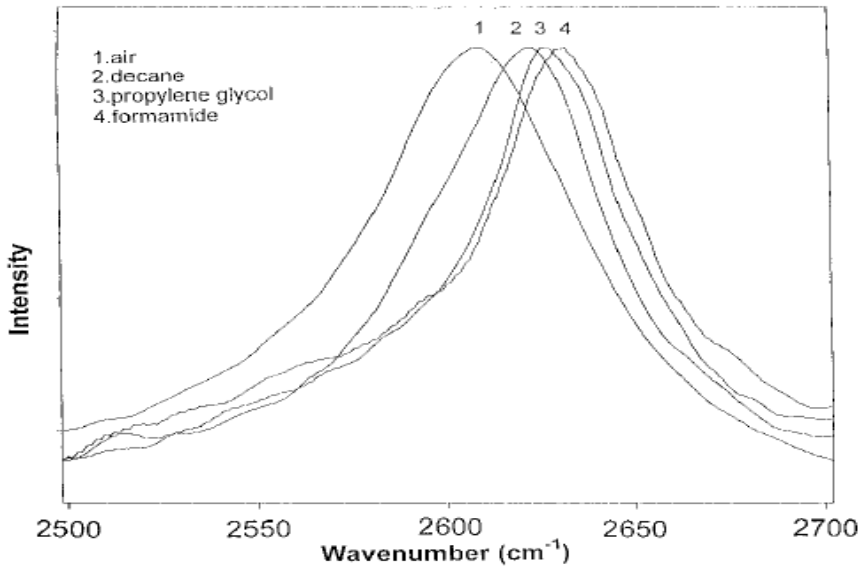

Figure 4.3 Effect of immersion of CNT aggregates on the frequency of D* band in Raman spectrum. Placing the nanotubes in liquids increases the wavenumber of the peak position compared to that in air (Wagner et al., 1999)

In another direction of studies, efforts have been taken on verifying that D* band of CNTs may strongly correlate with mechanical strain in the nanotube (Young et al., 2001). In a study by Zhao et al. (2001), they embedded CNTs (0.1wt %) in a polymer matrix (Rutapox L20 Epoxy Resin) to form CNT composite films. Under in-plane tensile straining to the film, under the Raman scanning, they found that the wavenumber shift of D* band was linear with the applied strain and the slope is about -1422cm^{-1}/strain. A similar study conducted by Wagner et al. (1999) also showed that the slope was about -

$1000cm^{-1}$/strain in the CNT/polycarbonate film. More importantly, they proposed that the external pressure (p) from polymer matrix is attributed to the mechanical (axial) stress (σ) on the tube as described:

$$\sigma = \frac{pR}{2t} \tag{4.3}$$

where σ is the stress in the axial direction of the nanotube, p is the pressure from the surrounding polymer matrix and R and t are the radius and thickness of the nanotube. Although the *in situ* method they proposed is able to obtain the applied strain data from both nanotubes and polymer matrix, the model however is not applicable to the cases concerned in this thesis for the reason that nanotubes in CNT films were not completely embedded into polymer matrix. As a result, the interfacial cohesion, instead of the external pressure, from surrounding polymer matrix was inclined to attribute to the axial stress on the tubes. The CNTs embedded in the polymer matrix exhibits a potential application as a nanoscale strain sensor.

4.5 Summary

In this chapter, several methods and models for estimating the stress transfer between CNT and polymer matrix in literature were reviewed. The conclusions drawn from these methods are summarized below.

(1) In CNT based films, the physical bonding including VDW and cohesion interaction play an important roles on the stress transition at the interface between CNTs and polymer matrix.

(2) The molecular simulation and TEM fragmentation observation estimated that the shear stress at the interface between CNT and polymer matrix is about 2.7 to 110 MPa and 500 MP up, receptively, which are an important reference for estimating the interfacial interaction in CNT films concerned in this thesis.

(3) In Raman microscopy, the D* band of CNTs strongly depends on mechanical strain on the nanotube. By using this *in situ* method, the mechanical strain on both nanotubes and polymer matrix can be obtained simultaneously. Experimental results have shown that the wavenumber shift of the D* band was linear with the applied strain in the film.

CHAPTER 5

MODELING PIEZORESISTIVE RESPONSE IN CNT NETWORKS

5.1 Introduction

Previously, it was discovered that the CNT films which are free of surfactants in CNT networks can exhibit a linear relationship between their conductance and applied in-plane strain (Miao et al., 2011). In this chapter, the modeling of piezoresistive response in CNT networks will be discussed. The objective of the study was to understand the mechanism which governs piezoresistive response in CNT networks. First, the percolation theory was applied to establish the relationship between the density and conductance of CNT networks to verify the hypothesis that the conductance of CNT networks follows the percolation theory. Then, two models were developed for describing piezoresistive response of CNT networks under in-plane straining: one for piezoresistive sensitivity (Gauge Factor) and the other for piezoresistive linearity.

5.2 Percolation and Conductance in CNT Networks

5.2.1 Materials and Method

Layer-by-Layer Spray Deposition: HiPCo Single-Wall Nanotubes (SWNTs) were obtained from the Unidym Inc. The randomly distributed CNT networks were formed on the surface of Polyethylene Terephthalate (PET, Melinex 451) substrate by using the LBL spray deposition. In the first step, a suspension of CNTs was first prepared with a CNT concentration of 0.8mg/ml plus 1%wt surfactant Sodium Dodecyl Sulfate (SDS Sigma and Aldrich). The suspension was sonicated for 30 minutes using a probe

ultrasonicator (Branson Sonifier 150) at 40 watts and then centrifuged for 30 minutes at 14000 rpm in the centrifuger (Eppendorf). The well centrifuged CNT-SDS solution was then carefully decanted into the spray gun for coating on a PET substrate. During the coating process, the substrate was heated through an aluminum plate to 80℃ by a 150 *W* infrared light bulb to prevent from the accumulation of solution in CNT networks. Spraying was done in pulses and after each pulse the substrate with CNT networks was dipped into distilled water to rinse off surfactant SDS. The CNT networks adhered to the substrate because of the strong adhesive forces between CNTs and the polymer substrate, which are a result of the hydrophobic property of CNTs. The density of CNTs was controlled by the number of pulses. Each spraying or pulse time yields one layer of CNT networks deposited on the substrate.

Several CNT films with different densities were fabricated by varying the number of pulses per sample. After the formation of CNT networks on the substrates, two parallel gold electrodes were sputtered on each film. These gold electrodes were used for electrical contacts and they had a separation distance (L) of 10mm and width (W) of 10 mm, as shown in Figure 5.1. To this point, multiple samples were fabricated by this method and ready for testing.

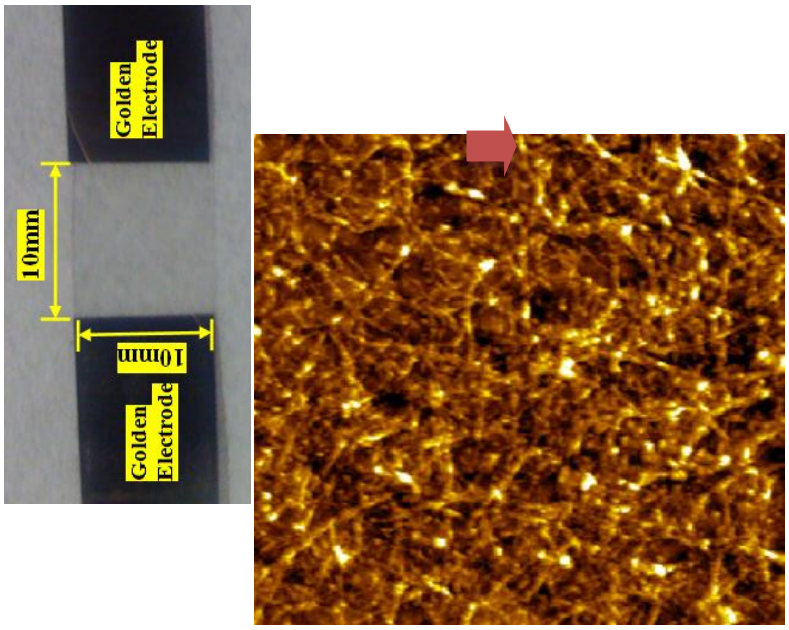

Figure 5.1 A CNT film sample prepared for conductance and density measurement: the randomly distributed CNT networks (AFM Image left) deposited on the PET substrate and two gold electrodes sputtered to form the electrical contact for CNT networks

Measurement and Instrument: A standard two-probe measurement to measure the resistance (R) of CNT networks between the two gold electrodes was taken. The measured resistance was then converted to sheet conductance σ (defined as $1/R_0$) where R_0 is equal to R (since L=W). Raman measurement with a Renishaw Microscope (785 nm excitation) was employed to examine the density in the CNT network in all samples. The amplitude at 1588 cm^{-1} shift was chosen to measure the density of CNTs, which is in compliance with the characterization of SWNTs identified by Keszler *et al.* (2004). In each sample, several spots within an area of CNT networks were selected and scanned. The scanned results were averaged to represent the amplitude at 1588 cm^{-1} wavenumber

shift, which is proportional to the density of CNTs in each sample, as shown in Figure 5.2. The validity of the Raman method refers to the work of Hagrasy *et al.* (2006). Accordingly, a relation between the density and conductance of CNT networks can be built from the measured results.

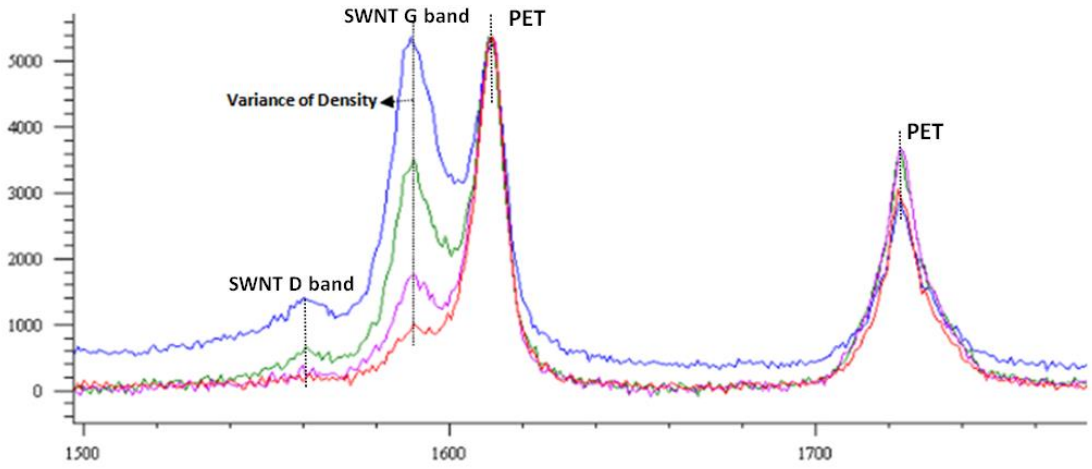

Figure 5.2 Variance of amplitudes (thus density) of count peaks in different film samples at the G bands (1588 cm^{-1}) of SWNTs

5.2.2 Results and Discussion

With the assumption that conductance in our CNT networks follows the percolation theory, CNTs are randomly distributed with no preferential direction, which further meets the stick percolation model (Pike et al., 1973). According to the stick percolation model, their conductance is dependent on the density in networks, which is further described by

$$\sigma \propto (N\text{-}N_c)^{\alpha} \qquad (5.1)$$

where σ refers to the conductance of CNT networks, N to the density of CNT networks, N_c to the critical density and α to the critical exponent , which is equal to 1.33 in a two dimensional region and 1.94 in a three dimensional region (Pike et al., 1973), respectively.

Using the information of the density of the CNT network obtained from the Raman spectroscopy and the two-probe measurement, a plot of sheet conductance σ versus density N of the CNT network for all the samples was shown in Figure 5.3. The best fit to the experimental result yields a value of α=1.938 (subsequently, $\sigma \sim (N- 0.95)^{1.938}$, note: Nc = 0.95). Although this experimental results is close to α=1.94, which sounds like that the CNT networks fabricated is a 3D structure, the author believes that the network fabricated is still a 2D structure (i.e., α=1.33). There are two reasons to support this speculation. First, in the fabrication, CNTs are randomly oriented in parallel with the surface of polymer substrate. Second, the thickness of the CNT network fabricated has little influence on their conductance according to the measurement with AFM (for the thickness) and conductance measurement on the film in the film plane. The discrepancy between 1.938 and 1.33 is caused by the experimental errors as well as assumptions. One of these assumptions is that all conducting sticks have the same conductivity, which is in line with the assumption that results in 1.33. However, in reality, our network system has 1/3 metallic tubes and 2/3 semi-conducting tubes (according to the product data sheet). It is noted that there is the so-called Schottky barrier (Straderman et al., 2004), which changes the conductance in the metallic–semiconducting junctions. In addition, percolation theory is based on the assumption that all sticks are in the same diameter and

length, which was not true in the condition of the author's experiment. Furthermore, any residual SDS surfactant in CNT networks may affect the conductance of the networks. In short, the CNT network in the CNT film fabricated in this study meets the stick percolation theory.

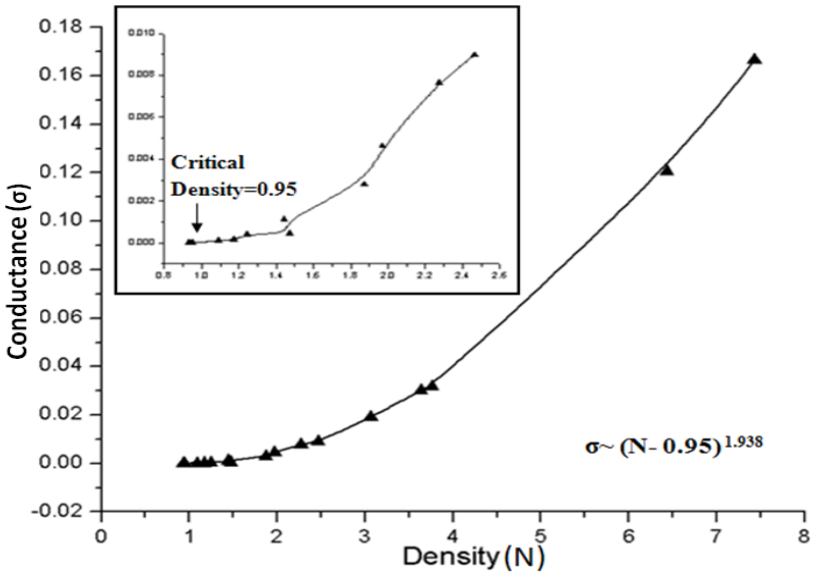

Figure 5.3 The relation between the density and conductance of CNT networks in the CNT film; the onset conduction is indicated by the amplitude value 0.95 on the inset figure when the first percolative path formed in CNT networks (Data analysis can be found in APPENDIX C)

5.2.3 Conclusion

The Layer-By-Layer Deposition method is a reliable approach to the formation of randomly distributed CNT networks in CNT films. Each spraying (pulse) can result in a direct increase of density in CNT networks, which can be further measured under Raman

microscopy. In CNT films, CNT networks follow the stick percolation model with the critical exponent coefficient in the model being 1.938

5.3 Modeling Piezoresistive Response in CNT Networks

5.3.1 Materials and Methods

Straining measurement for the samples fabricated with the method described in Section 5.2 is shown in Figure 5.4 (a). The measurement was performed at the Material Test Laboratory at the College of Engineering at the University of Saskatchewan. The size of test specimens followed the ASTM standard A370 (the sheet-type specimens), and the specimens were made from Aluminum6061 –T61. CNT film samples were first glued (using Loctite 402) onto the specimens after polishing, degreasing (using acidic surface cleaner) and naturalizing (using alkaline surface cleaner) onto the surface as shown in Figure 5.4(b). After overnight drying, the specimens were fixed in the tester (Instron 5500). The tester induced 0.04 tensile strains (in-plane) on the specimen at a crosshead speed of 0.2mm/min as shown in Figure 5.4(c).

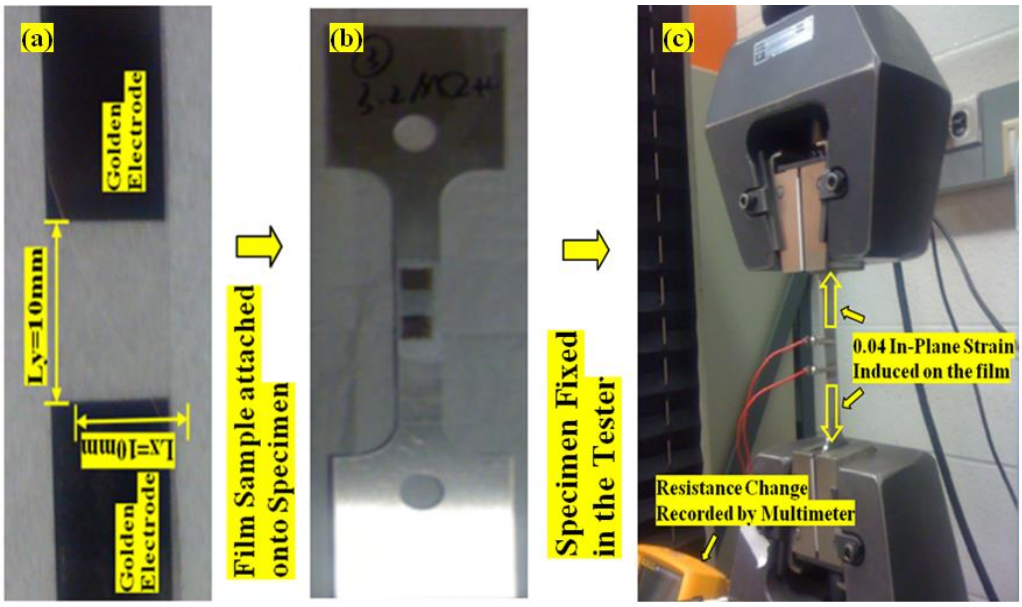

Figure 5.4 The film (a) glue onto the specimen (b) and the tester stretching the specimen to induce in-plane strains on the film (c)

During the tensile elongation, the changes in conductance of CNT films were recorded at every 0.005ε by the multimeter (Fluke 115) through the golden electrodes, and the circuit was supplied with a 10 mA DC current. Tensile displacement was recorded in the tester simultaneously to provide a base-line for comparison with the measured conductance. As the CNT film was stretched, the elongation of the film led to the change of conductance in CNT networks, which represents the piezoresistive response in strain detection. The two dependent variables, namely Gauge factor (representing the sensitivity of piezoresistive response) and linearity of piezoresistive response were then determined.

Before the experiment, a simulation was also performed by ANSYS 11.0 to verify that the uniform tensile strain (in-plane) is distributed on CNT networks. It can be seen in

Figure 5.5 that the CNT film (the rectangular plane in the centre) are attached onto the tensile test specimens (the block), which was elongated up to 0.3 tensile strain. In order to avoid CNT networks under non-uniform strain, the gold electrode area was made large enough (least 5*mm* x 10 *mm*) to cover the area with non-uniform strain at the both ends of the film, as shown Figure 5.5.

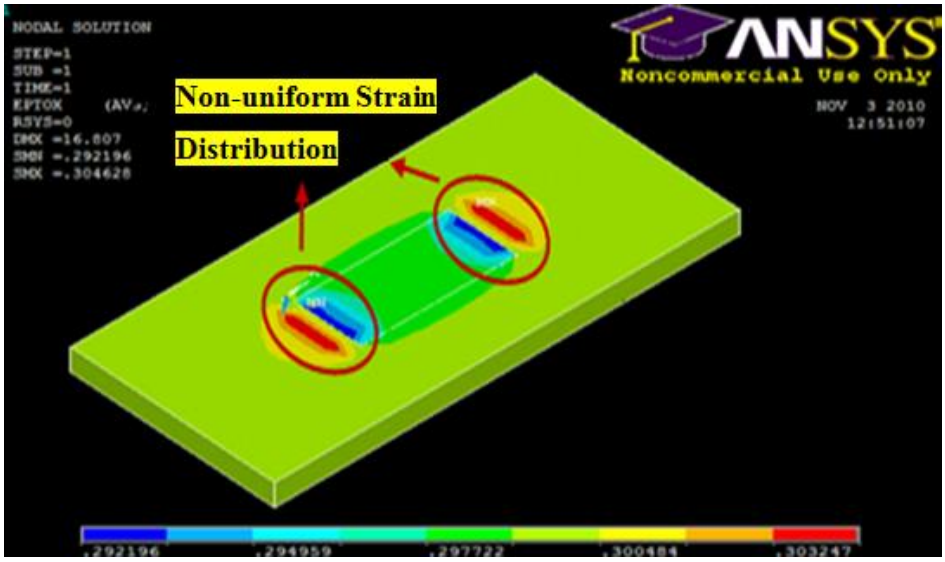

Figure 5.5 Tensile strain simulated on the test specimen to verify that in-plane strain is uniformly distributed on sensing material area (non-uniform area marked with circles)

5.3.2 Results and Discussions

In the preceding section, it has been found that the relation between percolation and conductance in CNT networks follows the stick percolation mode (Pike et al., 1973). The best fit to the experimental result yielded a value of α=1.938 (subsequently, $\sigma \sim (N - 0.95)^{1.938}$) with critical density of 0.95. When the CNT film is subject to in-plane tensile

straining (as ε_y) as shown in Figure 5.6, the area of CNT networks is changed, and the area variation can be described by

$$A+\Delta A= (L_y+ L_y \text{ x } \varepsilon_y) \text{ x } (L_x - \nu \text{ x } L_x \text{ x } \varepsilon_y) \quad (5.2)$$

where A refers to the original area of CNT networks, which is equal to 100 mm^2 ($L_y \times L_x$), ΔA is the area change, L_y and L_x are the separation distance and width, which are equal to 10 mm, ε_y is the in-plane strain, which is up to 0.04, and ν is Poisson's Ratio of Aluminum T61, which is equal to 0.33.

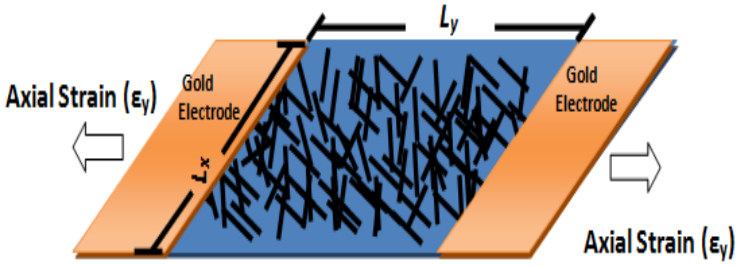

Figure 5.6 Schematic of a CNT film subject to in-plane straining

Therefore the area change (ΔA) gives rise to the new density (N_n) of CNT networks, which can be described by

$$N_n = \frac{N \text{ x } A}{A+\Delta A} \quad (5.3)$$

where N is the original density of CNT networks. From equation 5.3, one can see that the density of CNT networks decreases when the CNT film is subject to in-plane tensile straining. According to the percolation equation $\sigma \sim (N - 0.95)^{1.938}$, the conductance change ($\Delta\sigma$) due to the density change can be described by

$$\sigma - \sigma_n = \Delta\sigma, \text{ where } \sigma_n \sim (N_n - 0.95)^{1.938} \quad (5.4)$$

Piezoresistive response of CNT networks in the CNT film can thus be explained such that when the CNT film experiences a strain (in-plane), displacements of individual tubes on the substrate induce the density change in CNT networks, and this further leads to variations in the conductance of the film.

For the CNT film with a given conductance (σ), its piezoresistive response can be determined by the following procedure. Step 1: the original density (N) can be obtained by equation $\sigma \sim (N - 0.95)^{1.938}$; Step 2: when the CNT film is subject to a certain in-plane strain (εy), the changed density (N_n) is calculated from equations (5.2) and (5.3); Step 3: the conductance changes (Δσ) is calculated from equation (5.4); Step 4: the GF and linearity are calculated by $GF=\frac{\Delta\sigma/\sigma}{\varepsilon y}$ and Linearity= $d\sigma/d\,\varepsilon y$, respectively. Figure 5.7 shows a comparison of the prediction of gauge factor with the foregoing procedure and the experimental result of gauge factor from one sample. The two have an excellent agreement.

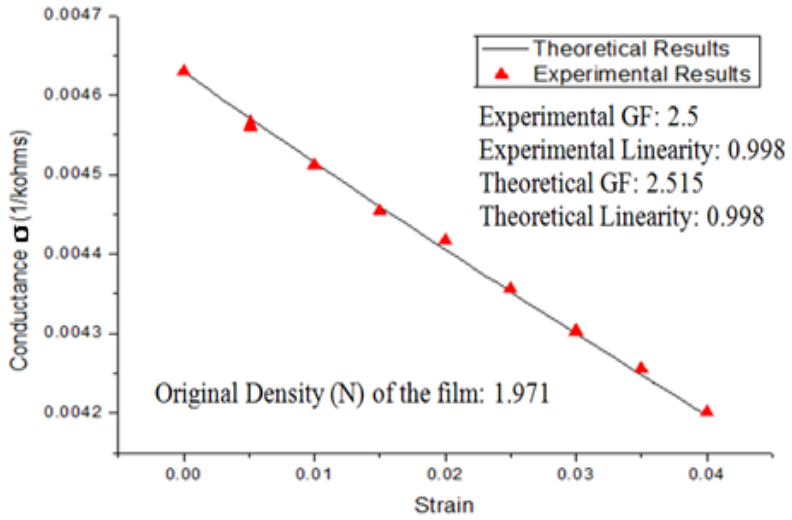

Figure 5.7 Comparison of the theoretical prediction of gauge factor (GF) and the experimental GF when the CNT film is subject to in-plane straining

Further using the procedure described above, the piezoresistive response in the CNT film with a different original density (*N*) subject to in-plane straining was calculated. As a result, the original density versus gauge factor and the original density versus piezoresistive linearity are shown in Figure 5.8 (a) and (b), respectively. From Figure 5.8 and Table 5.1, one can see that the theoretical prediction and experimental result are in good agreement.

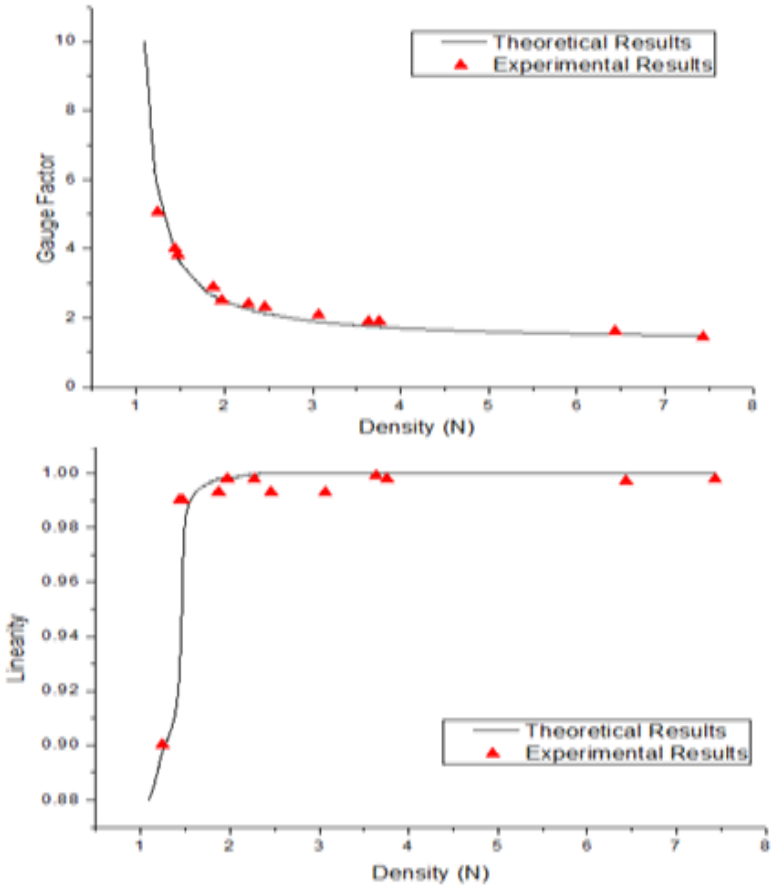

Figure 5.8 The effect of original density (*N*) on piezoresistive response in CNT networks: (top) gauge factor vs. original density (bottom) linearity vs. original density, including both experimental and theoretical results

Table 5. 1 The experimental results collected from 16 film samples

Density	GF	Linearity	Density	GF	Linearity
7.431	1.44	0.998	1.873	2.9	0.993
6.433	1.6	0.997	1.442	4	0.99
3.761	1.9	0.998	1.473	3.8	0.987

3.633	1.9	0.999	1.244	5.05	0.9
3.065	2.1	0.993	1.172	NA	NA
2.464	2.3	0.993	1.090	NA	NA
2.272	2.4	0.998	0.95	NA	NA
1.971	2.5	0.998	0.93	NA	NA

Further, Figure 5.8 shows that the increase of the original density of CNT networks leads to the decrease of gauge factor but the increase of piezoresistive linearity. This trend is consistent with the study reported by Martinez et al. (2010). In their study, the highest gauge factor was obtained in the lowest electrical conductivity (the lowest density) in polymeric composite films (conductive nanofillers as sensing materials), and vice versa. In addition, Figure 5.8 shows that there is an obvious trade-off between the GF and linearity when the density was less than 2. When the density was larger than 2, the GF decreased with a nearly constant linearity (approximately equal to 1). Therefore, the optimal density of the films should be around 2 for the CNT film which is subject to in-plane straining.

5.4 Conclusions

This chapter presented a study on modelling of piezoelectric resistance of CNT networks in the CNT film where both theoretical developments and experimental measurements were described. The results obtained from this study can conclude: (1) CNT networks in the CNT film follows the stick percolation model with the critical exponent of 1.938; (2)

the theoretical models, one for the relation between the density and gauge factor and one for the relation between the density and linearity for the CNT film subjected to in-plane straining, are accurate; (3) with these models, an optimal in-plane strain sensor built upon the CNT film should be such that its density is around 2.

CHAPTER 6

PIEZORESISTIVE RESPONSE IN ALIGNED CNT NETWORKS UNDER IN-PLANE STRAINING

6.1 Introduction

In this chapter, piezoresistive response in aligned CNT networks was investigated. In order to obtain aligned CNT networks, magnetic force was employed to align the CNTs in the films. The CNTs were first decorated with iron oxide nanoparticles to enhance their magnetic strength to facilitate their alignment. In the fabrication of CNT films, the decorated CNTs were deposited on the polymeric substrate in a magnetic field to form aligned CNT networks. Piezoresistive response of the networks was measured as the film was under in-plane straining.

6.2 Decoration of CNTs with iron oxide nanoparticles

The method used here to decorate CNTs with iron oxide nanoparticles was an adaptation of a previously reported synthesis by He et al. (2011).

6.2.1 Materials and Method

Acid oxidization (or functionalization): The 100 mg MWNTs (Shenzhen Nanotech Port) and 40mg SWNTs (Unidym Inc) were separately dispersed in a solution of 9 ml concentrated sulfuric acid (H_2SO_4) and 3 ml concentrated nitric acid (HNO_3) (3:1 volume ratio). Both MWNT and SWNT solutions were sonicated in a typical ultrasound bath (Branson 3510) for 3 hours as shown in Figure 6.1. After each hour, a sample of solution

was removed from both solutions, diluted (with distilled water) and centrifuged several times for Raman characterization (Renishaw Microscope 2000).

Figure 6.1 MWNTs and SWNTs dispersed in mixture of concentrated acid by sonication in ultrasound bath

After 3 hours sonication, both acid mixture containing CNTs was then diluted to 20% of its original concentration. The functionalized CNTs were filtered through the filter membrane (0.2 μm, Nalgene) with the aid of vacuum pump. Both SWNT and MWNT samples were washed several times vigorously with distilled water during filtration in order for them reach neutral pH. The sample powders were dried in the vacuum oven at 70 ºC overnight. To this point, the functionalized CNTs were ready for the decoration with iron oxide nanoparticles.

Decoration of CNTs with Iron Oxide Nanoparticles: Sodium Hydroxide (NaOH, Sigma & Aldrich) was first dissolved in Diethylene Glycol solution (DEG, Sigma &

Aldrich) for later use. The NaOH (1000 mg, 2.5 mmol) was added into 10mL of DEG (100 mg/ml) under nitrogen atmosphere and magnetic stirring. The mixture was heated to 120ºC for 1 hour and then maintained at 70ºC for later use.

It is noted that the functionalized MWNTs (f-MWNT) were obtained, but the functionalized SWNTs (f-SWNT) were severely damaged after the acid oxidization process and thus cannot be used in the decoration process (see later for details). Two feed ratios between iron oxide nanoparticles and f-MWNTs (5/1 and 1/1) were used in the decoration process.

In the feed ratio of 5/1 (w/w), the 30 mg f-MWNTs were dispersed in the 10 ml DEG in an ultrasonic bath (Branson 3510) for several minutes. The well dispersed mixture was then placed in a three-neck round-bottom flask equipped with a condenser which was located on a magnetic stirrer equipped with a heater, as shown in Figure 6.2. 540 mg $FeCl_3 \cdot 6H_2O$ (2 mmol, the iron content is about 150 mg) was then added and the mixture was maintained at 220 ºC for 30 minutes. The 2.5 mL pre-prepared NaOH/DEG solution was injected into the stirring mixture via a syringe. The resulting mixture was further maintained at220 ºC for 1 hour.

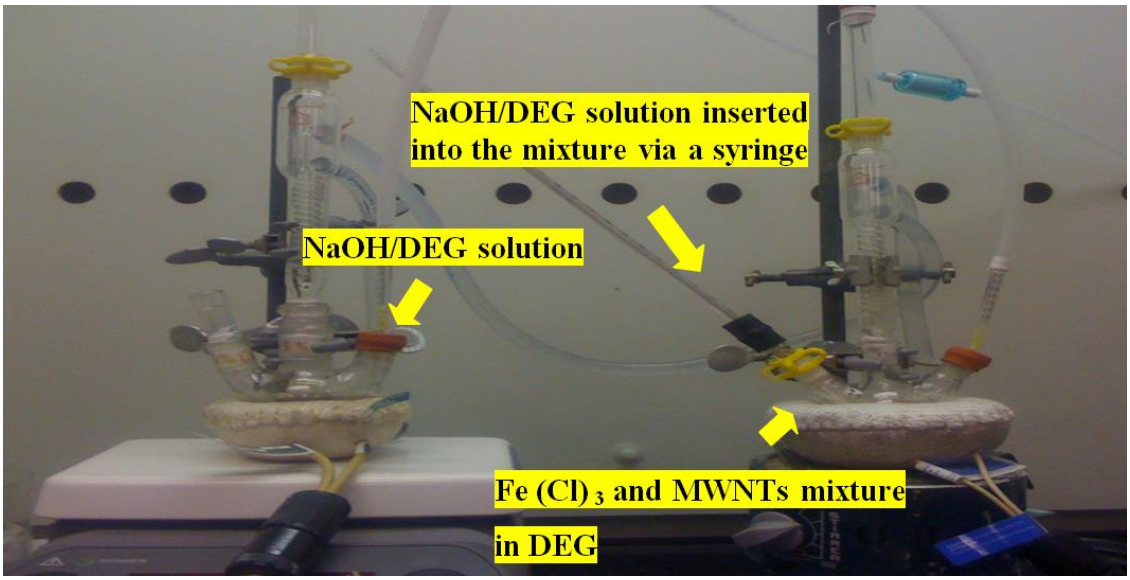

Figure 6.2 Experimental setups for the decoration process of f-MWNTs with iron oxide nanoparticles: the mixture placed in a three-neck round-bottom flask equipped with a condenser, located on a magnetic stirrer equipped with heater

After cooling down to room temperature, the mixture was separated by centrifugation (Beckman Coulter X-22R) at 15000 rpm , re-dispersed in ethanol and re-centrifuged for several times. The sample was then re-washed in distilled water and re-centrifuged for several times. The collected powder was dried in the vacuum oven at 60 ºC overnight. The same procedures were also followed to prepare the f- MWNTs with feed ratio 1/1(w/w), in which 30 mg f-MWNTs, 105mg $FeCl_3 \cdot 6H_2O$ (0.39 mmol, the iron content is about 30 mg) and 5 ml DEG solution (10 mg/ml) were used.

6.2.2 Results and Discussions

Acid Oxidization process was a common method used for the functionalization (or carboxylation) of CNTs. In general, oxidization tends to happen at the defect site on the

surfaces of CNTs, where functional group carboxylic acids (-COOH) can be formed at. However, with the acid oxidization process as designed before, Raman image showed that the functionalized SWNTs exhibit significant lower ratio between the intensity of D bands (1347 cm^{-1}) and that of G bands (1589 cm^{-1}) in comparison with the ratio for pristine SWNTs (Figure 6.3). According to a study by Shi et al. (2000), G band corresponds to the tangential modes of vibrations, while D band corresponds to the modes of vibration due to scattering from a defect which breaks the basic symmetry of graphene sheet. It can be seen from Figure 6.3 that the ratio between G and D bands in the SWNTs decreases from 6.84 (pristine) to 1.7 (3 hours oxidization), which suggests the presence of more defects on the surface of the SWNTs (due to the increase of oxidization time).

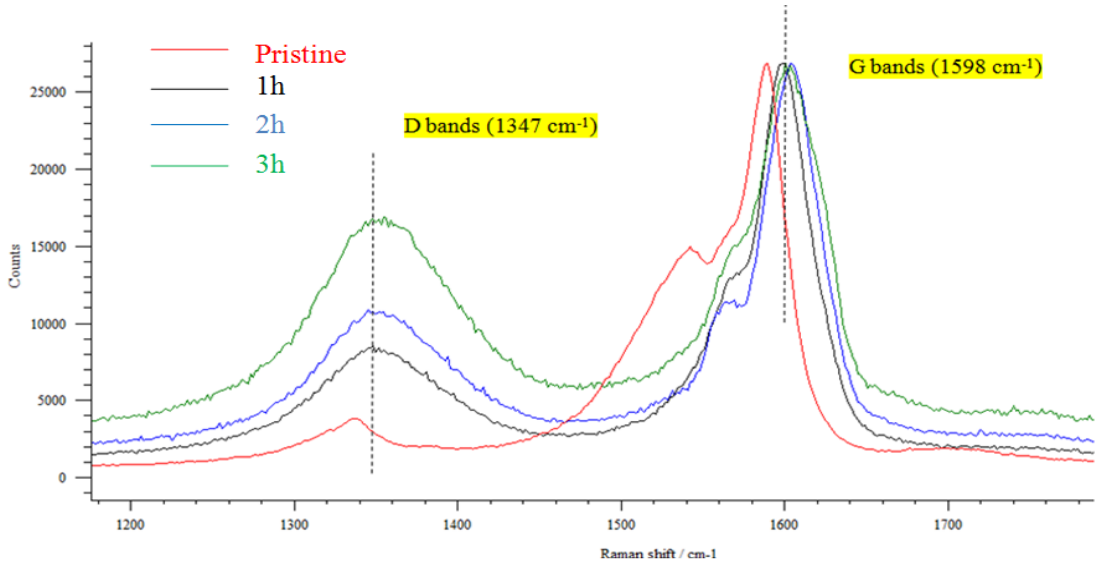

Figure 6.3 Raman microscopic results of SWNTs before and after acid oxidization process, ratio of G/D band: 6.84 (pristine), 3.2 (1 hour), 2.4 (2 hours) and 1.7 (3 hours)

In the same treatment, Raman microscope of the f-MWNTs showed that the ratio between G and D band increase from 0.94 (pristine tubes) to 1.15 (after 3 hours oxidization, Figure 6.4). The insignificant changes in the ratio of G/D bands suggest that MWNTs present fewer defects after the oxidization process as opposed to SWNTs. Due to the structural difference, the single layer of graphene in SWNTs appeared to be destroyed into amorphous carbon (evidenced by the decrease of the G/D ratio). Interestingly, a similar finding was reported by Zhang et al. (2004) where the layered structures of SWNT were destroyed during the nitric acid oxidization. As a result, SWNTs after the acid oxidization process are no long suitable for the decoration of iron oxide nanoparticles; as their single layered walls are destroyed, and thus they are not able to provide a platform for bonding with nanoparticles.

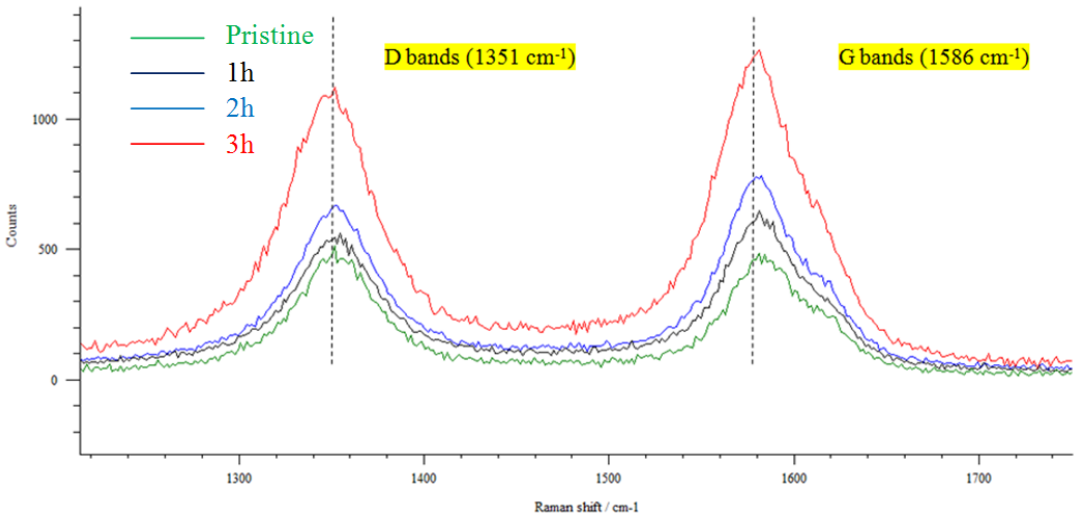

Figure 6.4 Raman microscopic results of MWNTs before and after acid oxidization process, ratio of G/D: 0.94 (pristine), 1.1 (1 hour), 1.1 (2 hours) and 1.15 (3 hours)

Decoration of CNTs with iron oxide nanoparticles: Electron Paramagnetic Resonance (EPR) spectroscopy was used to characterize the attached iron oxide nanoparticles. EPR spectra of the samples were shown in Figure 6.5. It can be seen that the decorated CNTs contain magnetite Fe_3O_4 and hematite α-Fe_2O_3 nanoparticles.

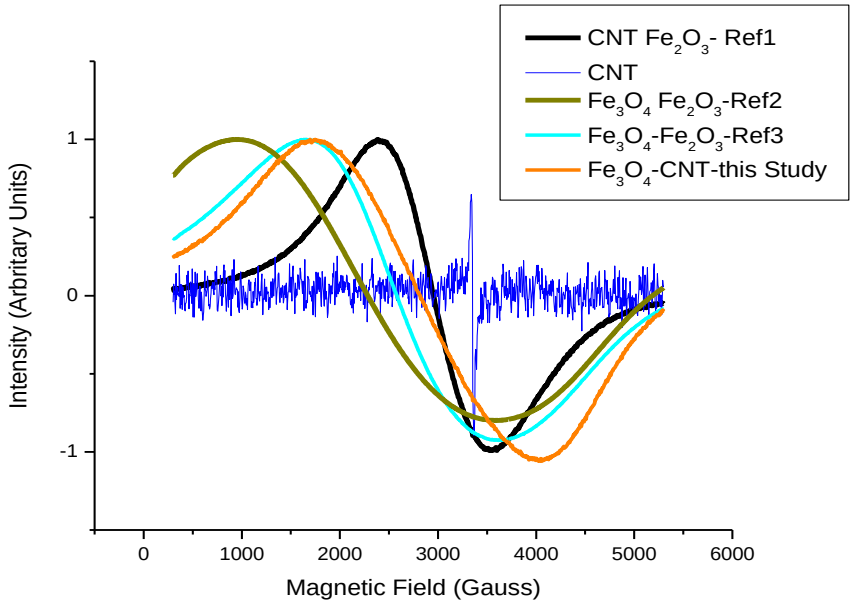

Figure 6.5 X band ESR spectra of the samples, showing that the attached nanoparticles are the mixture of Fe_3O_4 and Fe_2O_3 (reference samples courtesy of Dr. J. Zhou)

After the oxidization process, -COOH, as a carboxylic functional group, was attached to the defect site on the surfaces of CNTs, then the iron oxide nanoparticles would be able to covalently tethered to the oxidized defect sites on the outer surfaces of the CNTs during the sol-gel synthesis as shown in Figure 6.6.

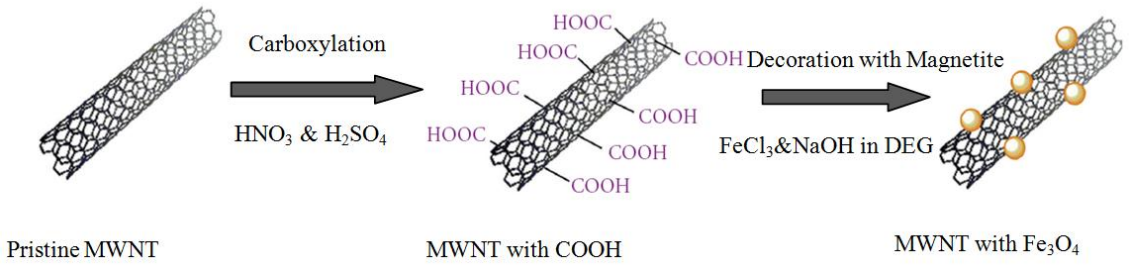

Figure 6.6 Schematic descriptions of carboxyl groups –COOH formed on the defect sites on the surfaces of the CNT; iron oxide nanoparticles attached onto the defect sites via –COOH binding

The precursor Fe (in $FeCl_3$) was first coordinated to the carboxyl groups –COOH on the surfaces of f-MWNTs in DEG solution. After adding the NaOH/DEG solution (OH^-) into the mixture, the Fe was then hydrolyzed and eventually dehydrated to generate magnetite Fe_3O_4 nanoparticles on the surface of MWTNs. During the aging process, some magnetite Fe_3O_4 nanoparticles were further oxidized and formed as hematite α-Fe_2O_3 nanoparticles. The relevant chemical reaction can be expressed by:

$$3Fe^{3+} + 8OH^- + \text{F-MWNT} \rightarrow \text{MWNT/}Fe_3O_4 + 4H_2O \quad (6.1)$$

$$2Fe_3O_4 + 0.5O_2 = 3\,Fe_2O_3 \quad (6.2)$$

Transmission Electron Microscopy (TEM) was used to observe the microstructure of the samples. For the two different feed ratios (5/1, 1/1), typical images were shown in Figure 6.7. It can be seen from the figure that the iron oxide nanoparticles are present as spherical nanoscale-crystals and located on the sidewalls of the tubes.

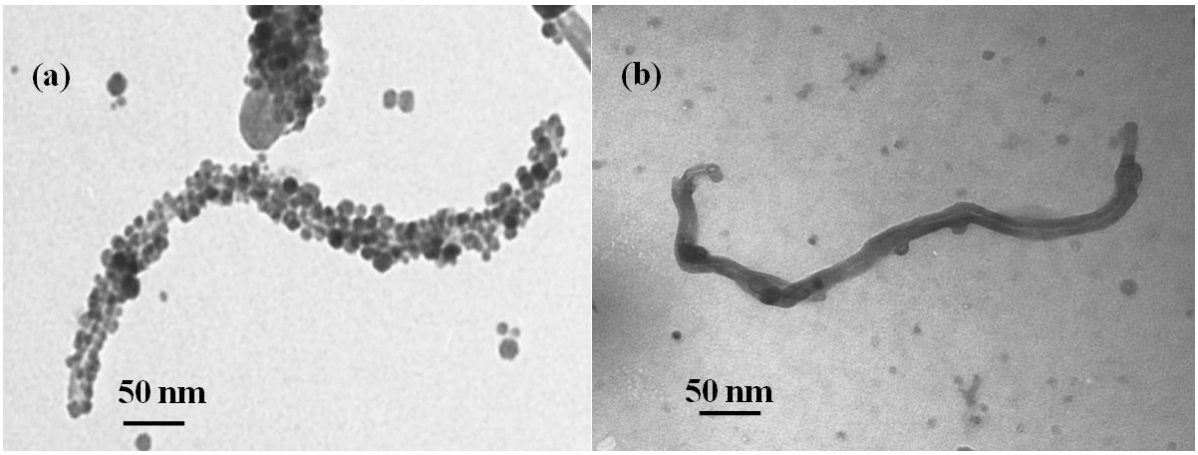

Figure 6.7 TEM images of decorated nanotubes: iron oxide nanoparticles attached on the outer surfaces of the tube with feed ratio of Fe/f-MWNTs (a) 5/1 and (b) 1/1

The CNTs decorated with iron oxide nanoparticles exhibited an enhanced magnetic susceptibility since the magnetite nanoparticles imparted their magnetic characteristics to the nanotube, as shown in Figure 6.8. In the fabrication of CNT films, the enhanced magnetic properties can facilitate the rotations of CNTs into alignments under the external magnetic force (discussed in subsequent section of this thesis).

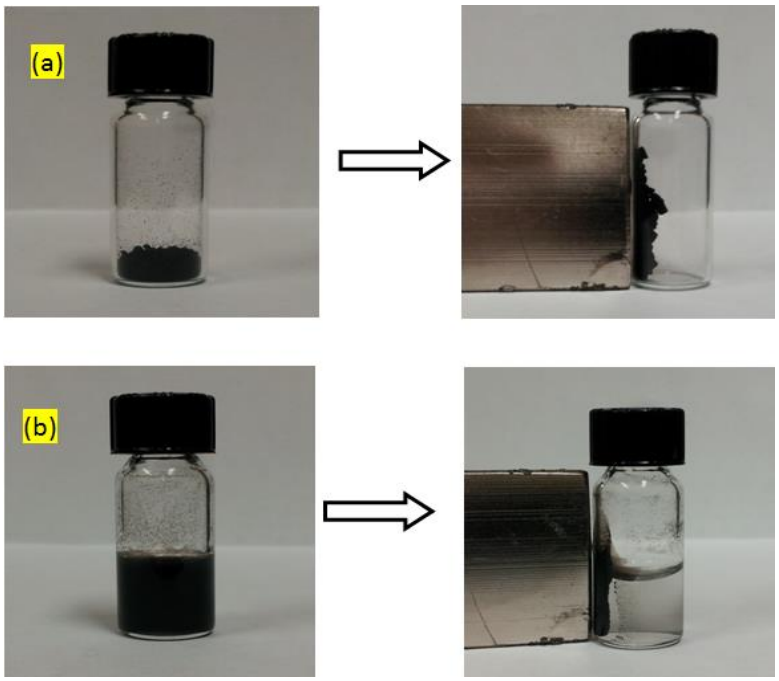

Figure 6.8 Decorated MWNTs with iron oxide nanoparticles exhibit enhanced magnetism as applied under a magnet field (a) in air and (b) in solution

6.2.3 Conclusion

Functionalization of SWNTs with acid treatment is difficult to be achieved, since their single layered walls were severely damaged. For MWNTs however, the functionalization happened on the defect site of their outer surfaces where the carboxylic acids group (-COOH) were formed.

In the decoration process, the iron oxide nanoparticles were generated and eventually attached on the surface of the MWNTs via covalent bonding with carboxylic acids (-COOH). The decorated CNTs with iron oxide nanoparticles exhibited enhanced magnetism.

6.3 Piezoresistive Response of Aligned CNT Networks

6.3.1 Materials and Methods

The CNTs decorated with iron oxide nanoparticles were used here to form aligned networks in the CNT films that were prepared with feed ratio of 5/1 (Fe/f-MWNTs) in the section 6.2.2.

A suspension of the decorated CNTs was prepared with a concentration of 0.25mg/ml in millipore water (used as received). The suspension was sonicated for 10 minute using a probe ultrasonicator (Branson Sonifier 150). The well dispersed solution was then decanted into the spray gun for coating onto the polymer substrate (PET, Melinex 451). During the coating process, the substrate was placed between a pair of magnets, where the substrate surface was parallel to the magnetic field (0.3T) as shown in Figure 6.9 (a). After each pulse of spraying, it can be seen that many isolated suspensions were produced and deposited on the substrate where tubes were oriented parallel to the direction of the externally applied magnetic field. After the solvent was eventually evaporated, the nanotubes were aligned on the substrate as shown in Figure 6.9 (b). The density of CNT networks was controlled by spraying volumes (or number of pulses). Five different spray volumes were used in fabricating CNT films, namely 2mL, 3mL 4mL, 5mL and 6mL.

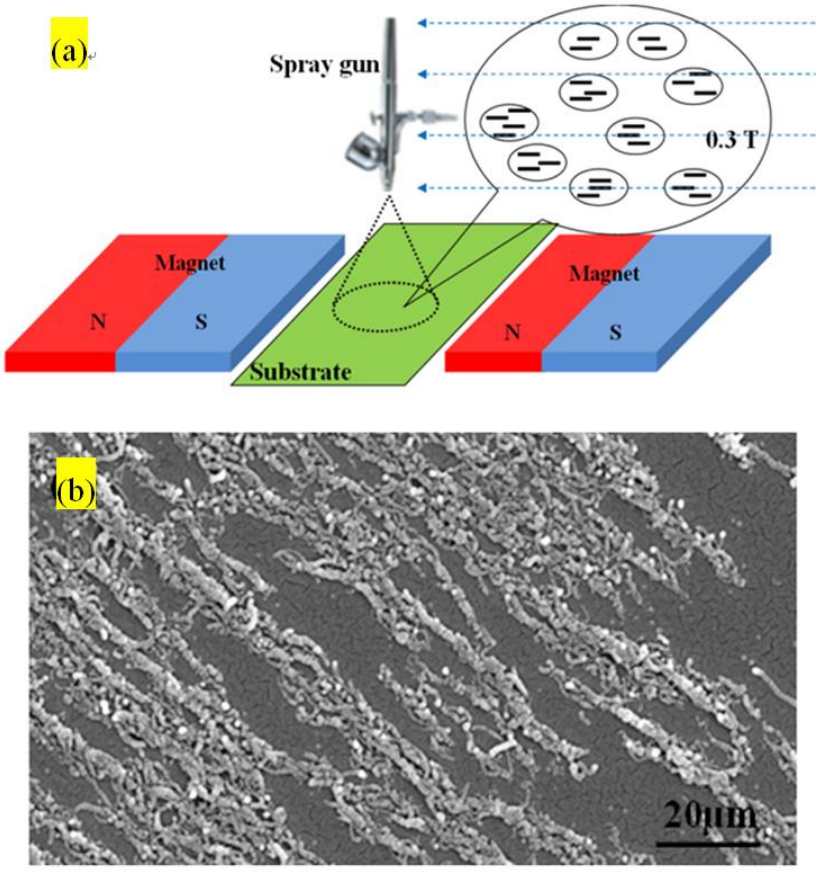

Figure 6.9 (a) Schematic description of spray deposition method used to fabricate aligned CNT networks; (b) Scanning Electron Microscope (SEM) image of aligned CNT networks fabricated by the spray deposition with the aid of magnetic field method (SEI 15Kev, WD 12mm, SS40)

Two parallel gold electrodes, with a separation distance (L) of 5mm and width (W) of 5 mm, were sputtered on the CNT film to function as electrical contacts. Three types of CNT networks were then made in between the electrical contacts as shown in Figure 6.10: (a) randomly distributed CNT networks (without magnetic field), (b) CNT networks aligned at 90º to the electrical contacts and (c) CNT networks aligned at 0º to the electrical contacts.

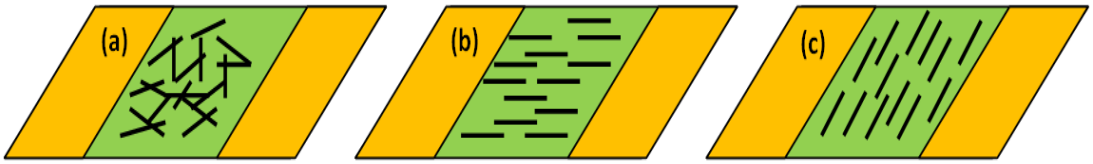

Figure 6.10 Schematic description of three types of configurations in CNT networks: (a) randomly distributed, (b) aligned at 90º to gold electrodes and (c) aligned at 0º to the gold electrodes

A solution was first prepared with 5% concentration of Polymethyl Methacrylate (PMMA, Sigma and Aldrich) in Chloroform (MG chemicals) at 70ºC while stirring. The transparent solution was then coated on the top of the formed CNT networks by a spin coater (Headway Research, PWM32) at 1000rpm for 1min (electrodes were masked during the coating). The electrical connection for strain detection was established by drying silver paste (MG chemical) on the gold electrodes with the twisted-strand wire to form two probes on both ends of the film (the overall contact resistance is less than 100Ω). To this point, all film samples were ready for in-plane strain testing. The complete structure of CNT films consist of the CNT networks sandwiched by the PMMA upper layer and the PET substrate, which is a type of CNT films for strain detection (Miao et al., 2012).

All film samples were first tested by the probe measurement (between gold electrodes) to obtain the sheet resistance R. The CNT films were then tested under the three points bending test at the Material Test Laboratory at the College of Engineering at the

University of Saskatchewan for piezoresistive measurement. The size of test bar (150mm x 30mm x 6mm) followed the ASTM D790, which were made from Polyvinyl Chloride (PVC). All CNT films were first attached (by Loctite 402) onto the centre of the PVC bar after polishing, degreasing and naturalizing the adhesion surface. The bars were then fixed in the three points bending tester where a cycled 4 mm maximum deflection was applied onto the middle of the span (120 mm) to induce a cycled 0.08 in-plane strain (pre-calibrated by a standard strain gauge) on the CNT film at crosshead speed 2 mm/min as shown in Figure 6.11.

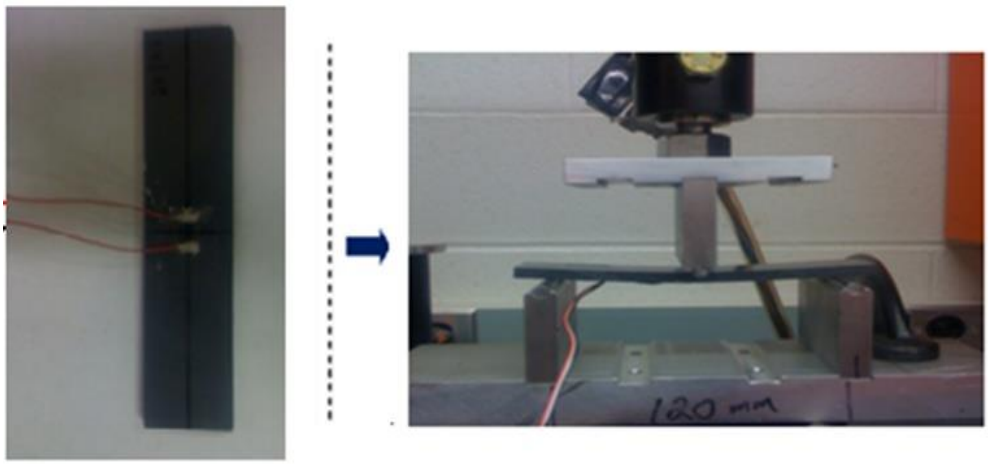

Figure 6.11 CNT film sample attached onto the centre of the PVC bar and fixed in the three points bending tester

After the film was subjected to a cycled load, its resistance (R) changes with respect to the applied strain (ε) were recorded by a digital multimeter. As shown in Figure 6.12, Gauge Factors (GF) (defined as $GF=\frac{\Delta R/R}{\varepsilon}$, where ε is an applied in-plane strain) were then

calculated based on the experimental results. The repeatability (%), defined as (R_{12min} – R_{0min}) / R_{0min}, was calculated for each film sample as well.

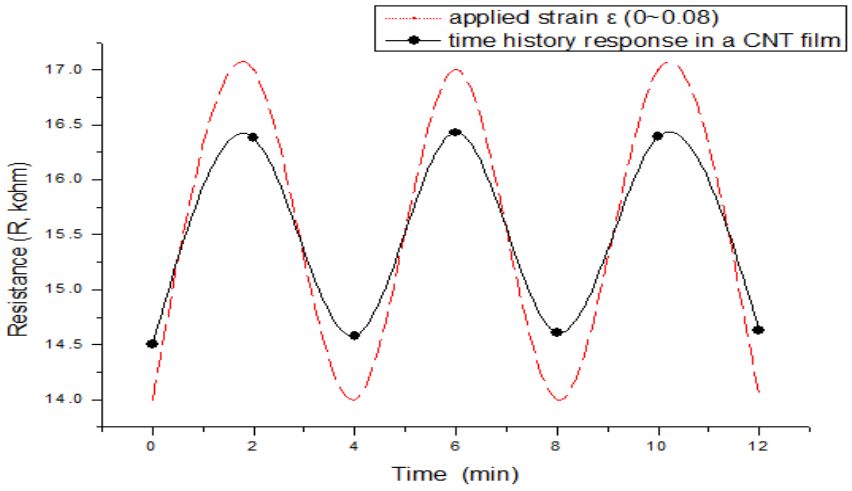

Figure 6.12 Representative time history response of the CNT film sample (solid line) subjected to a cycled strain ε 0~0.08 (dash line)

6.3.2 Results and Discussion

Two-probe measurements were performed on all three types of CNT networks and the resistance results were shown in Figure 6.13 and Table 6.1. For all three types of CNT networks prepared, the resistance decreases with the increase of spraying volumes (which increases the density of CNT networks). Straderman et al. (2004) suggested that the conductance through the tube to tube contacts should dominate the overall conductance of the network. Under the same spraying volume (thus the same density of CNT networks), it can be seen from Figure 6.13 that the CNT networks aligned at 90º to gold electrodes (thus 0º to the applied current passage) exhibit the lowest resistance. Such type

of aligned networks has the most tube-tube contacts; as a result it exhibits the lowest resistance. When CNTs are aligned at 0º to gold electrodes (thus 90º to the applied current passage), the shortage of tube-tube contacts severely increases the resistance in such networks.

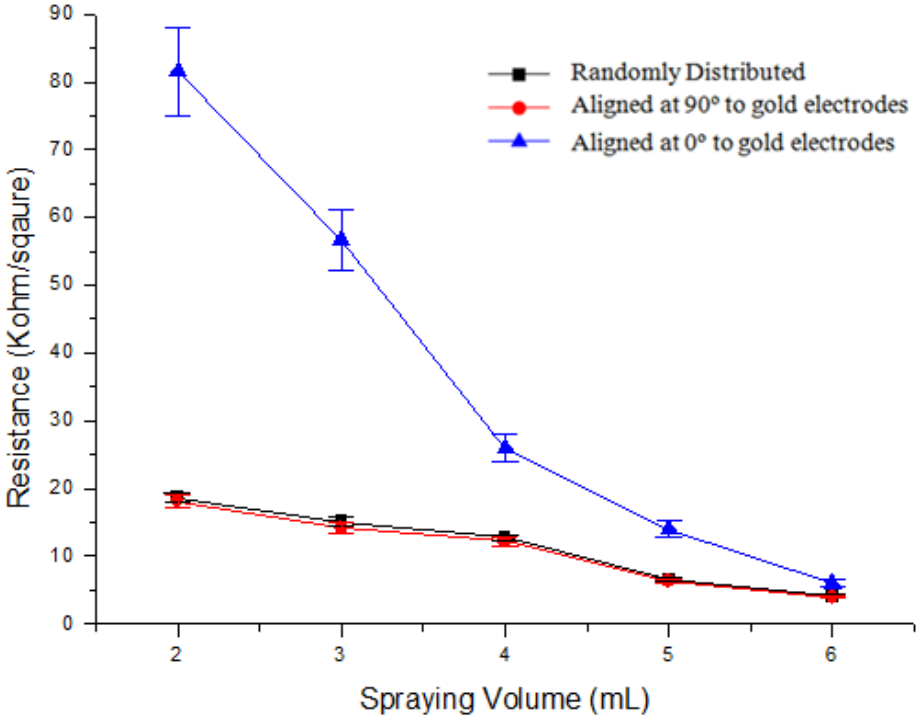

Figure 6.13 Resistance versus spraying volume in each type of CNT network

Table 6.1 Resistance versus spraying volume in three types of CNT network distributions (Calculation method see APPENDIX D)

Spray Volume (mL)	**Error**	**Randomly distributed (KΩ)**	**Error**	**Aligned at 90° to electrodes(KΩ)**	**Error**	**Aligned at 0° to electrodes(KΩ)**
2	±7%	18.6	±4%	18.1	±9%	81.535
3	±10%	15.125	±2%	14.2	±6%	56.655
4	±4%	12.715	±5%	12.18	±6%	25.95
5	±3%	6.575	±7.4%	6.7	±10%	14.01
6	±2%	4.13	±6.4%	3.95	±5%	6.07

The GFs of the network under in-plane straining are shown in Figure 6.14 and Table 6.2. In all three types of CNT networks, it can be seen that the GF decreases with the increase of spraying volumes. Under the same spraying volume, the GF of the networks aligned at 0º to the gold electrodes has the highest values, while the GF obtained from the networks aligned at 90º to the gold electrodes has the lowest values and the GF values of the randomly distributed networks are between those of the two aligned networks. The foregoing results can be explained by the mechanism of Straderman et al. (2004). To the CNT networks aligned at 0º to the gold electrodes (thus 90º to the applied strain), the tube-tube contacts are affected most by the straining, so the conductance is most affected, which further gives the highest GF in the film. In contrast, to the CNT networks aligned

at 90º to the gold electrodes (thus 0º to the applied strain), the tube to tube contacts are affected least by the applied stain, thus exhibiting the lowest GF in the film. To the CNT networks randomly distributed, the tube to tube contacts affected between the two aligned CNTs networks.

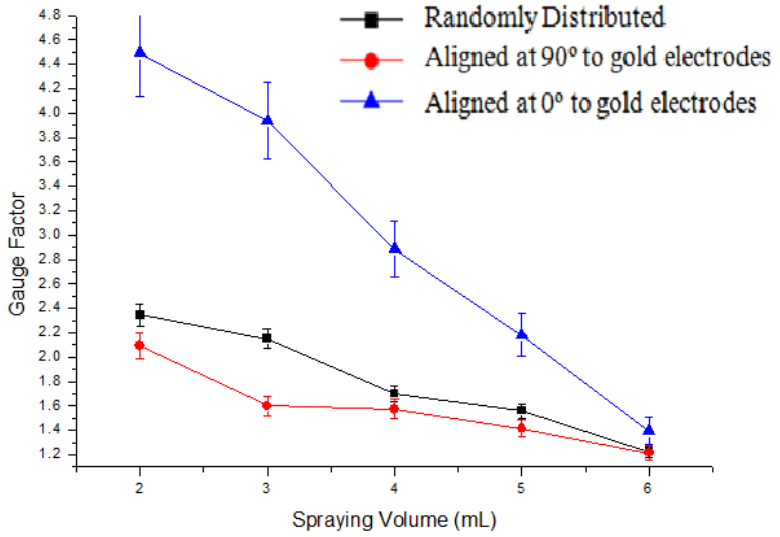

Figure 6.14 Gauge factors versus spraying volume in each type of CNT network

Table 6.2 Gauge factors versus spraying volume in three types of CNT network distributions (Calculation method sees APPENDIX D)

Spray Volume (mL)	Error	Randomly distributed	Error	Aligned at 90° to electrodes	Error	Aligned at 0° to electrodes
2	±9%	2.345	±5%	2.095	±6%	4.49
3	±5%	2.15	±6%	1.6	±7%	3.935
4	0	1.7	±7%	1.575	±5%	2.885
5	±4%	1.56	±4%	1.415	±16%	2.18
6	±2%	1.225	±3%	1.215	±3%	1.395

The repeatability for the three types of CNT film is listed in Table 6.3. It can be seen from the table that both CNT networks randomly distributed and aligned at 90° to the gold electrodes exhibit the similar repeatability value varying from 0.43% to 1.25%. The CNT networks aligned at 0° to the gold electrodes however exhibit severe resistance reduction ranging from -6% to -27%. The foregoing result can be attributed to the uncertainty of tube rotation (clockwise, counter clockwise). First, CNT tend to rotate to align with the direction of applied straining (Jin et al., 1998; Ajayan et al., 1994). Second, to the tube which is perpendicular to the straining direction, the course that the tube rotating to the straining direction can be either clockwise or counter clockwise, which one of the two is an uncertain event, thus suggesting the poor repeatability of the CNT films aligned at 0° to the gold electrodes.

Table 6.3 Repeatability for three types of CNT network distributions after a cycled in-plane straining (note: the calculation method is seen in APPENDIX D)

Spray Volume (mL)	**Randomly distributed #1**	**Randomly distributed #2**	**Aligned at 90° to electrodes #1**	**Aligned at 90° to electrodes #2**	**Aligned at 0° to electrodes #1**	**Aligned at 0° to electrodes #2**
2	0.50%	0.70%	0.60%	1.30%	-30%	-24%
3	0.50%	0.36%	0.90%	0.70%	-22%	-27%
4	0.80%	1.70%	0.50%	0.70%	-17%	-15%
5	0.70%	0.90%	1.30%	1.10%	-18%	-9.60%
6	0.90%	0.90%	1.20%	1%	-5.10%	-7.50%

6.3.3 Conclusion

First, with the enhanced magnetism, the CNTs decorated with iron oxide nanoparticles can be well aligned to the direction of the externally applied magnetic field (0.3T) so as to form aligned CNT networks on the polymer substrate by spraying deposition.

Second, the configuration of CNT networks (or distribution of CNTs) in the film with respect to the direction of straining is an important factor to determine piezoresistive response (sensitivity and repeatability). In particular, the CNT networks aligned at 90º to the gold electrodes and at 0º to the gold electrodes have the lowest and highest GF, respectively.

Third, the CNT networks aligned at 0° to the gold electrodes are not suitable for in-plane strain detection. The randomly distributed CNT networks are best suitable for in-plane strain detection.

6.4 Conclusions

(1) Functionalization of SWNT by acid treatment method is difficult to be achieved, but for MWNTs, the method is highly possible.

(2) Decoration of iron oxide nanoparticles on MWNTs is highly feasible and achieved. The decorated CNTs with iron oxide nanoparticles exhibited enhanced magnetism.

(3) In CNT films, aligned CNT networks were achieved on the polymer substrate by spraying deposition under an externally applied magnetic field.

(4) The configuration of CNT networks in CNT films with respect to the direction of straining is an important factor to determine piezoresistive response.

(5) The randomly distributed CNT networks are best suitable for in-plane strain detection, with regard to the sensitivity and repeatability.

CHAPTER 7

INTERACTION OF CARBON NANOTUBE WITH POLYMER MATRIX IN CNT FILMS UNDER IN-PLANE STRAINING

7.1 Introduction

The nature of CNT films in structure is that CNTs as conductive tubes are distributed on or within polymer matrix. When the CNT film is under in-plane straining, the tubes displace with the substrate, which causes the conductance of the film change. This change mechanism, as now known, is due to reconfiguration of the CNT networks. During the reconfiguration process, the bonding between the nanotube and polymer matrix can likely be a significant factor (Liao et al., 2003).

In this chapter, a study on the interaction between the CNT and polymer matrix for the CNT film (fabricated with the approach developed in this thesis) is presented. The goals of the study were (i) to examine the slipping phenomenon and (ii) to develop a model which describes the underlying mechanism. Two types of films were studied: CNT-only films (regular films) and sandwiched CNT films (CNTs are in between polymer matrix).

7.2 Materials and Methods

Fabrication Process: The SWNTs (HiPCo-CNTs) was purchased from Unidym Inc. The fabrication method for CNT films was same as proposed formerly by Miao et al. (2010). The concentration of 0.05mg/ml of SWNTs suspension (the 1 wt% Sodium Dodecyl Sulfate as surfactant removed afterwards in the fabrication) was sonicated for 2 hours and

deposited on the Polyethylene Terephthalate substrate (PET, Melinex 329). The CNT films with 1, 3, 5 layered networks were fabricated respectively. It should be noted that a long sonication hour, low concentration of the suspension and low number of layered dispositions were used to ensure the dispersion of CNT bundles into individual tubes to avoid the situation where tubes stay in the bundle (Ajayan et al., 2000).

CNT films with the sandwiched structures can also be made where CNT networks are located in between two polymer layers. The fabrication method for such films has been proposed by Miao et al. (2012). In this chapter, 0.05mg/ml suspension of SWNTs (the 1wt% Sodium Dodecyl Sulfate as surfactant removed afterwards in the fabrication) was sonicated for 2 hours and deposited on the PET (Melinex 329) substrate and then 3 wt% of PMMA/chloroform (Sigma and Aldrich) solution were spin coated on the top of formed networks. The CNT film sandwiched samples with 1, 3, 5 layered networks were fabricated, respectively.

Both types of film samples were first tested under the Instron Tester 1122 and their mechanical properties were shown about the same with yield point of 4%~5% at 1kN tensile load.

A homemade mini tensile tester was designed for this study and was fabricated at the Engineering Workshop at the University of Saskatchewan. The structural details of the tester are seen in Appendix B. Both film samples were cut and fixed in the tensile tester with 25 mm long, as shown in Figure 7.1. During the tensile test, film samples were

elongated upon the rupture point in the unit step of 0.5 mm, which was half turn on the handle of the tester.

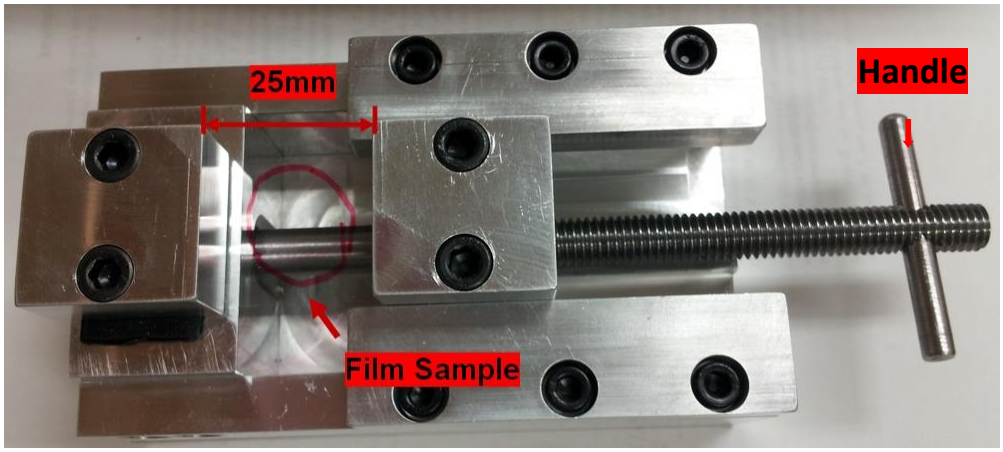

Figure 7.1 The CNT film sample fixed in the homemade mini tensile tester with 25mm of original length

Raman Characterization: Raman measurement (with a Renishaw Microscope 2000) was used in this study to examine the wavenumber of the D* band on nanotubes in the films (owing to its suitability to study carbon materials, see the previous discussion in section 4.4). After the film samples were placed in the home-made tensile tester, Raman spectra were obtained in the backscattering geometry with 785nm line of 1.5mW laser (x50 lenses and 1% laser power used). The polarized laser beam was focused on the film samples with about the 2 μm diameter laser spot.

The laser polarization direction in Raman microscopy was set to be parallel to the applied tensile straining. The spectroscopy in Raman selected out the signal from the nanotubes

lying along the polarization direction. In both film samples, nanotubes were randomly distributed on the polymeric substrate. Therefore only the tubes with mechanical strain along with the applied tensile load were examined within the laser scanning spot (Wagner et al., 2001). In the tensile test, Raman scanning was performed and recorded after each 0.5 mm (0.02 ε) elongation. As a result, the wavenumber of the D* band was the average value (automatically calculated in the system) from tubes whose alignments were along with the tensile loading directions.

7.3 Results and discussion

In both film samples, nanotubes were embedded or partially embedded in polymeric matrix. Prior to the testing, there has already been some D* band wavenumber shift due to the pre-stress induced from the interaction between the tubes and polymer matrix, as shown in Figure 7.2. It can be seen from the figure that the peak position of the wavenumber of the D* Band on tubes from both film samples increases with respect to their peak position in air at room temperature and pressure. Under the room condition, the atmosphere pressure (1atm) is small compared with the external pressure from the surrounding polymer matrix. As a result, such shifts in both film samples are a consequence of the polymer matrix where nanotubes apparently responded to the external force. In both type films, the D* band wavenumber of tubes was about the same among different numbers of layered networks (different network densities). Therefore, the Van der Waals (VDW) interaction among CNT bundles was not the major external force compared with the applied external force on the tubes from surrounding polymer matrix.

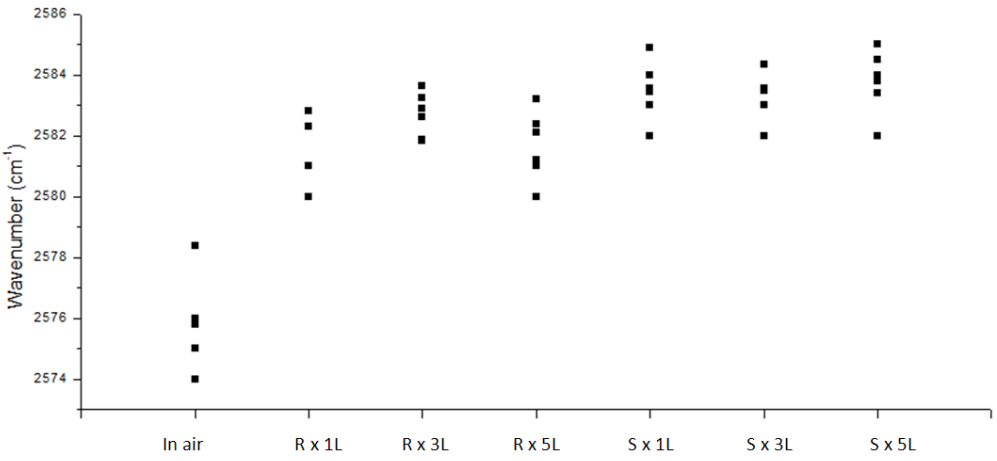

Figure 7.2 The peak position of the D* band wavenumber of tubes in both film samples with respect to their peak position in air; the number of layered networks, represented by 1L,3L,5L; Regular and Sandwiched types of films represented by capital R and S, respectively

When both film samples were subjected to the in-plane straining, the mechanical strain was transformed from surrounding polymer matrix to the tube, which caused the D band* wavenumber peak shift linearly with respect to the applied strain. The experimental results obtained from the regular CNT films were shown in Figure 7.3. The change in wavenumber with respect to the applied tensile strain has constant values of -51.75cm^{-1}/strain up to 0.12ε.

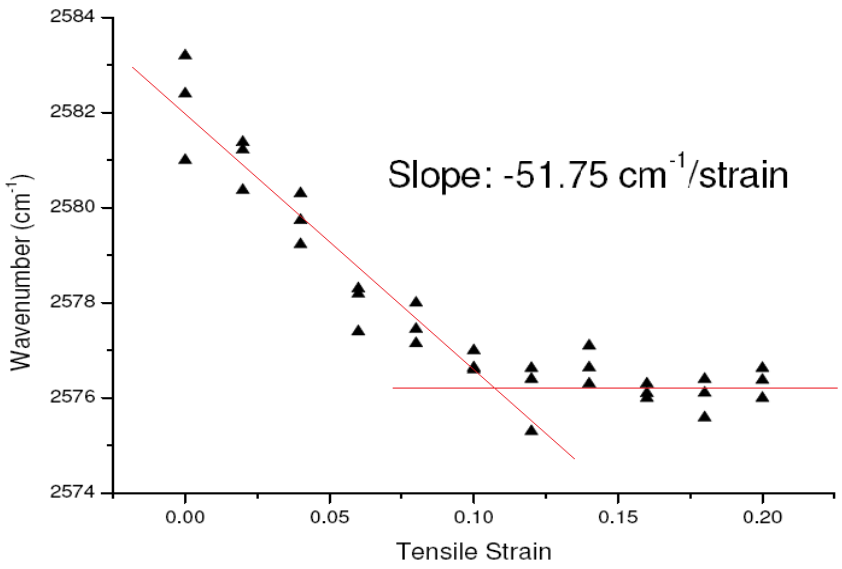

Figure 7.3 The change in wavenumber of the D* band of nanotubes with respect to the applied tensile strain in regular CNT films

For the film with the sandwiched structure, the wavenumber shifts of the D* band with respect to the applied in-plane strain was shown in Figure 7.4. By comparing with regular films, the wavenumber peak shifts linearly with the applied strain at constant value of -135.3cm^{-1}/strain and up to 0.25ε point, where the upper PMMA layer started to peel off from the PET substrate.

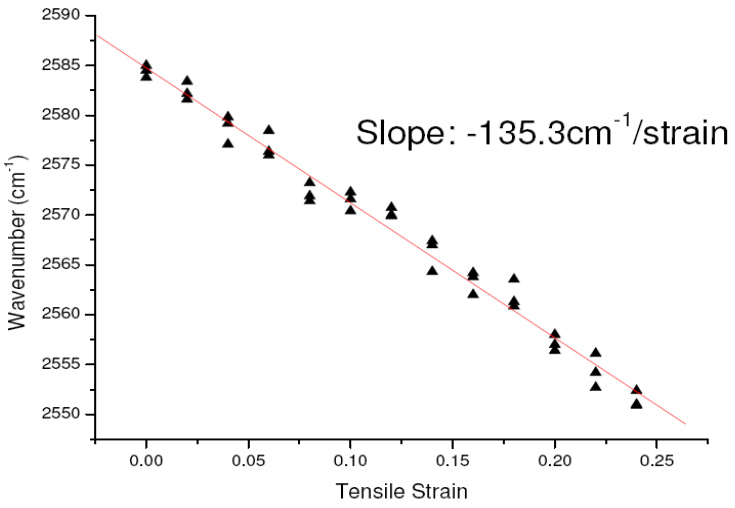

Figure 7.4 The change in wavenumber of the D* band of nanotubes with the applied tensile strain in sandwiched type of CNT films

In CNT composite films, Wagner et al. (1999) proposed that the nanotubes were completely embedded into the polymer matrix. When the film was under in-plane straining, their model showed that the external pressure (p) from the surrounding polymer matrix is attributed to the axial stress (σ) on the tube, as described by

$$\sigma = \frac{pR}{2t} \qquad (7.1)$$

where σ is the stress in the axial direction, p is the pressure and R and t are the radius and thickness of the nanotube. This model was, however not applicable to the situation here due to the following reasons: 1) p in their model refers to the internal pressure rather than to the external one; 2) In the films of the present study, nanotubes were partly embedded into polymer matrix, whereas their model assume that the nanotubes are completely embedded in the polymer matrix. A new model is needed for the CNT films in the present study. Figure 7.5 shows a schematic model of the present situation, where the

tube is placed in the middle of the polymer matrix and aligned along with the applied tensile load F.

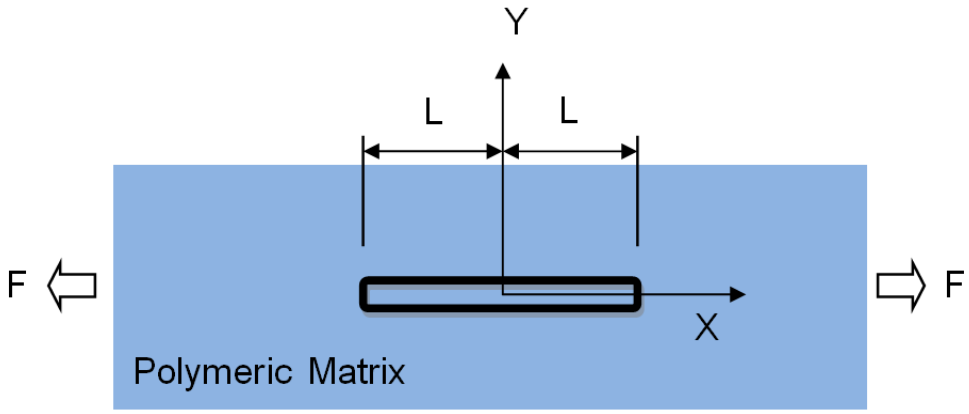

Figure 7.5 The schematic model of the tube placed in the middle of the polymer matrix and aligned along with applied tensile load F

Under the applied tensile load F, the interactions of the tube with polymer matrix can be categorized into two situations. In the first situation, the interfacial cohesion between the tube and polymeric matrix was strong enough so that no slipping can happen at the interface. As results, the strain ε_c from the tube can be described as

$$\varepsilon_c = \varepsilon_p = \frac{F}{EpAp} \tag{7.2}$$

, where ε_p is the strain from polymer matrix, F is the applied tensile load, E_p is the elastic modulus of the polymeric matrix and A_p is the cross section area of the polymeric matrix. Details of derivation of all equations in this chapter are attached in Appendix A. According to equation 7.2, the strain ε_c from the tube and the strain ε_p from the polymeric matrix have the same constant value.

In the second situation, the interfacial cohesion between the tube and polymeric matrix was not strong enough so that the slipping happens at the interface. In this situation, the tube was considered as a smooth bar (hollow cylinder, nanotubes were cut after the sonication process) and its surface roughness was assumed to be the same along the tube. In this situation, the interfacial cohesion F_v with the polymeric matrix is constant along the tube, which can be expressed by

$$F_v(x) = \alpha, \ -L<x<L \tag{7.3}$$

where α is a constant. The strain ε_c from the tube can therefore be described by

$$\varepsilon = \begin{cases} \dfrac{2\pi r\alpha(x+L)}{EcAc}, (-L < x < 0) \\ \dfrac{2\pi r\alpha(x-L)}{EcAc}, (0 < x < L) \end{cases} \tag{7.4}$$

where r is the radius of the tube, E_c is the elastic modulus of the tube and A_c is the cross section area of the tube. According to equation 7.4, the strain ε_c on the tube was no longer a constant and is not the same as the strain ε_p (constant value) in the polymeric matrix.

In the CNT composite films, Zhao et al. (2001) proposed that the stress on tubes was equal to the stress in the polymer matrix. The slope of wavenumber of the D* band on tubes was about -1422cm^{-1}/strain for their case. In the films of the present study, the slopes were about -51.75cm^{-1}/strain for regular film and -135.3cm^{-1}/strain for the sandwich film, respectively. Since the shifts of the D* band wavenumber were sensitive to breathing modes (mechanical strain) along the tube axis, the lower slope value in the film samples in present study demonstrates that the nanotubes experience less axial strain in comparison with the nanotubes in CNT composite films. Therefore, it is reasonable to

conclude that the stress transition in CNT composite films belong (or close) to the first situation (equation 7.2) while the stress transition in CNT films in the present study belong to the second situation (equation 7.4).

In both film samples, the slipping (ε_{slip}) at the interface can be described by

$$\varepsilon_{slip} = \varepsilon_p - \varepsilon_C = \begin{cases} \dfrac{F}{E_p A_p} - \dfrac{2\pi r\alpha(x+L)}{E_C A_C}, -L < x < 0 \\ \dfrac{F}{E_p A_p} - \dfrac{2\pi r\alpha(L-x)}{E_C A_C}, 0 < x < L \end{cases} \tag{7.5}$$

and the average strain ratio between polymeric matrix (ε_p) and the tube (ε_c) can be described by

$$\frac{(\varepsilon_p)_{avg}}{(\varepsilon_C)_{avg}} = \frac{FE_C A_C}{E_p A_p \pi r\alpha L} \tag{7.6}$$

where $\dfrac{E_C A_C}{E_p A_p \pi r L}$ is a constant and $(\varepsilon_p)_{avg}$ is equal to ε_p. According to equation 7.6, the $(\varepsilon_c)_{avg} / (\varepsilon_p)_{avg}$ ratio was determined by α/F value. The tensile test performed on Instron 1122 has further shown that both film samples in the present study have the same mechanical properties (thus the same F value). In the films with the sandwiched structures, the tubes experienced higher interfacial cohesion (α) from the upper PMMA layer as compared with the tubes in the regular films. The $(\varepsilon_c)_{avg} / (\varepsilon_p)_{avg}$ ratio was thus supposed to be higher in the film with the sandwiched structure than that in the regular

film. This proposition was in consistent with the experimental results in the present study that the slope (-135.3cm^{-1}/strain) obtained from the films with the sandwiched structure are about 3 times greater than the slope (-51.75cm^{-1}/strain) from the regular films.

Under in-plane straining, the previous study has shown that the nanotubes displace with the polymer matrix upon the rupture points of the films (Miao et al., 2011). However, the wavenumber D* band shifts in both films stopped at the applied tensile strain of 0.1 and 0.25, respectively. Similar tendency also appeared in CNT composite films (Zhao et al., 2001). It is reasonable to conclude that the slipping at the interface between the tube and polymer matrix happens in the entire process of straining. When the bondings between the tube and polymer matrix were broken by the slipping, the bonding area on the tube decreased gradually to the point where the bonding area (thus straining area) become so small that the Raman signals cannot detect the variation (since the signal was the averaged value of the entire tube). As a result, the shift of the D* band wavenumber stopped and the tube however, with a small area bonded with the polymer matrix, continuously displaced in the films.

According to equation 7.4, the strain ε_c value (thus stress σ_c) decreases gradually from the centre of the tube to its both ends. In contrast, the slipping at the interface was inclined to start initially from both ends (low straining area) to the middle (high straining area) on the tube. The simulation result by Ansys 11.0 was shown in Figure 6 (solid 45, contact pairs, mapped mesh to the curved lines). The simulation model (Figure 6a) included the tube with its surface partially bonded with polymer matrix. The elastic modulus of the

tube and polymer matrix was estimated as 1TPa and 3GPa, respectively. The interfacial cohesion (physical bonding) was predetermined as 5MPa, which was within the range of the results (less than 10MPa) by Mader et al. (1996) and close to the simulation results (about 2MPa) by Frankland et al. (2002). When the polymer matrix was under in-plane straining, the shear stress density on the tube decreased gradually from the middle to its both ends, as shown in Figure 7.6 (b) - (f). Therefore, the slipping at the interface (low straining area) started to happen from both ends to the middle. According to Kelly and Tyson model as described as (Kelly et al., 1965)

$$\tau_c = \left(\frac{\sigma_c(L_c)}{2(L_c/D_c)}\right)\left(1 - \frac{{d_c}^2}{{D_c}^2}\right) \tag{7.7}$$

where d_c (1.6nm) and D_c (2nm) are the inner and outer diameters of the tube respectively, L_c (800nm after 4 hours sonication (Hecht et al., 2006)) is the length of the tube. Because the shear stress at the interface was taken as 3-35MPa (as shown in Figure 7.6), this translates to an interfacial normal stress in the tube between 6.6GPa~78GPa according to equation 7.7 (normal stress of 50GPa was estimated by Wagner et al., 1997). Since the elastic modulus of the tube was about 1TPa, it was thus much easier to slide the nanotube with polymer matrix than to break it.

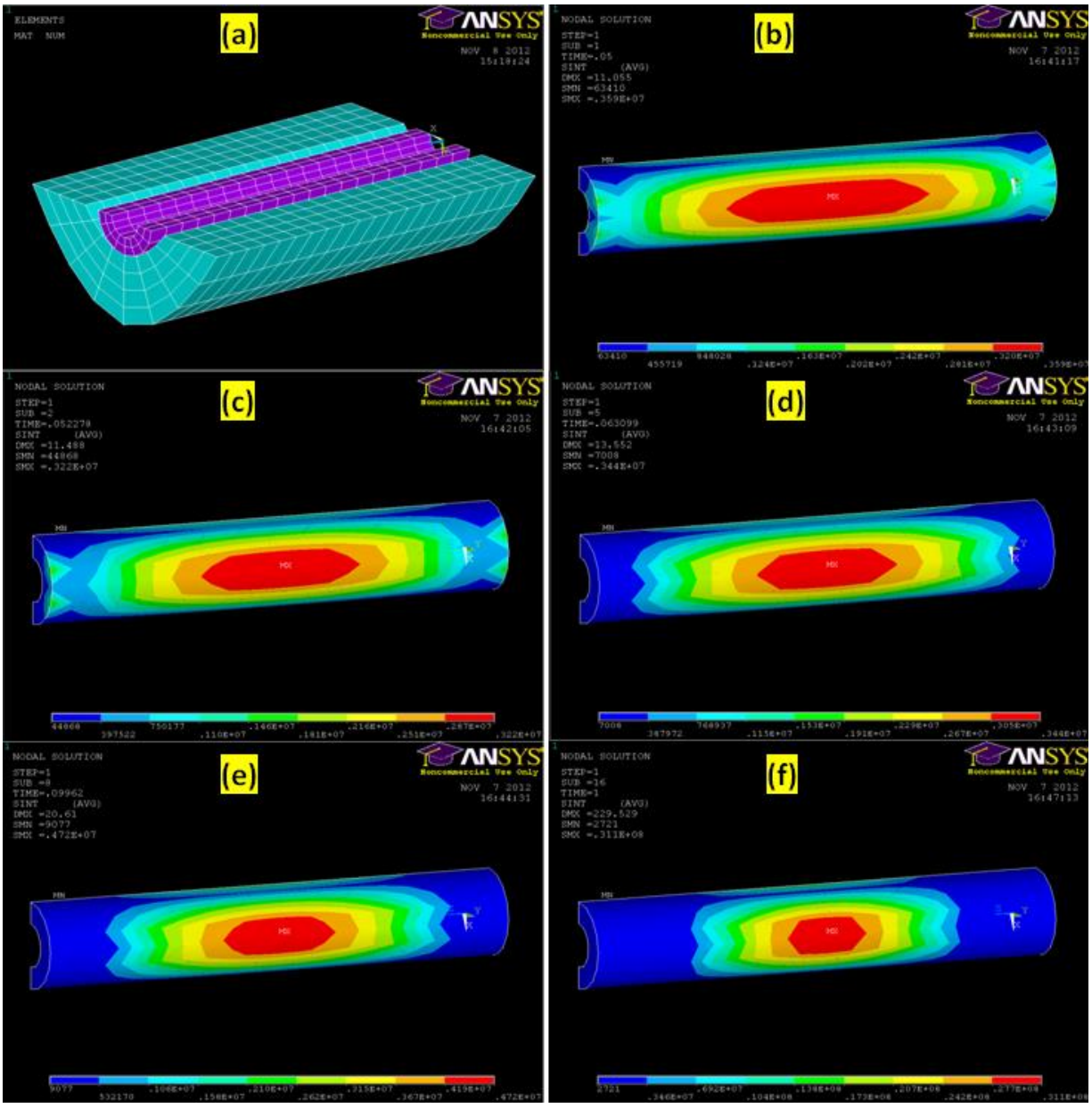

Figure 7.6 (a) Nanotube partly bonded with polymer matrix and the tensile stress applied gradually to the polymer matrix, (b) ~ (f) the shear stress intensity on the tube when the applied tensile stress to the polymer matrix increases to:(b)2MPa, (c) 5MPa, (d)10MPa (e)17MPa (f) 35Mpa

7.4 Conclusions

Two types of CNT films were fabricated for in the present study. When the film was subjected to an in-plane straining, it was found that the D band* wavenumber peak shifts linearly with the applied strain. As compared with CNT composite films, the low slope value in CNT films in the present study suggests that the slipping occur at the interface between the tube and polymer matrix in the process of in-plane straining.

The new model built in the present study is also in agreement with the experimental results that the bonding between the tube and the polymer matrix in CNT films can be broken due to the slipping.

CHAPTER 8

CONCLUSION AND RECOMMENDATIONS

8.1 Overview and Conclusions

The CNT based films can be used for strain detection, which is one of the most encouraging finding recently. There are two types of CNT based films for strain detection, namely CNT composite film and CNT film. The major difference between them is that the CNT film is free of polymeric surfactant while the CNT composite film contains polymeric surfactant. Several methods are available in the literature to fabricate them, which are the buckypaper method, molding transfer method, Layer-by-Layer deposition method and CVD method.

This thesis was focused on the in-plane strain detection with CNT films. This was motivated by less understanding of mechanisms underlying CNT films as an in-plane strain sensor. More specifically, there was no study on the relationship between the performance of CNT film sensors and their structures such as density of CNT networks and configuration of CNT networks. Methods for fabrication of CNT films with different configurations especially aligned CNT networks in large scale were not available. Last, mechanism that governs interactions between the CNTs and polymer matrix, for CNT films was not clear in the literature. The specific objectives of this thesis study were defined as:

(1) To study the relation between conductance and density in randomly distributed CNT networks of CNT films, in particular whether the stick percolation model is valid to the CNT networks of the films.

(2) To develop a method to fabricate CNT films with aligned CNT networks and to investigate piezoresistive response of these films. A care must be taken that in the literature, there were methods available for fabricating aligned CNT networks but not for CNT films.

(3) To study the interaction of the nanotubes with the polymer matrix of CNT films under in-plane straining. It is noted that in the literature, there were studied on this problem but not on CNT films in particular.

The thesis first presented three comprehensive literature reviews related to the research objectives. In particular, the mechanism of piezoresistive response in CNT networks as well as the corresponding mathematical model was reviewed in Chapter 2. In Chapter 3, methods for fabricating aligned CNT networks were reviewed, which are potentially applicable to CNT films. In Chapter 4, the literature regarding interaction between the nanotube and the polymer matrix was reviewed, as well as the technique and the developed model to study the interaction.

In Chapter 5, the CNT films with randomly distributed CNT networks were fabricated by the Layer-by-Layer deposition method. The relation between density and conductance in CNT networks was established. The models were developed to describe the relationship between their density and gauge factor and the relationship between their density and linearity in CNT networks.

In Chapter 6, a method based on magnetic alignment and spray deposition was proposed to fabricate aligned CNT networks for CNT films. CNTs (MWNTs) were first decorated with iron oxide nanoparticles to enhance their magnetism. Under the external magnetic field, the nanotubes decorated with iron oxide nanoparticles were rotated into one direction to form aligned networks. The CNT films with aligned CNT networks were further investigated under to two probe conductive measurements and strain detections.

In Chapter 7, Raman microscopy was employed to study the axial strain on the nanotube. In particular, the D band* wavenumber peak of CNTs was taken to study the interaction the nanotube and polymer matrix when the CNT film was under the in-plane straining.

The following conclusions can be drawn from this thesis:

(1) Randomly distributed CNT networks of CNT films follow the stick percolation model with the critical exponent coefficient (α) in the model being 1.938.

(2) The theoretical models developed in Chapter 5, one for the relation between the density and gauge factor and one for the relation between the density and linearity for the

CNT film subjected to in-plane straining, are accurate. Based on these models, an optimal in-plane strain sensor built upon the CNT film should be such that its density is around 2.

(3) Decoration of SWNTs with iron oxide nanoparticles is difficult to be achieved by the proposed method, but for MWNTs, this method is highly feasible and achieved. The decorated CNTs with iron oxide nanoparticles exhibited enhanced magnetism.

(4) The CNT films with aligned CNT networks were achieved by spray deposition with the aid of externally applied magnetic field. The configuration of CNT networks in CNT films with respect to the direction of straining is an important factor to determine piezoresistive response.

(5) When the CNT film were subjected to the in-plane straining, it was found that the D band* wavenumber peak shifts linearly with the applied strain, which was the consequence of inducing axial strain on the tubes from polymer matrix.

(6) The low slope value in CNT films indicate that the slipping occurs at the interface between the tube and polymer matrix in the process of in-plane straining. The new model developed in Chapter 7 is also in agreement with the experimental results that the bonding between the tube and the polymer matrix in CNT films can be broken due to the slipping.

8.2 Major Contributions of Thesis

This thesis research has generated several "firsts", implying the contributions to the field of CNT networks for strain detection. All contributions are summarized in the following:

(1) Provision of a mathematical model based on the percolation theory to describe the piezoresistive response in randomly distributed CNT networks as the films are under in-plane straining.

(2) Fabrication of aligned CNT networks with uniform distribution and in large scale for CNT films, which can be used in strain detection.

(3) Discovery of the influence of piezoresistive response from the configuration of CNT networks in CNT films with respect to the direction of straining.

(4) Proof of slipping situation existing at the interface between the tube and the polymer matrix in CNT films under in-plane straining.

8.3 Future work

Future works are expected to improve this thesis work. First, the theoretical percolation model is based on the same conducting sticks. However, CNT networks contain both metallic and semiconducting tubes, where the Schottky Barrier can arise between their interconnections to affect their conductance, causing the major discrepancy in the present study between the theoretical and experimental results. The hypothesis here is that non-mixed CNTs (either metallic or semiconductive) would more follow the percolation model. The testing of this hypothesis should be an interesting future work. Meanwhile, investigation of a more accurate model for the mixed CNTs is an interesting future work as well.

Second, the CNT films (MWNT in this case) with aligned CNT networks were fabricated in this study, the fabrication method, however, required the nanotubes to be decorated with iron oxide nanoparticles. The CNT networks decorated with iron oxide nanoparticles however can reduce the conductance of CNT films. Therefore, it is worth to develop a new approach to form aligned CNT networks without a need of decorating iron oxide nanoparticles.

Finally, the governing principle for two aligned CNT networks of the CNT film is not known yet. It is likely the same as that for random distributed CNT networks of the CNT film. Nevertheless, this needs to be confirmed.

REFERENCES

Ajayan, M. P.; Schadler, L.S.; Giannaris, C.; Rubio, A.; 2000. Singe-walled carbon nanotube-polymer composite: strength and weakness. Advanced Materials, 12:10.

Ajayan, P.M.; Stephan, O.; Colliex, C.; Trauth, D.; 1994. Aligned Carbon Nanotube Arrays Formed by Cutting a Polymer Resin—Nanotube Composite. Science Journal, 265:1212.

Ali-zade, R.A.; 2009. Kinetics of first stage of formation magnetite nanoparticles prepared by chemical precipitation method. doi:10.1088/1742-6596/153/1/012041.

Anand, S.; Mohapatra, M.; 2010. Synthesis and applications of nano-structured iron oxides/hydroxides- a review. Journal of Engineering, Science and Technology, 2:8:127-146.

Broadbent, S.; Hammersley, J.; 1957. Percolation processes I. crystals and mazes. Cambridge Philosophical Society, 53: 629–641.

Bunde, A.; Kantelhardt, J.W.; 1996. Introduction to Percolation Theory Part (A). Available online: http://www.physik.uni-halle.de/Fachgruppen/kantel/11-99-springer_polen_buch.pdf.

Bunde, A.; Dieterich, W.; 2000, Percolation in composites. Journal of eletroceramics, 5:2: 81-92.

Cao, F.; Zhong, K.; Gao, A.; Chen, C.; Li, Q.; Chen, Q.; 2007. Reducing reaction of Fe_3O_4 in nanoscopic reactors of a-CNTs. Physical Chemistry B, 111: 7: 1724–1728

Chen, W.; Pan, X.; Willinger, M.G.; Su, D.S.; Bao, X.; 2006. Facile autoreduction of iron oxide/carbon nanotube encapsulates. The American Chemical Society, 128: 10: 3136–3137.

Chun, Y.S.; Shin, J.Y.; Song, C.E.; Lee, S.G.; 2008. Palladium nanoparticles supported onto ionic carbon nanotubes as robust recyclable catalysts in an ionic liquid. Chemical Communications, 8: 942–944.

Choi, H.C.; Shim, M.; Bangsaruntip, S.; Dai, H.; 2002. Spontaneous reduction of metal ions on the sidewalls of carbon nanotubes. The American Chemical Society, 124: 9058–9059.

Choi, E.S.; Brooks, J.S.; Eaton, D.L.; Al-Haik, M.S.; Hussaini, M.Y.; Garmestani, H.; Li, D.; Dahmen, K.; 2003. Enhancement of Thermal and Electrical Properties of Carbon Nanotube Polymer Composites by Magnetic Field Processing. Journal of Applied Physics, 94:9.

Cochrane, C.; Koncar, V.; Lewandowski, M.; Dufour, C.; 2007. Design and development of a flexible strain sensor for textile structures based on a conductive polymer composite. Sensors, 7: 473-492.

Day, T.M.; Unwin, P.R.; Wilson, N.R.; Macpherson, J.V.; 2005.Electrochemical Templating of Metal Nanoparticles and Nanowires on Single-Walled Carbon Nanotube Networks. The American Chemical Society, 127:10639-10647.

Dharap, P.; Li, Z.L.; Nagarajaiah, S.; Barrera, E.V; 2004. Flexural strain sensing using carbon nanotube film sensor. Sensor Review, 24: 271–273.

Domingo, C.; Rodriguez-Clemente, R.; Blesa, M.; 1994. Morphological properties of α-FeOOH, γ-FeOOH and Fe_3O_4 obtained by oxidation of aqueous Fe (II) solutions. Colloid and Interface Science, 165: 244-252.

Dresselhaus, S.G.; Dresselhaus, G., 2004, Physical Properties of Carbon Nanotubes. Imperial College Press, 30-80.

Dresselhaus, G.; Rao, A. M.; Richter, E.; Bandow, S.; Chase, B.; Eklund, P. C.;Williams, K. A.; Fang, S.; Subbaswamy, K. R.; Menon, M.; Thess, A.; Smalley, R. E.; Dresselhaus, M. S.; 1997. Diameter-Selective Raman Scattering from Vibrational Modes in Carbon Nanotubes. Science, 275:187-191.

Feller, J.F.; Linossier, I.; Grohens, Y.; 2002. Conductive polymer composites: Comparative study of poly (ester)-short carbon fibers and poly (epoxy)-short carbon fibers mechanical and electrical properties. Materials Letters, 57: 64-71.

Frankland, S.J.V.; Caglar, A.; Bremmer, D.W and Griebel, M.; 2002. Molecular simulation of the influence of chemical cross-links on the shear strength of carbon nanotube polymer interfaces. The Journal of Physics Chemistry B, 106:3046-3048.

Gruner, G.; Artukovic, E.; Kaempgen, M.; Hecht, D.S.; 2005. Transparent and flexible carbon nanotube transistors. Nano Letter, 5: 4: 757- 760.

Haggnemueller, R.; Gommans, H.H.; Rinzler, A.G.; Fischer, J.E.; Winey, K.I.; 2000. Aligned Single-Wall Carbon Nanotubes in Composites by Melt Processing Methods. Chemical Physics Letter, 330:219-224.

Haus, J.; 2010. Optical Sensor Basics and Applications. Wilety-VCH, 30-130.

Hecht, D.S.; Thomas, D.; Hu, L.B.; Ladous, C.; Lam, T.; Park, Y.; Irvin, G.; Drzaic, P.; 2007. Carbon-nanotube film on plastic as transparent electrode for resistive touch screens. Available online: http://www.unidym.com/files/CNT_Film_on_Plastic.pdf.

Hecht, D.; Hu, L.B.; Grünera, G.; 2004. Percolation in transparent and conducting carbon nanotube networks. Nano Letters, 4:12:2513-2517

Hecht, D.; Hu, L.B.; Grünera, G.; 2006. Conductivity scaling with bundle length and diameter in single walled carbon nanotube networks. Applied Physics Letter, 89: 133112-133115.

Horner, O.; Neveu, S.; Montredon, S.; Siaugue, J.M.; Cabuil, V.; 2009. Hydrothermal synthesis of large maghemite nanoparticles: influence of the pH on the particle size, Nanoparticles Research, 11:5: 1247-1250.

He, H.H.; Gao, C., 2011. Synthesis of Fe_3O_4/Pt Nanoparticles Decorated Carbon Nanotubes and Their Use as Magnetically Recyclable Catalysts. Nanomaterial, doi:10.1155/2011/193510.

Hedberg, J.; Dong, L.F.; Jiao, J.; 2005. Air flow technique for large scale dispersion and alignment of carbon nanotubes on various substrates. Applied Physics Letters, 86: 143111.

Iijima, S.; Ajayan, S.; Ichihashi, P.M.; 1991. Growth model for carbon nanotubes. Physics Review Letter, 69: 3100–3103.

Jang, J.; Lee, K.J.; Kim, Y.; 2005. Fabrication of polyimide nanotubes and carbon nanotubes containing magnetic iron oxide in confinement. Chemical Communications, 30:3847–3849.

Jiang, L.Y.; Tan, H.L.; Wu, J.; Huang, Y.G.; Hwang, K.C.; 2009. Continuum modeling of interfaces in polymer matrix composites reinforced by carbon nanotubes. Nanoscale Research Letters, 303: 7573.

Jin, L.; Bower, C.; Zhou, O.; 1998. Out-of-Plane Mosaic of Single Wall Carbon Nanotube Films. Applied Physical Letter, 84:2171-2177.

Kaempgen, M.; Dusberg, G.S.; Roth, S.; 2005. Transparent carbon nanotube coatings. Applied Surface Science, 252: 425-429.

Kaempgen, M.; Roth, S.; 2006. Transparent and flexible carbon nanotube/polyaniline pH sensors. Journal of Electroanalytical Chemistry, 586:72-76.

Kaniyoor, A.; Jafri, R.I.; Arockiadoss, T.; Ramaprabhu, S.; 2009. Nanostructured Pt decorated graphene and multi walled carbon nanotube based room temperature hydrogen gas sensor. Nanoscale, 1: 3: 382–386.

Kang, I.; Schulz, M.J.; Kim, H.J.; Shanov, V.; Shi, D.L.; 2006. A carbon nanotube strain sensor for structural health monitoring. Smart Materials, 15: 737–748.

Kelly, A.; Tyson, W.R.; 1965. Tensile properties of fiber-reinforced metal: Copper/Tungsten and Copper/molybdenum. Journal of the Mechanics and Physics of Solid, 13:6:329-338.

Kim, Y.J.; SHIN, T.S.; Choi, H.D.; Kwon, J.H.; Chung, Y.C.; Yoon, H.G.; 2005. Electrical conductivity of chemically modified MWNT/epoxy composites. Carbon, 43:23.

Korneva, G.; Ye, H.; Gogotsi, Y.; 2005. Carbon nanotubes loaded with magnetic particles. Nano Letters, 5:5: 879–884.

Kuznetsova, A.; Mawhinney, D. B.; Naumenko, V.; Yates, J. T., Jr.; Liu, J.; Smalley, R. E.; 2000. Enhancement of adsorption inside of single-walled nanotubes: opening the entry ports. Chemical Physics Letters, 321:292-296.

Lauren, S.; Forge, D.; Port, M.; Roch, A.; Robic, C.; Vaner, L.; 2008. Magnetic Iron Oxide Nanoparticles: Synthesis, Stabilization, Vectorization, Physicochemical Characterizations, and Biological Applications. Chemical review, 108:2064-2110.

Lay, M.D.; Duncan, A.; Zhang, Q.H.; Vichchulada, P.; 2009. Macroscopic Electrical Properties of Ordered Single-Walled Carbon Nanotube Networks. Applied Materials and Interfaces, 2:467-473.

Lay, M.D.; Duncan, A.; Zhang, Q.H.; Vichchulada, P.; 2009. Percolation in Networks of Aligned SWNTs Formed with Laminar Flow Deposition. Journal of Mater Science, 44: 1206-1211.

Li, W.; Gao, C.; Qian, H.; Ren, J.; Yan, D.; 2006.Multiaminofunctionalized carbon nanotubes and their applications in loading quantum dots and magnetic nanoparticles. Materials Chemistry, 16: 19: 1852–1859.

Li, J.T.; Zhang, S.L.; 2009. Finite-size scaling in stick percolation. Physical Review E, 80: 040104.

Liao, K.; Wong, M.; Paramsothy, M.; Xu, X.J.; Ren, Y.; Li, S.; 2003. Physical interaction at carbon nanotube-polymer interface. Polymer, 44: 7757-7764.

Liao, K.; Li, S.; 2001. Interfacial characteristics of a carbon nanotube-polystyrene composite system. Applied Physics Letter, 79: 4225.

Liang, X.G.; Lukes, J.R.; Tien, C.L.; 1998. Anisotropic thermal conductance in the thin layer of disordered packed spheres. The 11th International Heat Transfer Conference, 7:31-35.

Liptak, B.G.; 2003. Process Measurement and Analysis 1. CRC Press, 622-1333.

Liu, S.; Song, X.H.; Gan, Z.Y.; Lv, Q.; Cao, H.; Yan, H.; 2009. Controllable fabrication of carbon nanotube-polymer hybrid thin film for strain sensing. Microelecticnic Engineering, 86: 11: 2330-2333.

Lordi, V.; Yao, N.; 2000. Molecular mechanics of binding in carbon-nanotube-polymer composites. Journal of Materials Research, 15: 2770.

Lynch, J.P.; Kenneth, J.; Nicholas, A.; 2008. Inductively coupled nanocomposite wireless strain and pH sensor. Smart Structure and System, 4: 531-548.

Lynch, J.P.; Loh, K.J.; Shim, B.S.; Kotov, N.A.; 2007. Tailoring piezoresistive sensitivity of multilayer carbon nanotube composite strain sensors. Journal of Intelligent Material Systems and Structures, 19: 747-749.

Mader, E.; Jacobasch, H.J.; Grundke, K.; Gietzelt, T.; 1996. Influence of an optimized inter-phase on the properties of polypropylene glass fiber composites. Composites Part A, 27:9:907-912.

Martinez, F.; Obieta, G.; Uribe, I.; Skiora, T.; Ochoteco, E.; 2010. Polymer-based self-standing flexible strain sensor. Journal of Sensors, 2010: doi:10.1155/2010/65

Miao, Y.; Chen, L.; Lin, Y.; Sammynaiken, R.; Zhang, W.J.; 2011. On finding of high piezoresistive response of CNT films with surfactants for in-plane strain detection. Journal of Intelligent Material Systems and Structures, 22:18:2155-2159.

Miao, Y.; 2010. A new strain sensor based on CNT films. Available online: http://library2.usask.ca/theses/available/etd-08172010-165151/.

Miao, Y.; Yang, Q. Q.; Sammynaiken, R.; Zhang, W.J.; 2012. The multi-wall carbon nanotube film sensor for in-plane strain detection. The 3rd International Conference on Nanotechnology: Fundamentals and Applications.

Miao, Y.; Lin, Y.; Chen, L.; Sammynaiken, R.; Zhang, W.J.; 2011. Optimization of piezoresistive response of pure carbon nanotubes networks as in-plane strain sensors. Review of Scientific Instruments, 82:12:126104.

Miao, Y.; Yang, Q. Q.; Sammynaiken, R.; Zhang, W.J.; Chen, L.; 2012. Modeling of piezoresistive response of carbon nanotube network based films under in-plane straining by percolation theory. Applied Physics Letter, 101:063120.

Miguel, A.C.; Grzelczak, M.; Maceira, V.S.; Giersig, M.; Diaz, R.; 2005. Alignment of Carbon Nanotubes under Low Magnetic Fields through Attachment of Magnetic Nanoparticles. Physical Chemistry B, 109:19060-19063.

Minot, E.D.; Park, J.Y.; Brink, M.; McEwen, P.L.; 2002. Tuning carbon nanotube band gaps with strain. Physics Reviews Letters, 90: 15.

Mladenovic, D.; Hutchins, J.; Tran, E.; Lu, S.; 1998. Elements for Modeling Diffused Piezoresistor Temperature Coefficient and Sensitivity. Technical Proceedings of the 1998 International conference on modeling and simulation of Microsystems, C4:145-150.

Mohammed, A.S.; Moussa, W.A.; Lou, E.; 2008. High sensitivity MEMS strain sensor: design and simulation. Sensors, 8:2642-2661.

Niyogi, S.; Hamon, M. A.; Hu, H.; Zhao, B.; Bhowmik, P.; Sen, R.; Itkis, M. E.; Haddon, R. C.; 2002. Chemistry of Single-Walled Carbon Nanotubes. Accounts of Chemical Research, 35:1105–1113.

Paloniemi, H., Lukkarinen, M.; Aaritalo, T.; Areva, S.; Leiro, J.; Heinonen, M.; Haapakka, K.; Luddari, J.; 2006. Layer-by-Layer electrostatic self-assembly of single-wall carbon nanotube polyelectrolytes. Langmuir, 22: 74–83.

Peijs, T.; Bilotti, E.; Reynolds, C. T.; Zhang, R.; Deng, H.; 2009. A novel concept for highly oriented carbon nanotube composite tape or fibres with high strength and electrical conductivity. Macromolecular Materials and Engineering, 294:749- 755.

Pike, G.E.; Seager, C.H.; 1973. Percolation and conductivity: a computer study. I. Physical Review B, 10:1421-1434.

Qiu, J.; Li, Q.; Wang, Z.; Sun, Y.; Zhang, H.; 2006. CVD synthesis of coal-gas-derived carbon nanotubes and nanocapsules containing magnetic iron carbide and oxide. Carbon, 44:12: 2565–2568.

Richard, C.; Doan, B.T.; Beloeil, J.C; Bessodes, M.; Scherman, D.; 2008. Noncovalent functionalization of carbon nanotubes with amphiphilic Cd^{3+} chelates: toward powerful T1 and T2 MRI contrast agents. Nano Letters, 8:1:232-236.

Salvetat, J.P.; Andrew, G.; Briggs, D.; Bonard, J.M.; Kulik, A. J.; 1999. Elastic and shear moduli of single-walled carbon nanotube ropes. Physics Review Letters, 82: 944.

Shin, D.H.; Yoon, K.H.; Kwon, O.H.; Min, B.G.; Hwang, C.; 2006. Surface resistivity and rheological behavior of carboxylated MWNT/PET composite film. Journal of Apply Polymer Science, 99:900.

Shi, D.L.; He, H.; Lian, J.; Chaud, X.; Bud'ko, S.L.; Beaugnon, E.; Wang, L.M.; Ewing, R.C.; Tournier, R.; 2005. Magnetic Alignment of Carbon Nanotubes in Polymer Composites and Anisotropy of Mechanical Properties. Journal of Applied Physics, 97:064312-064319.

Shi, Z.; Lian, Y.; Zhou, X.; Gu, Z.; Zhang, Y.; Iijima, S.; 2000. Single-wall carbon nanotube colloids in polar solvents. Chemical Communications, 461–462.

Stadermann, M.; Papadakis, S.J.; Falvo, M.R.; Fu, Q.; Liu, J.; Fridman, Y.; Boland, J. J.; Superfine, R.; Washburn, S.; 2005. Exponential decay of local conductance in single-wall carbon nanotubes. Physics Review B, 72: 245406-245410.

Sugimoto, T.; Sakata, K.; Muramatsu, A.; 1993. Formation mechanism of monodisperse pseudocubic α-Fe2O3 particles from condensed ferric hydroxide gel. Colloid and Interface Science, 159: 2:372-382.

Tannenbaum, R.; Kim, T.; Nunnery, G.A.; Jacob, K.; Schwartz, J.; Liu, X.T.; 2010. Facile Alignment of Carbon Nanotubes Mediated by Tethered Maghemite Nanoparticles. Material Research Society, 1258: R04:05.

Thostenson, E.T.; Chou, T.W.; 2006. Carbon nanotube networks: sensing of distributed strain and damage for life prediction and self healing. Advanced Materials, 18:2837-2841.

Tombler, T.M.; Zhou, C.W.; Alexseyev, L.; Kong, J.; 2000. Reversible electromechanical characteristics of carbon nanotubes under local-probe manipulation. Nature, 405: 769-772.

Tuinstra, F.; Koenig, J. L.; 1970. Raman Spectrum of Graphite. Journal of Chemical Physics, 53:1126-1130.

Wagner, H.D.; Feldman, Y.; Lourie, O.; Tenne, R.; 1998. Stress-induced fragmentation of multiwall carbon nanotube in a polymeric matrix. Applied Physics Letter, 72:188-190.

Wagner, H.D.; Wood, J.D.; Frogley, M.D.; Meurs, E.R.; Prins, A.D.; Peijs, T.; Dunstan, D.J.; 1999. Mechanical Response of Carbon Nanotubes under molecular and macroscopic pressure . Journal of Physical Chemistry:103:10388-10392.

Wagner, H.D.; Wood, J.R.; Zhao, Q.; 2001. Orientation of carbon nanotubes in polymers and its detection by Raman spectroscopy. Composites Part A, 32:391-399

Wagner, H.D.; Lourie, O.; Cox, D. M.; 1998. Buckling and collapse of embedded carbon nanotubes, Physical review letters, 81: 1638–1641.

Walters, D.A.; Casavant, M.J.; Qin, X.C.; Huffman, C.B.; Boul, P.J.; 2001. In-plane-Aligned Membranes of Carbon Nanotubes. Chemical Physics Letter, 338:14-20

Xue, Q.B.; Yan, K.Y.; Zheng, B.Q.; Hao, L.Z.; 2007. The interface effect of the effective electrical conductivity of CNT composite. Nanotechnology, 18: 255705.

Yamamoto, K.; Aktia, S.; Nakayama, Y.; 1996. Orientation of Carbon Nanotubes Using Electrophoresis. Applied Physics, 35:917-923.

Yang, X.; Zhou, Z.Y.; Wu. Y.; Xiao, M.F.; 2007. Measurement and simulation of carbon nanotube's piezoresistance property by a micro/nano combine structure. Journal of Pure &Applied Physics, 45: 282-286.

Yong, L.; Lu, W.W.; Jun, L.K.; Guo, H.C.; 2003. Piezoresistive effect in carbon nanotube films. Chinese Science Bulletin, 48: 2: 125-127.

Young, R.J.; Cooper, C.A.; Halsall, M.; 2001. Investigation into the deformation of carbon nanotubes and their composites through the use of Raman spectroscopy. Composite Part A, 32:401-411.

Yu, R.; Chen, L.; Liu, Q.; Lin, J.; Tan, K.; Ng, S. C.; Chan, H.; Xu, G.; Andy Hor, S. T.; 1998. Platinum Deposition on Carbon Nanotubes via Chemical Modification. Chemical Physics Letters, 10: 718-721.

Zhang, X.F.; Sreekumar, T.V.; Liu, T.; Kumar, S.; 2004. Properties and Structure of Nitric Acid Oxidized Single Wall Carbon Nanotube Films. Physical Chemistry B, 108:16435:16440.

Zhang, M.; Yudasaka, M.; Iijima, S.; 2004. Diameter enlargement of single-wall carbon nanotubes by oxidation. Physical Chemistry, 108:149-153.

Zhao, Q.; Frogely, D.M.; Wagner, D.H.; 2001. The use of carbon nanotubes to sense matrix stress around a single glass fiber, Composites Science and Technology, 61:2139-2143.

APPENDXI A

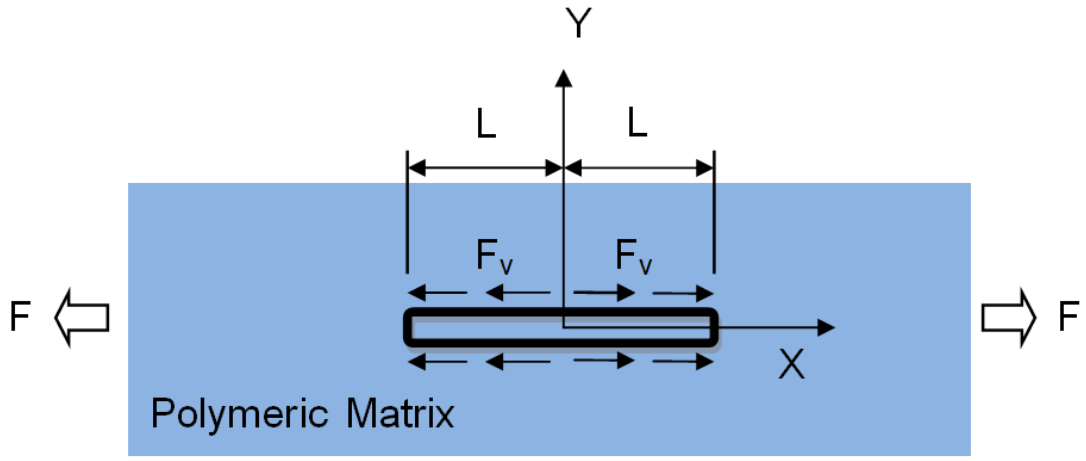

Figure A.1 Schematic model of the tube placed in the middle of the polymeric matrix and aligned along with applied tensile load F

In the 1st situation, no slipping happens at the interface. The stress in polymer matrix σ_p can be described as:

$$\sigma_p = \frac{F}{A_p} = E_p \varepsilon_p \tag{A.1}$$

, where F is the tensile load, A_p is the cross sectional area, E_p is the elastic modulus of polymeric matrix and ε_p is the strain in polymeric matrix. Therefore, the strain in polymeric matrix ε_p can be described as:

$$\varepsilon_p = \frac{du_p}{dx} = \frac{F}{E_p A_p} \tag{A.2}$$

, where u_p is the displacement of any point in the polymer and can be described as:

$$u_p = \frac{F}{E_p A_p} x + C_1 \tag{A.3}$$

From symmetry as shown in Fig.A1, at $x=0$, $u_p=0$, $C_1=0$ and thus u_p can be described as:

$$u_p = \frac{F}{E_p A_p} x \tag{A.4}$$

When no slipping happens at the interface between the tube and polymeric matrix, the displacement of the tube u_p can be described as:

$$u_C = u_p = \frac{F}{E_p A_p} x \tag{A.5}$$

Therefore, the strain on the tube ε_c can be described as:

$$\varepsilon_C = \frac{du_C}{dx} = \frac{F}{E_p A_p} \tag{A.6}$$

In the 2nd situation, slipping happens at the interface between the tube and polymeric matrix. As shown in Fig.2, the tube is considered as a smooth bar (hallow cylinder) and its surface roughness thus is the same along the tube. As a result, the interfacial cohesion F_v with polymer matrix is constant on the surface of the tube as described as:

$$F_v = F_v(x), \tag{A.7}$$

$$F_v(x) = \alpha, \ -L < x < L \tag{A.8}$$

, where F_v is the force per surface area (dA) and α is a constant.

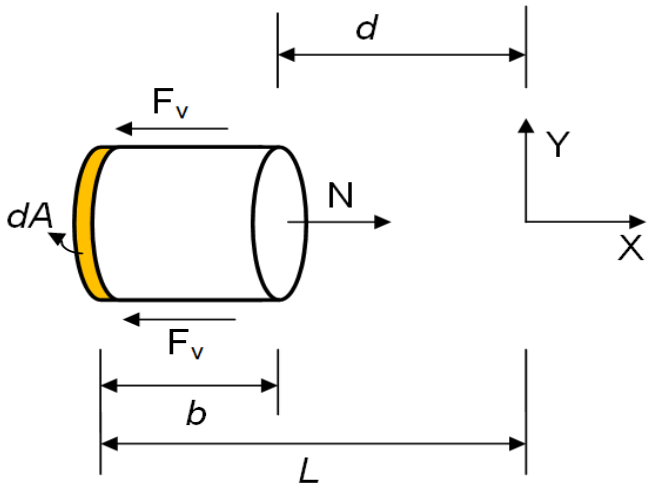

Figure A.2 Free body diagram of the tube (the same coordinate system used as in Figure A.1)

If we assume the wall of the tube is thin, the wall thickness t thus can be described as:

$$t = r_o - r_i \text{ and } t << r_i, \tag{A.9}$$

$$r_o \approx r_i \approx r \tag{A.10}$$

where r_o and r_i are the outer and inner radius of the tube respectively, r is the radius of the tube. Therefore, the stress applied on the tube N can be described as:

$$\sum F_X = 0 = N - \int F_V dA, dA = 2\pi r dx \tag{A.11}$$

From symmetry as shown in Fig.A1, the N thus can be described as:

$$N = 2\pi r \int_{-L}^{x} F_V dx, -L < x < 0$$

$$N = 2\pi r \int_{x}^{L} F_V dx, 0 < x < L \tag{A.12}$$

Since the F_v is a constant, the N on the tube can be described as:

$$N = \begin{cases} 2\pi r\alpha(x+L), -L < x < 0 \\ 2\pi r\alpha(L-x), 0 < x < L \end{cases} \tag{A.13}$$

As a result, the stress σ_c and strain ε_c on the tube can be described:

$$\sigma_C = \frac{N}{A_C}$$

$$\varepsilon_C = \frac{\sigma_C}{E_C} = \frac{N}{E_C A_C} \tag{A.14}$$

where E_c is the elastic modulus of the tube and A_c is the cross sectional area of the tube. Therefore the strain ε_c on the tube can be described as:

$$\varepsilon_C = \begin{cases} \dfrac{2\pi r\alpha(x+L)}{E_C A_C}, -L < x < 0 \\ \dfrac{2\pi r\alpha(L-x)}{E_C A_C}, 0 < x < L \end{cases} \tag{A.15}$$

The slipping at the interface ε_{slip} thus can be described as:

$$\varepsilon_{slip} = \varepsilon_p - \varepsilon_C = \begin{cases} \dfrac{F}{E_p A_p} - \dfrac{2\pi r\alpha(x+L)}{E_C A_C}, -L < x < 0 \\ \dfrac{F}{E_p A_p} - \dfrac{2\pi r\alpha(L-x)}{E_C A_C}, 0 < x < L \end{cases} \tag{A.16}$$

Since the Raman polarized laser selects the average signal from the tube, the average strain of polymeric matrix $(\varepsilon_p)_{avg}$ and the tube $(\varepsilon_c)_{avg}$ can be described respectively as:

$$(\varepsilon_p)_{avg} = \frac{F}{E_p A_p}$$

$$(\varepsilon_C)_{avg} = \frac{1}{2L}\int_{-L}^{L} \varepsilon_C dx$$

$$(\varepsilon_C)_{avg} = \frac{1}{2L}\left\{\frac{2\pi r\alpha}{E_C A_C}\left(\frac{x^2}{2} + Lx\right)\right\}\Bigg|_{-L}^{0} + \frac{1}{2L}\left\{\frac{2\pi r\alpha}{E_C A_C}\left(Lx - \frac{x^2}{2}\right)\right\}\Bigg|_{0}^{L}$$

$$(\varepsilon_C)_{avg} = \frac{2\pi r\alpha L}{E_C A_C} \tag{A.17}$$

The ratio between the average stain of the polymeric matrix and the tube can be described as:

$$\frac{(\varepsilon_p)_{avg}}{(\varepsilon_C)_{avg}} = \frac{FE_C A_C}{E_p A_p \pi r\alpha L} \tag{A.18}$$

where $\frac{E_C A_C}{E_p A_p \pi r L}$ is a constant.

APPENDIX B

Homemade Mini Tensile Tester; Unit (mm)

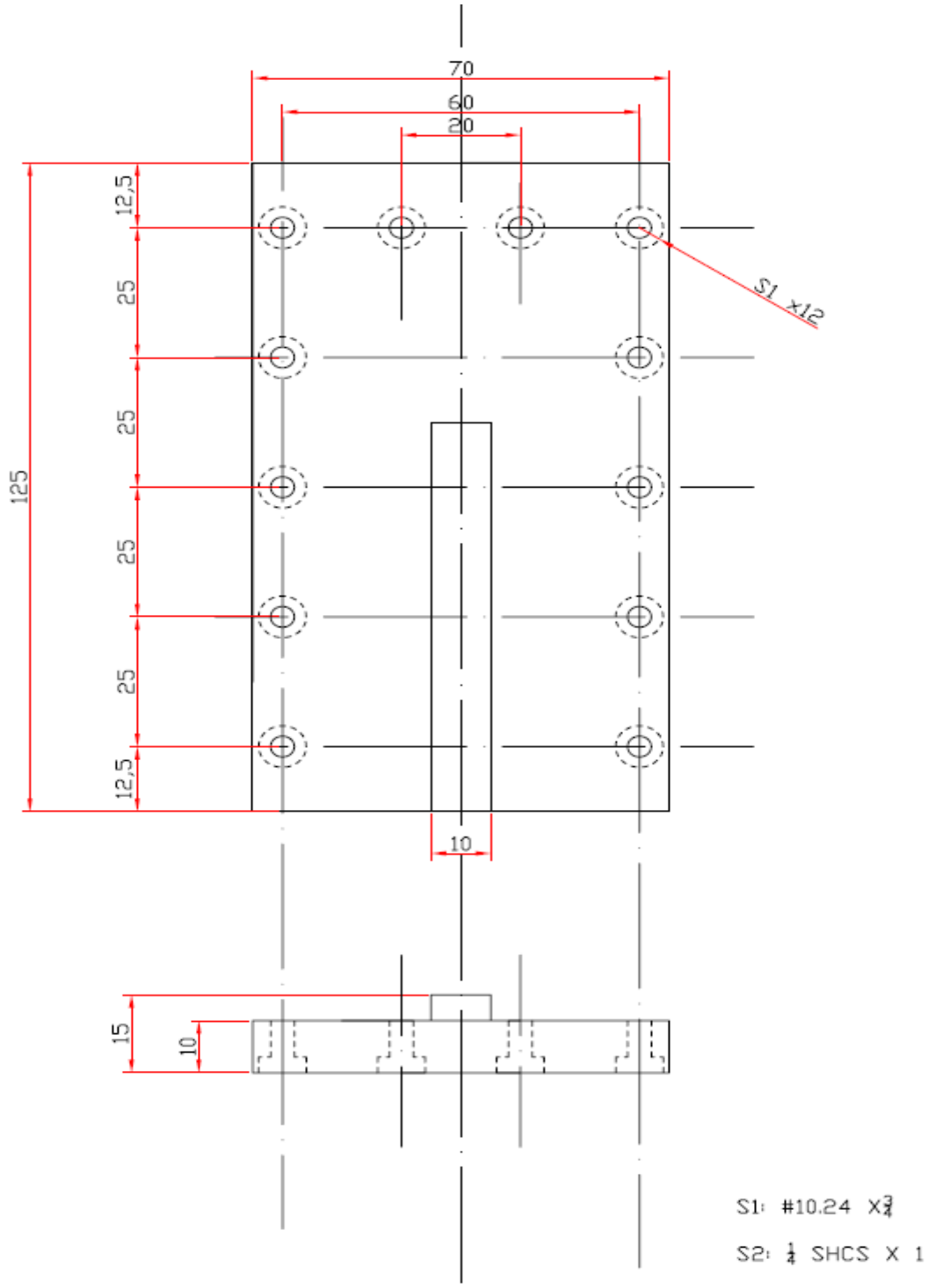

Figure B.1 Base Board (x1), AISI 4130

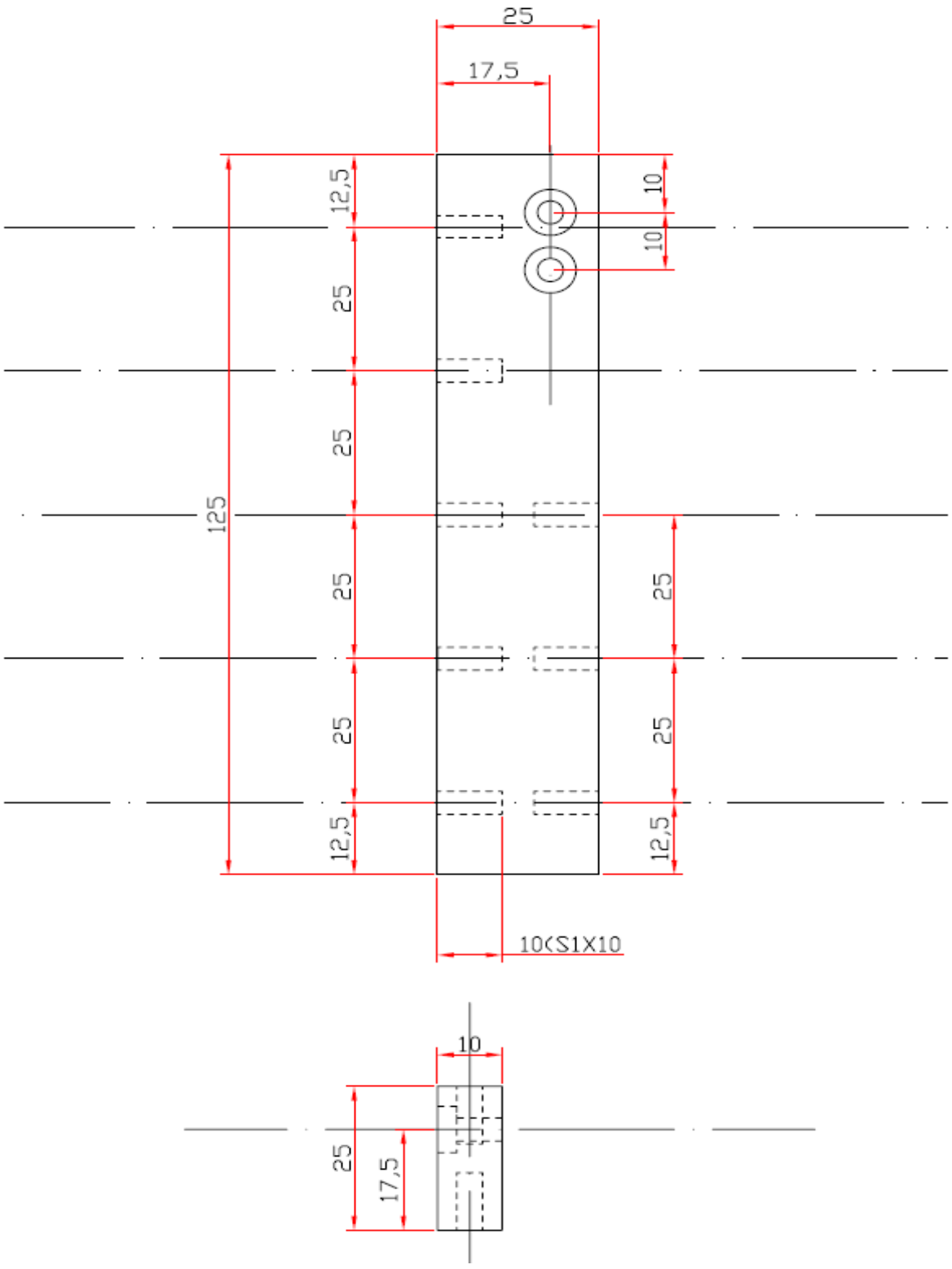

Figure B.2 Left Side Wall (x1), Installed on the left side of baseboard, AISI 4130

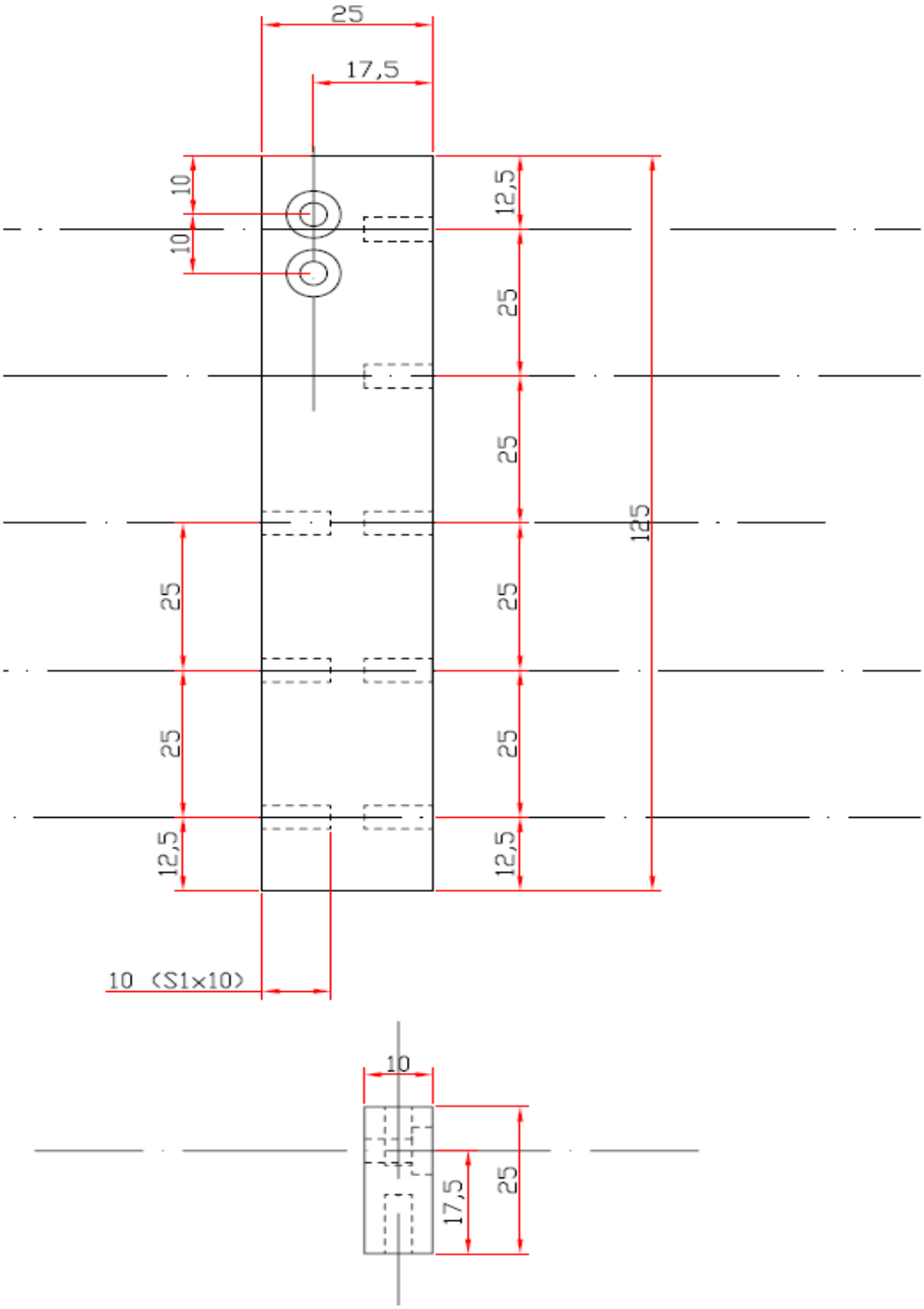

Figure B.3 Right Side Wall (x1), Installed on the right side of base board, AISI 4130

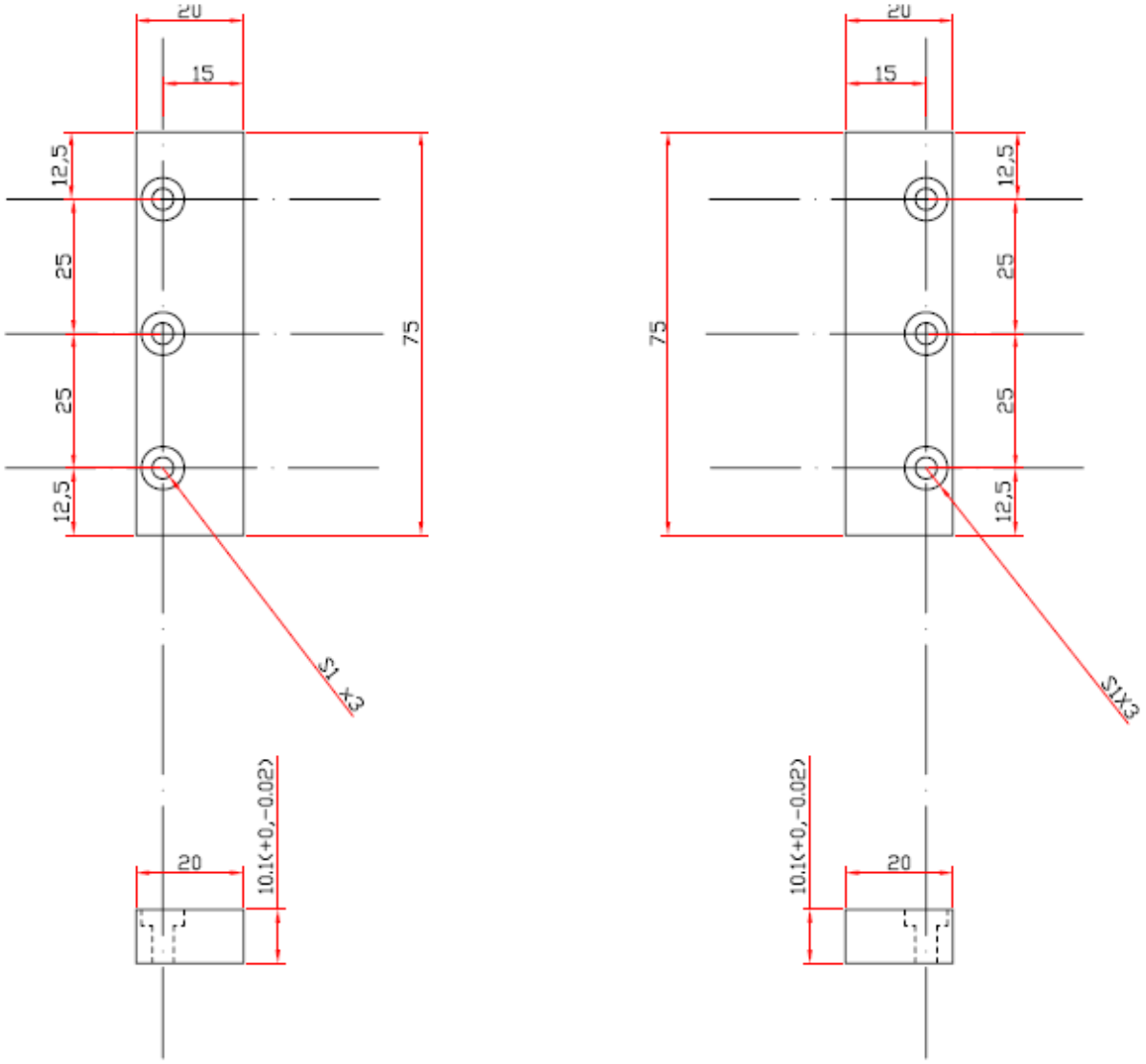

Figure B.4 Fasten Boards (Left and Right x1), Installed on the top of side walls respectively, AISI 4130

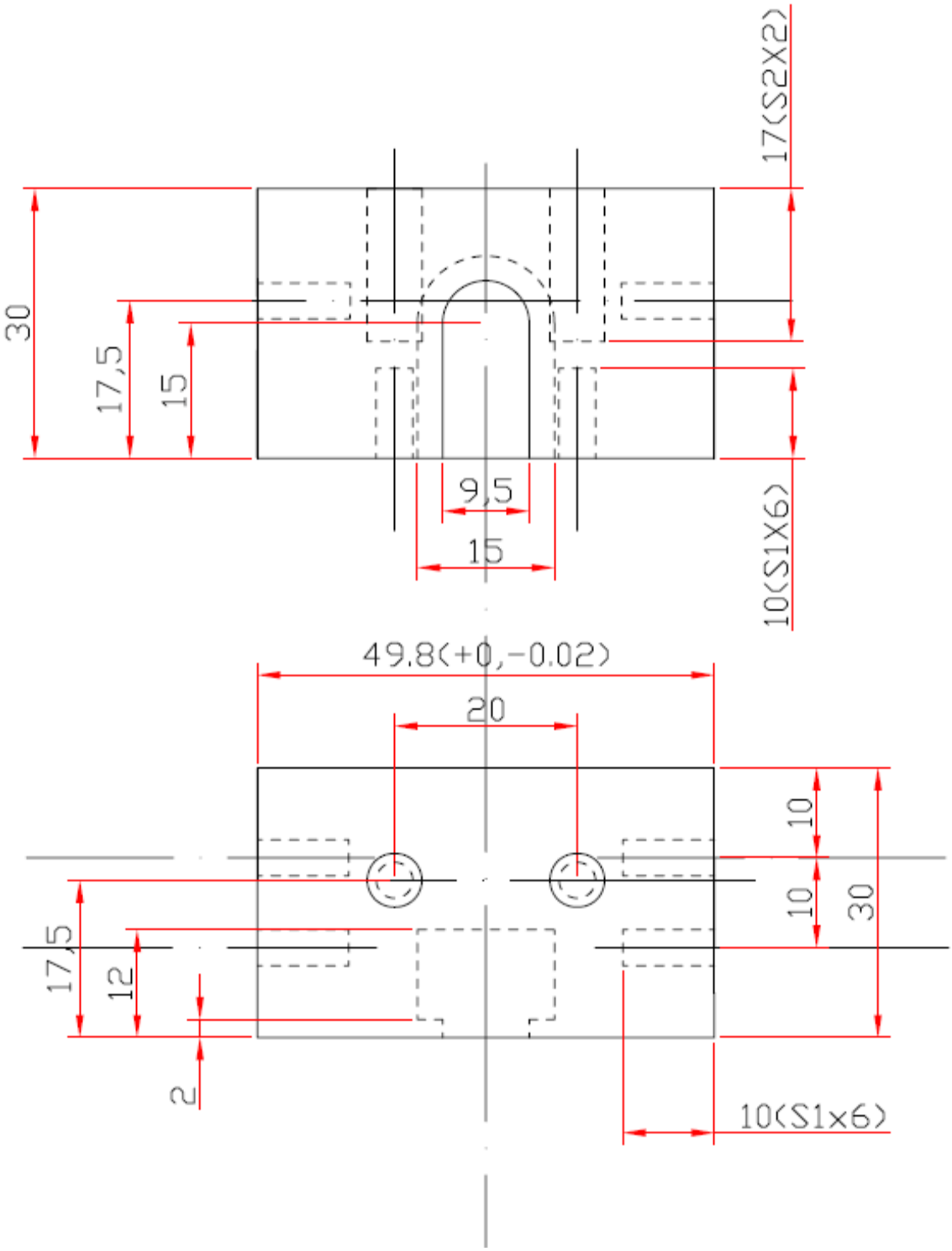

Figure B.5 Unmovable block(x1), Fixed on the end of base board and between two side walls, AISI 4130

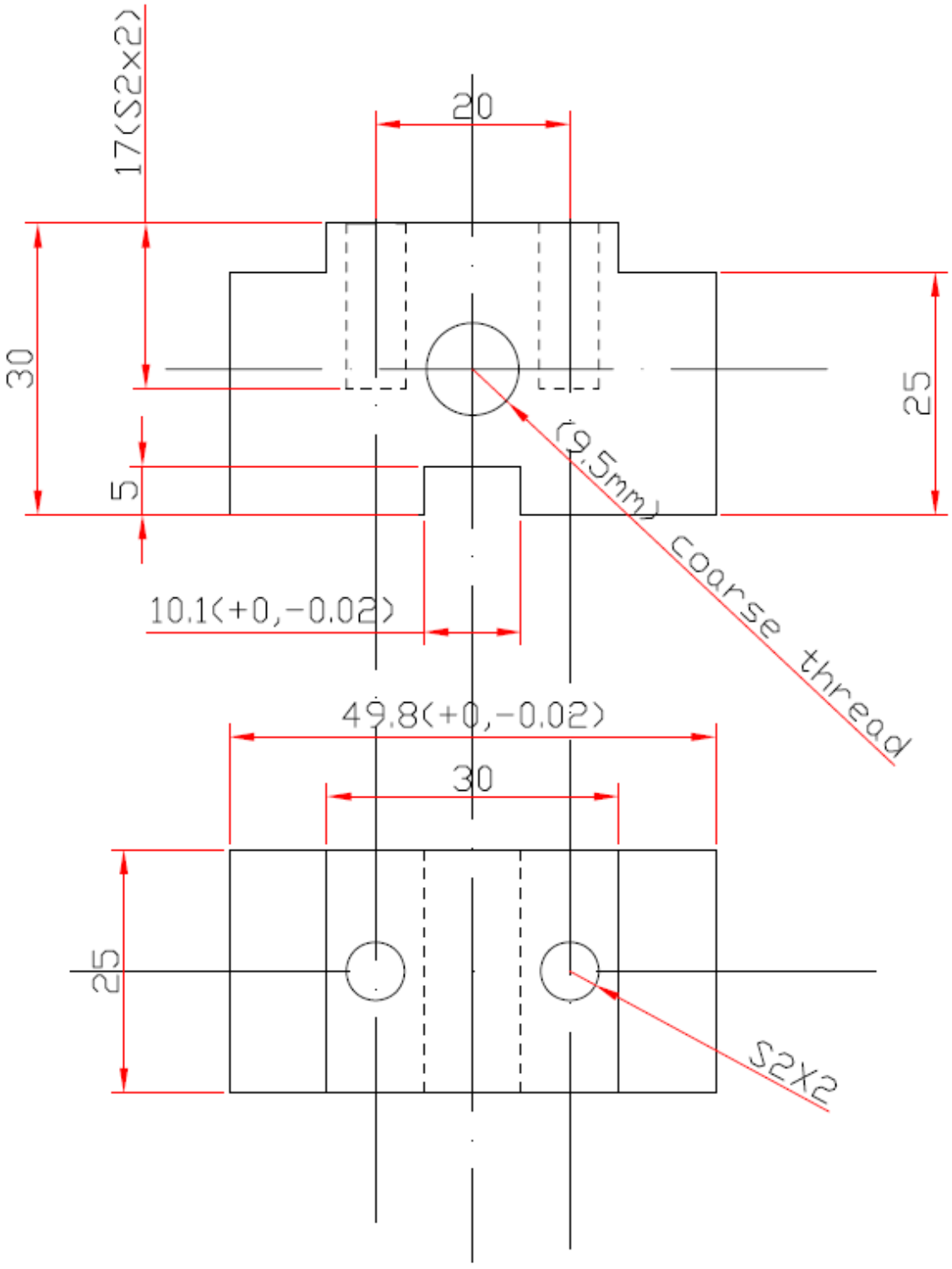

Figure B.6 Movable block(x1), Slide on the base board, AISI 4130

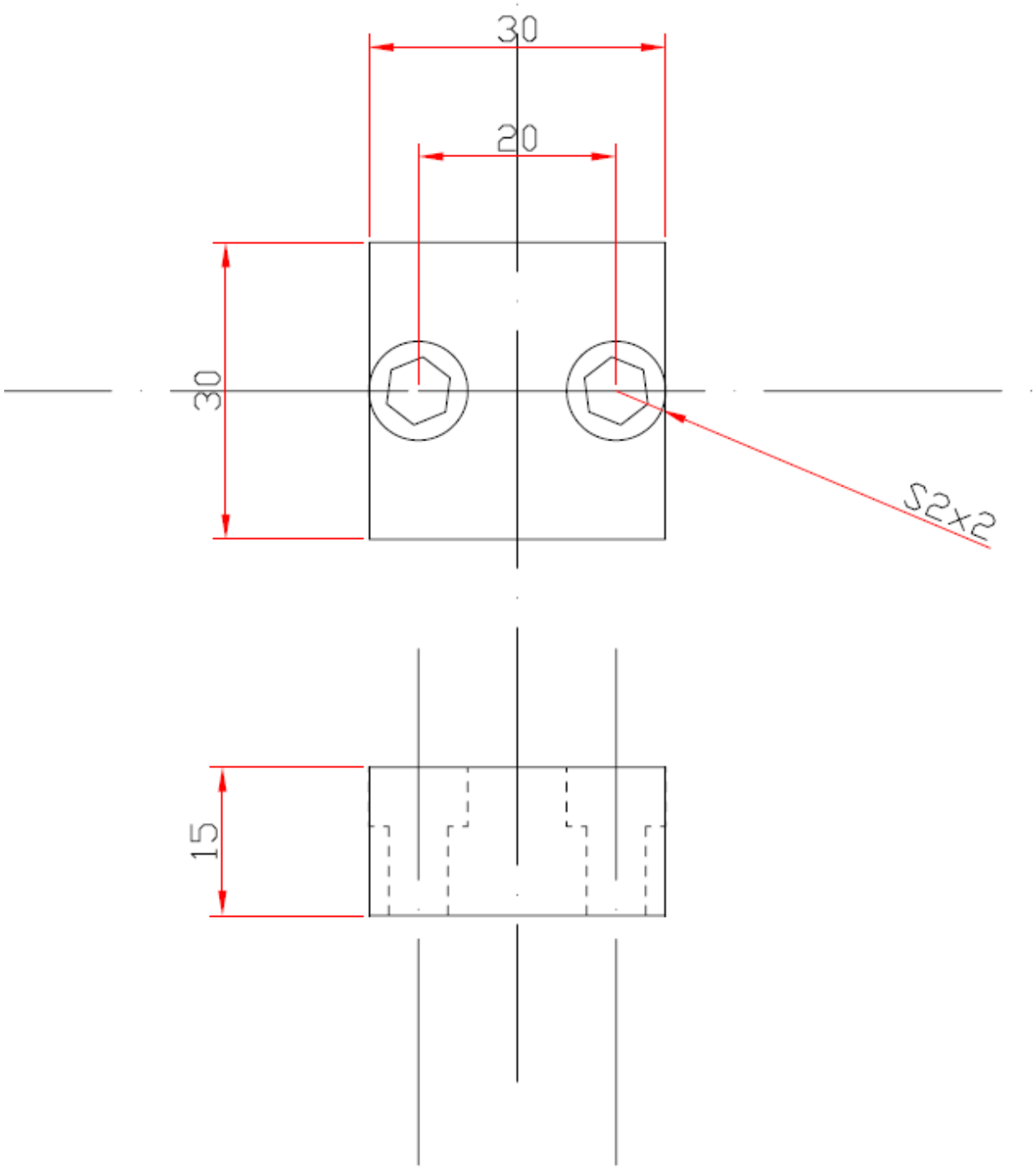

Figure B. 7 Fasten blocks(x2), Installed on top of the unmovable and movable blocks respectively, PVC

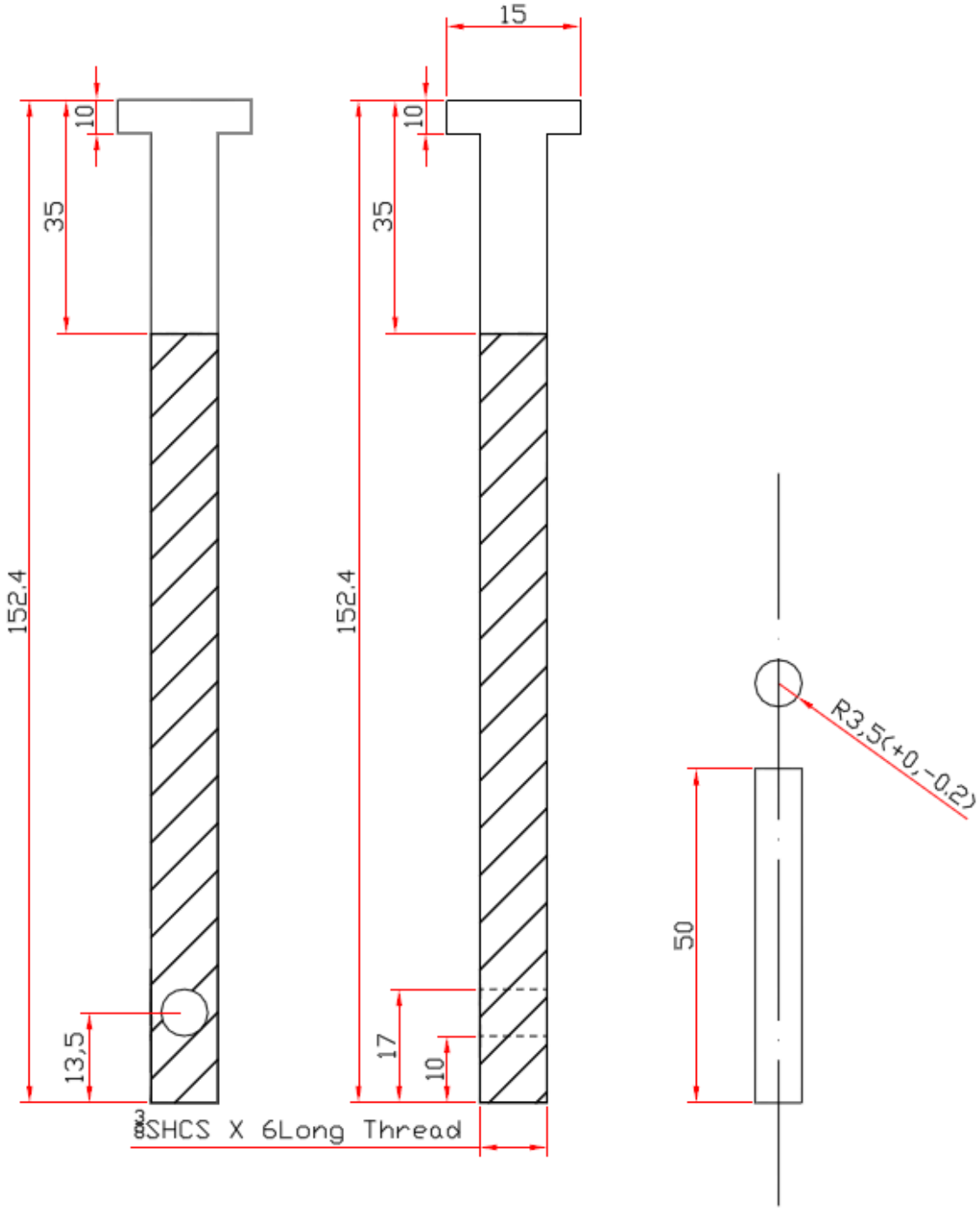

Figure B.8 Thread shaft (x1), Installed through the movable block and fixed the end at unmovable block, AISI 4130

APPENDIX C

Iteration History[b]

Iteration Number[a]	Residual Sum of Squares	Parameter e
0	15.410	1.938

Derivatives are calculated numerically.

a. Major iteration number is displayed to the left of the decimal, and minor iteration number is to the right of the decimal.

b. Run stopped after 0 iterations. Optimal solution is found.

Parameter Estimates

Parameter	Estimate	Std. Error	95% Confidence Interval	
			Lower Bound	Upper Bound
e	1.938	.013	1.910	1.966

ANOVA[a]

Source	Sum of Squares	df	Mean Squares
Regression	2517.391	1	2517.391
Residual	15.410	13	1.185
Uncorrected Total	2532.801	14	
Corrected Total	1900.742	13	

Dependent variable: VAR00001

a. R squared = 1 - (Residual Sum of Squares) / (Corrected Sum of Squares) = .992.

APPENDIX D

Experiment results

Spray Volume 2mL											
		Aligned 0 (Sample1)						Aligned 0 (Sample 2)			
	Strain	1	2	3	4		Strain	1	2	3	4
	0	88.5	77.21	69.53	61.23		0	74.57	69.4	60.2	56.6
	0.08	118.42	102.75	95.42			0.08	101.77	98.87	83.6	
GF	4.22		Repeatability		30%	GF	4.76		Repeatability		24%
		Aligned 90 (Sample1)						Aligned 90 (Sample 2)			
	Strain	1	2	3	4		Strain	1	2	3	4
	0	18.8	18.68	18.74	18.92		0	17.4	17.52	17.5	17.63
	0.08	21.66	21.54	21.82			0.08	20.44	20.39	20.51	
GF	1.9		Repeatability		0.60%	GF	2.2		Repeatability		1.3%
		Randomly Distributed (Sample1)						Randomly Distributed (Sample2)			
	Strain	1	2	3	4		Strain	1	2	3	4
	0	20	19.96	20.08	20.1		0	17.2	17.27	17.29	17.32
	0.08	23.4	23.32	23.43			0.08	20.68	20.53	20.57	
GF	2.12		Repeatability		0.50%	GF	2.57		Repeatability		0.50%

Calculation Methods

Average Resistance= (88.5+74.57)/2=81.535 (Error: ±9%)

GF= (118.42-88.5)/88.5=4.22

Average GF= (4.22+4.76)/2=4.49 (Error: ±6%)

Repeatability= (61.23-88.5)/88.5= -30%

APPENDIX E

Permission to Use Figures

Figure 1.2

Confirmation Number: 11122748
Order Date: 09/11/2013

Requestor type	Academic institution
Format	both print and electronic
Portion	image/photo
Number of images/photos requested	1
With minor editing privileges	no
In the following language(s)	Original language of publication
The requesting person/organization	Yu (Paul) Miao
Author/Editor	Yu (Paul) Miao
Title	PhD thesis: ON UNDERSTANDING OF PIEZORESISTIVE RESPONSE IN CARBON NANOTUBE NETWORKS UNDER IN-PLANE STRAINING
Publisher	University of Saskatchewan
Expected publication date	Nov 2013
Estimated size (pages)	130

Figure 1.3

License Number 3231580816518

License date	Sep 17, 2013
Licensed content publisher	Elsevier
Licensed content publication	Applied Surface Science
Licensed content title	Transparent carbon nanotube coatings
Licensed content author	M. Kaempgen,G.S. Duesberg,S. Roth
Licensed content date	15 October 2005
Licensed content volume number	252
Licensed content issue number	2
Number of pages	5
Type of Use	reuse in a thesis/dissertation
Portion	figures/tables/illustrations
Number of figures/tables/illustrations	1
Format	both print and electronic
Are you the author of this Elsevier article?	No
Will you be translating?	No
Order reference number	
Title of your thesis/dissertation	ON UNDERSTANDING OF PIEZORESISTIVE RESPONSE IN CARBON NANOTUBE NETWORKS UNDER IN-PLANE STRAINING
Expected completion date	Sep 2013
Estimated size (number of pages)	130
Elsevier VAT number	GB 494 6272 12
Permissions price	0.00 USD
VAT/Local Sales Tax	0.00 USD / 0.00 GBP
Total	0.00 USD

Figure 1.4

License Number	3231581384983
License date	Sep 17, 2013
Licensed	Springer

content publisher	
Licensed content publication	Chinese Science Bulletin
Licensed content title	Piezoresistive effect in carbon nanotube films
Licensed content author	Yong Li
Licensed content date	Jan 1, 2003
Volume number	48
Issue number	2
Type of Use	Thesis/Dissertation
Portion	Figures
Author of this Springer article	No
Country of republication	other
Title of your thesis / dissertation	ON UNDERSTANDING OF PIEZORESISTIVE RESPONSE IN CARBON NANOTUBE NETWORKS UNDER IN-PLANE STRAINING
Expected completion date	Sep 2013
Estimated size(pages)	130
Total	0.00 USD

Figure 2.1

License Number	3234970633669
License date	Sep 23, 2013
Licensed content publisher	Nature Publishing Group
Licensed content publication	Nature
Licensed content title	Reversible electromechanical characteristics of carbon nanotubes underlocal-probe manipulation
Licensed content author	Thomas W. Tombler, Chongwu Zhou, Leo Alexseyev, Jing Kong, Hongjie Dai et al.

Licensed content date	Jun 15, 2000
Type of Use	reuse in a thesis/dissertation
Volume number	405
Issue number	6788
Requestor type	academic/educational
Format	print and electronic
Portion	figures/tables/illustrations
Number of figures/tables/illustrations	1
Figures	Fig 2.1
Author of this NPG article	no
Your reference number	
Title of your thesis / dissertation	ON UNDERSTANDING OF PIEZORESISTIVE RESPONSE IN CARBON NANOTUBE NETWORKS UNDER IN-PLANE STRAINING
Expected completion date	Sep 2013
Estimated size (number of pages)	130
Total	0.00 USD

Figure 2.3

Title:	Finite-size scaling in stick percolation
Author:	Jiantong Li and Shi-Li Zhang
Publication:	Physical Review E
Publisher:	American Physical Society
Date:	Oct 19, 2009

PERMISSION/LICENSE IS GRANTED FOR YOUR ORDER AT NO CHARGE

This type of permission/license, instead of the standard Terms & Conditions, is sent to you because no fee is being charged for your order. Please note the following:

- Permission is granted for your request in both print and electronic formats, and translations.
- If figures and/or tables were requested, they may be adapted or used in part.
- Please print this page for your records and send a copy of it to your publisher/graduate school.

- Appropriate credit for the requested material should be given as follows: "Reprinted (adapted) with permission from (COMPLETE REFERENCE CITATION). Copyright (YEAR) American Chemical Society." Insert appropriate information in place of the capitalized words.
- One-time permission is granted only for the use specified in your request. No additional uses are granted (such as derivative works or other editions). For any other uses, please submit a new request.

Figure 2.4

License Number	3231590549852
Order Date	Sep 17, 2013
Publisher	AIP Publishing LLC
Publication	Applied Physics Letters
Article Title	Conductivity scaling with bundle length and diameter in single walled carbon nanotube networks
Author	David Hecht, Liangbing Hu, George Grumner
Online Publication Date	Sep 27, 2006
Volume number	89
Issue number	13
Type of Use	Thesis/Dissertation
Requestor type	Student
Format	Print and electronic
Portion	Photograph/Image
Number of Photographs/Images	1
Title of your thesis / dissertation	ON UNDERSTANDING OF PIEZORESISTIVE RESPONSE IN CARBON NANOTUBE NETWORKS UNDER IN-PLANE STRAINING
Expected completion date	Sep 2013
Estimated size (number of pages)	130
Total	0.00 USD

Figure 2.5 and Figure 2.6

Title:	Percolation in Transparent and Conducting Carbon Nanotube Networks
Author:	L. Hu,D. S. Hecht, and, and G. Grüner*
Publication:	Nano Letters
Publisher:	American Chemical Society
Date:	Dec 1, 2004

Figure 2.7 and Figure 3.3

Title:	Macroscopic Electrical Properties of Ordered Single-Walled Carbon Nanotube Networks
Author:	Pornnipa Vichchulada, Qinghui Zhang, Alicia Duncan, and Marcus D. Lay
Publication:	Applied Materials
Publisher:	American Chemical Society
Date:	Feb 1, 2010

This type of permission/license, instead of the standard Terms & Conditions, is sent to you because no fee is being charged for your order. Please note the following:

- Permission is granted for your request in both print and electronic formats, and translations.
- If figures and/or tables were requested, they may be adapted or used in part.
- Please print this page for your records and send a copy of it to your publisher/graduate school.
- Appropriate credit for the requested material should be given as follows: "Reprinted (adapted) with permission from (COMPLETE REFERENCE CITATION). Copyright (YEAR) American Chemical Society." Insert appropriate information in place of the capitalized words.
- One-time permission is granted only for the use specified in your request. No additional uses are granted (such as derivative works or other editions). For any other uses, please submit a new request.

Figure 3.1 and Figure 3.2

License Number	3231591173499
License date	Sep 17, 2013
Licensed content publisher	Springer
Licensed content publication	Journal of Materials Science (full set)
Licensed content title	Percolation in networks of aligned SWNTs formed with laminar flow deposition
Licensed content author	Qinghui Zhang
Licensed content date	Jan 1, 2009
Volume number	44
Issue number	5
Type of Use	Thesis/Dissertation
Portion	Figures
Author of this Springer article	No

Title of your thesis / dissertation	ON UNDERSTANDING OF PIEZORESISTIVE RESPONSE IN CARBON NANOTUBE NETWORKS UNDER IN-PLANE STRAINING
Expected completion date	Sep 2013
Estimated size(pages)	130
Total	0.00 USD

Figure 3.4 and Figure 3.7

License Number	3231591490456
License date	Sep 17, 2013
Licensed content publisher	Cambridge University Press
Licensed content publication	MRS Online Proceedings Library
Licensed content title	Facile Alignment of Carbon Nanotubes Mediated by Tethered Maghemite Nanoparticles
Licensed content author	Il Tae Kim, Karl I Jacob, Justin Schwartz, Xiaotao Liu and Rina Tannenbaum
Licensed content date	Jan 1, 2010
Volume number	1258
Issue number	-1
Start page	0
End page	0
Type of Use	Dissertation/Thesis
Requestor type	Not-for-profit
Portion	Figure
Number of Figure requested	2
Order reference number	
Territory for reuse	North America Only
Title of your thesis / dissertation	ON UNDERSTANDING OF PIEZORESISTIVE RESPONSE IN CARBON NANOTUBE NETWORKS UNDER IN-PLANE STRAINING
Expected completion date	Sep 2013

Estimated size(pages)	130
Billing Type	Invoice
Billing address	4 hardy cres
	Saskatoon, SK s7h3e7
	Canada
Total	0.00 USD

Figure 3.5

License Number	3231600181205
License date	Sep 17, 2013
Licensed content publisher	Elsevier
Licensed content publication	Carbon
Licensed content title	CVD synthesis of coal-gas-derived carbon nanotubes and nanocapsules containing magnetic iron carbide and oxide
Licensed content author	Jieshan Qiu,Qixiu Li,Zhiyu Wang,Yufeng Sun,Hongzhe Zhang
Licensed content date	October 2006
Licensed content volume number	44
Licensed content issue number	12
Number of pages	4
Type of Use	reuse in a thesis/dissertation
Portion	figures/tables/illustrations
Number of figures/tables/illustrations	1
Format	both print and electronic
Are you the author of this Elsevier article?	No
Will you be translating?	No
Order reference number	
Title of your thesis/dissertation	ON UNDERSTANDING OF PIEZORESISTIVE RESPONSE IN CARBON NANOTUBE NETWORKS UNDER IN-PLANE STRAINING
Expected completion date	Sep 2013
Estimated size (number	130

of pages)	
Elsevier VAT number	GB 494 6272 12
Permissions price	0.00 USD
VAT/Local Sales Tax	0.00 USD / 0.00 GBP
Total	0.00 USD

Figure 3.6

Title:	Carbon Nanotubes Loaded with Magnetic Particles
Author:	Guzeliya Korneva et al.
Publication:	Nano Letters
Publisher:	American Chemical Society
Date:	May 1, 2005

PERMISSION/LICENSE IS GRANTED FOR YOUR ORDER AT NO CHARGE

This type of permission/license, instead of the standard Terms & Conditions, is sent to you because no fee is being charged for your order. Please note the following:

- Permission is granted for your request in both print and electronic formats, and translations.
- If figures and/or tables were requested, they may be adapted or used in part.
- Please print this page for your records and send a copy of it to your publisher/graduate school.
- Appropriate credit for the requested material should be given as follows: "Reprinted (adapted) with permission from (COMPLETE REFERENCE CITATION). Copyright (YEAR) American Chemical Society." Insert appropriate information in place of the capitalized words.
- One-time permission is granted only for the use specified in your request. No additional uses are granted (such as derivative works or other editions). For any other uses, please submit a new request.

Figure 4.1

Title:	Molecular Simulation of the Influence of Chemical Cross-Links on the Shear Strength of Carbon Nanotube−Polymer Interfaces
Author:	S. J. V. Frankland, A. Caglar, D. W. Brenner, and M. Griebel
Publication:	The Journal of Physical Chemistry B
Publisher:	American Chemical Society

Date: Mar 1, 2002

Figure 4.2

License Number	3231600551945
Order Date	Sep 17, 2013
Publisher	AIP Publishing LLC
Publication	Applied Physics Letters
Article Title	Stress-induced fragmentation of multiwall carbon nanotubes in a polymer matrix
Author	H. D. Wagner, O. Lourie, Y. Feldman, R. Tenne et al.
Online Publication Date	Jan 12, 1998
Volume number	72
Issue number	2
Type of Use	Thesis/Dissertation
Requestor type	Student
Format	Print and electronic
Portion	Figure/Table
Number of figures/tables	1
Title of your thesis /	ON UNDERSTANDING OF PIEZORESISTIVE RESPONSE IN CARBON NANOTUBE NETWORKS UNDER IN-PLANE STRAINING

dissertation	
Expected completion date	Sep 2013
Estimated size (number of pages)	130
Total	0.00 USD

Figure 4.3

Title:	Mechanical Response of Carbon Nanotubes under Molecular and Macroscopic Pressures
Author:	Jonathan R. Wood et al.
Publication:	The Journal of Physical Chemistry B
Publisher:	American Chemical Society
Date:	Nov 1, 1999

This type of permission/license, instead of the standard Terms & Conditions, is sent to you because no fee is being charged for your order. Please note the following:

- Permission is granted for your request in both print and electronic formats, and translations.
- If figures and/or tables were requested, they may be adapted or used in part.
- Please print this page for your records and send a copy of it to your publisher/graduate school.
- Appropriate credit for the requested material should be given as follows: "Reprinted (adapted) with permission from (COMPLETE REFERENCE CITATION). Copyright (YEAR) American Chemical Society." Insert appropriate information in place of the capitalized words.
- One-time permission is granted only for the use specified in your request. No additional uses are granted (such as derivative works or other editions). For any other uses, please submit a new request.

Curriculum Vitae

Yu (Paul) Miao graduated from China Jiliang University (Hangzhou, P.R. CHINA) in 2006 with B.Sc degree in the major of Mechanical Engineering. From 2006 to 2008, he was a mechanical engineer (entry level) at the SBS Bühnentechnik Gmbh in Dresden, Germany and his works included composing technical specifications and detailed designing of hoist systems and hydraulic lifters. In 2008, he moved to Canada for a M. Sc. degree study at the Mechanical Engineering at the University of Saskatchewan and received the M. Sc. degree in 2010. After that, he continued to study for a PhD degree at the same department. In his PhD study, he has contributed to several original articles in international journals and conferences listed as follows:

Journals:

(1) **Miao, Y**.; Yang, Q. Q.; Sammynaiken, R.; Zhang, W.J.; Chen, L.; 2012. Modeling of piezoresistive response of carbon nanotube (CNT) network based films under in-plane straining by percolation theory. Applied Physics Letter, 101:063120.

(2) **Miao, Y**.; Yang, Q. Q.; Sammynaiken, R.; Zhang, W.J.; Maley, J.; Schatte, J.; 2013. Influence of aligned CNT Networks on Piezoresistive Response in CNT Films under In-plane straining. Applied Physics Letter, 102:233106.

(3) **Miao, Y**.; Yang, Q. Q.; Sammynaiken, R.; Zhang, W.J.; Maley, J.; 2013. Interaction of Carbon Nanotube (CNT) with polymer matrix in CNT films under the in-plane straining. Under preparation

Conferences:

(1) **Miao, Y**.; Yang, Q. Q.; Sammynaiken, R.; Zhang, W.J.; 2012. The multi-wall carbon nanotube (MWNT) film sensor for in-plane strain detection. The 3rd International Conference on Nanotechnology: Fundamentals and Applications, (Montreal, Canada, 2012)